

DISSERTATION

DEMOGRAPHIC PROCESSES IN FOREST TREES IN THE ROCKY MOUNTAINS

Submitted by

Arne Buechling

Department of Horticulture and Landscape Architecture

In partial fulfillment of the requirements

For the Degree of Doctor of Philosophy

Colorado State University

Fort Collins, Colorado

Summer 2017

Doctoral Committee:

Advisor: Patrick H. Martin

Bill Bauerle

Peter M. Brown

Tony Cheng

Copyright by Arne Buechling 2017

All Rights Reserved

ABSTRACT

DEMOGRAPHIC PROCESSES IN FOREST TREES IN THE ROCKY MOUNTAINS

Forests provide numerous ecological and economic services including regulation of biogeochemical cycles, fiber production, watershed protection, as well as less tangible aesthetic and recreational benefits. Forests are being substantially altered by a range of consumptive uses related to expanding human population and economies. Superimposed on other anthropogenic impacts is global climate change. Global circulation models unambiguously reveal the role of greenhouse gas forcings associated with industrial processes in driving global temperature trends (Hanson *et al.* 2005). Meteorological observations indicate that global mean temperature has increased by approximately 0.6 °C over the past century relative to a base 1951 to 1980 period, with record high temperatures occurring in 2010. Paleoclimatic reconstructions based on proxy data indicate that modern rates of warming may be unprecedented in the context of the past 1000 years. Rates of warming are geographically heterogeneous. Temperature anomalies in the Rocky Mountain ecoregion, for example, are 2–3 times higher than the global mean temperature increase. Some models and observational data suggest that temperature trends are elevation dependent with greater warming at high altitudes and with greater increases in daily minimum temperatures than maximum temperatures. Documented increases in minimum temperature is associated with earlier spring thaw events, driven by minimum temperatures that exceed 0 °C and a lengthening of the growing and fire seasons.

In the Rocky Mountains, an altered climate system is projected to result in a higher frequency and intensity of drought events. Precipitation over the previous 100 years lacks clear

trends across the region as a whole, but models of snow water equivalent (SWE) indicate declining moisture availability since the mid-20th century. Early spring snowmelt and warming driven increases in rates of evapotranspiration may correlate with reduced stream flow and declines in effective soil moisture late in the growing season. Warming temperatures and reductions in moisture availability have been associated with significant increases in area burned by wildfire in some forest systems, particularly at high elevations where climate variability rather than fuel conditions is the primary driver of fire activity. Changing climate may also be expanding the ranges and altering the dynamics of forest insects, such as the mountain pine beetle (*Dendroctonus ponderosae*), resulting in extensive tree mortality.

The recent widespread acceptance of climate change has highlighted the need for regional and species specific adaptation strategies. However, a lack of reliable projections describing the responses of organisms and communities to climate change has been identified as a major impediment to the development and implementation of climate adaptation strategies within federal agencies. Potential vegetation responses include migration to track preferred habitats or adaptation through phenotypic or genetic plasticity. Heat stress and prolonged drought have been associated with rapid shifts in the range limits of ponderosa pine (*Pinus ponderosa*) and in significantly elevated rates of background tree mortality for tree species and forest environments worldwide. Mortality events associated with physiological stress or environmental disturbances may accelerate changes in the distributions of long-lived tree species that might otherwise persist in sub-optimal environments.

The distribution and abundance of plants are largely determined by physiological, life history, and ecosystem processes, and how these processes interact or respond to climate. A mechanistic understanding of these processes and their physiological thresholds is required to

accurately predict forest response to climate change. The 2007 Intergovernmental Panel on Climate Change working group has argued that current predictive vegetation models are limited by a failure to adequately quantify relationships between climate, critical life history processes, and disturbance regimes.

The main objective of this research is to quantify life history processes for select tree species in the Rocky Mountain ecoregion. Specifically, non-linear regression models will be developed to quantify variation in both tree fecundity and growth as a function of climate variables, edaphic gradients, and competition. Comprehensive field data will be used to train flexible functions in a maximum likelihood framework. Competing models representing alternative hypotheses will be evaluated using information theory. The overarching objective of this project is to provide detailed quantitative life history information that may subsequently be used to parameterize dynamic simulation models for the prediction of forest response to alternative future climate scenarios. An additional component of this research involves the reconstruction of historical temperatures in the southern portion of the Rocky Mountain ecoregion using chronologies of radial growth from several high elevation tree species occurring in northern Colorado and southern Wyoming. Historical temperatures have been reconstructed for northern portions of the Rocky Mountain ecoregion. A comparable reconstruction for the southern portion of the region has not been developed. Global climate models predict that parts of the Rockies may experience future climates with no previous analogs. Historical temperature reconstructions based on proxy indicators will provide historical context for both modern climate variation and simulations of future conditions.

ACKNOWLEDGEMENTS

This research was only possible through the generosity of friends, family, advisors, and mentors. I wish to thank everyone who shaped this work and contributed to its completion.

We gratefully acknowledge our field and lab assistants, Lee Arnold, Kevin Bolland, Ben Gannon, and Carrie Howard, who endured rain and snow, difficult terrain, and long hours. Erin Birtwistle in particular was a partner in these endeavors for every year of the entire 6-year duration of the project.

Many thanks to my committee, Peter Brown, Bill Bauerle and Tony Cheng, for their support. Peter Brown in particular provided much helpful advice regarding tree ring analyses. Tong Cheng additionally provided generous funding via the Colorado Forest Restoration Institute, which sustained progress on this work at critical times.

My principle advisor, Patrick Martin, seeded the intellectual goals of this work and guided progress as the research evolved over time. His patient style of mentoring and guidance was appreciated. He also ensured consistent and essential funding over the many years that were required to bring this research to completion.

Charles Canham of the Cary Institute of Ecosystem Studies provided invaluable training and guidance in statistical methods and computer modeling. His knowledge, expertise, and experience to a large extent shaped the direction and outcomes of this project. His kind and gentle approach were much appreciated.

Friends and family in Canada took care of me during difficult times, providing me with financial help and a place to sleep and work when needed. Friends also provided intellectual discussion that tuned statistical questions and interpretations. In particular, I thank my parents,

Karl and Inge Buechling, and friends, Irving Kwok, Maureen Ryan, Lori Wahn, and Pat Wahn.

I'm also grateful to all the teachers at Elan for helping to keep me grounded.

We thank the US Forest Service and National Park Service for data and access to study sites. In particular we thank Lance Asherin at the USFS for years of seed collection and lab analyses, and Kelly Elder for supplying weather station data for the Fraser Experimental Forest.

TABLE OF CONTENTS

ABSTRACT.....	ii
ACKNOWLEDGEMENTS	v
CHAPTER 1 CLIMATE DRIVERS OF SEED PRODUCTION IN <i>PICEA ENGELMANNII</i> AND RESPONSE TO WARMING TEMPERATURES IN THE SOUTHERN ROCKY MOUNTAINS.....	1
Synopsis.....	1
Introduction	2
Materials and methods.....	5
Study Site.....	5
Seed collection and growth increment sampling.....	6
Climate analyses	7
Seed production analyses	7
Statistical models used to determine the climate drivers of seed rain.....	9
Tree growth analyses	11
Results	12
Climate trends.....	12
Temporal and spatial patterns of seed production	13
Climate effects on seed rain	15
Discussion	17
Reproductive dynamics	17
Climate effects on seed rain	18
Trends in seed output.....	21
Data Accessibility.....	24

Tables	25
Figures	28
REFERENCES	34
CHAPTER 2 CLIMATE AND COMPETITION EFFECTS ON TREE GROWTH IN ROCKY MOUNTAIN FORESTS.....	41
Synopsis.....	41
Introduction	42
Materials and methods.....	45
Study area	45
Growth data	46
Growth models	48
Model specification and evaluation.....	52
Results	53
Discussion	56
Data Accessibility.....	63
Tables	64
Figures.....	67
REFERENCES	71
CHAPTER 3 A TEMPERATURE HISTORY FROM HIGH ELEVATION TREE SPECIES IN THE SOUTHERN ROCKY MOUNTAINS OF WESTERN NORTH AMERICA	76
Synopsis.....	76
Introduction	77
Materials and methods.....	80
Study area	80
Growth data	81

Climate data.....	83
Growth - climate relationships	84
Temperature reconstruction.....	86
Model specification	87
Results and Discussion.....	88
Tables	96
Figures	104
REFERENCES	110
APPENDIX.....	117
Appendix S1.1: Comparison of PRISM and TopoWx Gridded Temperature Datasets	117
Appendix S2.1: Distribution of field samples	119
Appendix S2.2: Growth models based on seasonal climate	120

CHAPTER 1 CLIMATE DRIVERS OF SEED PRODUCTION IN *PICEA ENGELMANNII*
AND RESPONSE TO WARMING TEMPERATURES IN THE SOUTHERN ROCKY
MOUNTAINS¹

Synopsis

Seed production by *Picea engelmannii* was monitored at 13 sites distributed across a ~670 m elevation gradient for 40 years. Time series of annual seed output was investigated for evidence of masting behavior and trends in seed abundance over time. We used regression models in a likelihood framework to examine climate effects on seed production for critical periods in the species' reproductive cycle. We rigorously evaluated the performance of two gridded climate datasets, PRISM and TopoWx, before using associated variables as predictors in the seed models. Seed production at these sites does not strictly conform to the classic masting concept. Seed abundance was highly variable over time and strongly synchronized among sites, but mast years could not be objectively identified due to intermediate levels of seed output. Model results indicate that climate conditions across multiple years cumulatively determine reproductive output. High seed rain is associated with elevated summer temperatures in the year that seeds are dispersed, low spring snowfall in the year preceding seed dispersal when buds are initiated, and reduced spring snowfall in a so-called priming year two years prior to seed dispersal. Low spring precipitation putatively increases growing season length and resource accumulation in seed trees. Linear models identified significant positive trends in seed output

¹ This research was originally published in the *Journal of Ecology*: Buechling, A., Martin, P.H., Canham, C.D., Shepperd, W.D. & Battaglia, M.A. (2016) Climate drivers of seed production in *Picea engelmannii* and response to warming temperatures in the southern Rocky Mountains. *Journal of Ecology* 104, 1051-1062.

over time. Anomalous aridity and summer warmth in the latter half of the study period were highly favorable for seed production and were associated with increases in seed abundance. The increases in seed output observed in this study may promote population fitness of *P. engelmannii* in the face of changing climate regimes and increasing frequencies of fire and insect related tree mortality in the Rocky Mountains. Since this species lacks a persistent seed bank, re-colonization of disturbed areas or dispersal to shifting habitats depends on adequate production of seed by surviving trees, which, according to these analyses may be moderately enhanced by current climate trends. However, some evidence also indicates that increases in seed output will ultimately be constrained by threshold high temperatures in the seed maturation year.

Introduction

Historical reconstructions of climate suggest that modern rates of climate warming may be unprecedented in the context of the past 1000 years (Mann *et al.* 1999) and evidence is accumulating that forests are becoming increasingly vulnerable to these climate trends. Temperature stress and drought have been implicated in elevated rates of canopy tree mortality for multiple tree species worldwide (van Mantgem *et al.* 2009; Allen *et al.* 2010). Rising temperatures have also been associated with more frequent wildfire (Littell *et al.* 2009) and severe insect outbreaks (Raffa *et al.* 2008), compounding the effects of heat stress on forest dynamics. As an example, an extreme drought event in the American southwest during the 1950s caused widespread mortality and range contraction of *Pinus ponderosa* and *Pinus edulis* (Allen & Breshears 1998; Macalady & Bugmann 2014). The facility of trees to recolonize sites after disturbance or disperse seed to shifting habitats depends, in part, on their inherent reproductive capacity (Angert *et al.* 2011). Warming temperatures have been associated with depressed seed output in some species (Redmond *et al.* 2012), suggesting that climate change may affect not

only rates of disturbance and tree mortality, but also life history processes that determine the potential of an affected population to recover from disturbance.

The phenology of flowering and seed production has been widely studied for a range of plant species across multiple scales, from the stand level to the level of individual flower (Fenner 1998). Two noteworthy patterns emerge from previous studies that may have significant implications for seedling recruitment following disturbance and adult mortality; seed production is often highly variable from year to year, and individuals of a species are highly synchronized over space and time (Silvertown 1980; Kelly & Sork 2002). Synchronization appears to be a ubiquitous characteristic of the reproductive biology of plant taxa globally (Koenig & Knops 2000), and this synchronization may encompass large geographic areas for some tree species (Koenig & Knops 1998; Schauber *et al.* 2002; Liebhold *et al.* 2004). Reproductive processes that are synchronized and additionally periodic, so that well-defined intervals separate seed crops, are commonly classified as masting or mast seeding processes (Janzen 1976; Kelly 1994, Herrera *et al.* 1998).

The physiological mechanisms determining both variability and synchronization of seed output remain poorly understood (Piovesan & Adams 2001; Rees *et al.* 2002; Smaill *et al.* 2011; Koenig & Knops 2014; Pearse *et al.* 2014). Spatial synchronization of seed production across large areas suggests that climate may be an important driver of seed production via the so-called Moran effect (Hudson & Cattadori 1999). Indeed, high temperatures and / or drought conditions during the period of reproductive bud initiation have frequently been correlated with elevated seed output (Daubenmire 1960; Woodward *et al.* 1994; Houle 1999; Piovesan & Adams 2001; Selås *et al.* 2002; Schauber *et al.* 2002; Roland *et al.* 2014). Experimental treatments in nursery settings have also demonstrated enhanced reproductive response to drought or heat stress in

some species (Holmsgaard & Olsen 1966; Ross 1985). Duff & Nolan (1958) hypothesized that stress-induced seed production may be related to within-plant competition for finite resources. Specifically, environmental conditions that depress vegetative growth early in the growing season result in enhanced initiation and development of ovulate cone structures in late summer. This hypothesis is supported by observations that large seed crops are dependent on the successful initiation of reproductive buds and that high failure rates in the initiation of bud primordia are common (Forcella 1981, Harrison & Owens 1983; Owens 1995).

An alternate hypothesis gaining empirical support involves history and antecedent processes. Previous studies have identified relationships between climate variation in years preceding reproductive bud initiation and subsequent levels of seed output (Woodward *et al.* 1994; Piovesan & Adams 2001; Richardson *et al.* 2005; Roland *et al.* 2014). Climate may affect external resource supplies that are essential for the synthesis of reproductive tissue. For example, Smaill *et al.* (2011) identified correlations between seed abundance and climate factors in years preceding reproductive bud initiation that putatively increase rates of nitrogen mineralization in soils.

The objective of this study is to explore long term relationships between climate and the reproductive biology of *Picea engelmannii* Parry ex Engelm. (Engelmann spruce) in subalpine forests of the Rocky Mountains in North America. These forests provide critical ecosystem services and are likely to experience rapid ecological changes due to accelerated warming rates relative to lower elevation regions (Pepin *et al.* 2015). We examined a 40-year record of seed abundance from a subalpine forest in central Colorado for evidence of masting behavior, trends in seed production over time, and potential tradeoffs between tree growth and reproductive effort. The reproductive cycle in *P. engelmannii* is a complex process that spans multiple years

(Owens & Blake 1985). Seeds that mature and are dispersed in a given (current) year are initiated in late summer of the preceding year. Non-linear regression models were constructed to quantify the importance of climate factors on seed production across all phases of this reproductive cycle. Model selection and information theory were used to evaluate two main hypotheses: (1) reproductive bud development is stress induced, following Duff & Nolan (1958); (2) seed production depends on internal plant resources, such as carbohydrate or nutrient reserves, acquired in years preceding seed bud initiation or seed maturation. These hypotheses are not strictly independent as environmental stress during the spring season of the bud initiation year could influence seed production through either of these pathways.

Materials and methods

Study Site

The study site is located within Fraser Experimental Forest (39° 51' N, 105° 55' W) in the Rocky Mountains of central Colorado. Fraser is a dedicated research area managed by the United States Forest Service (Alexander & Watkins 1977). Thirteen 0.16 ha seed collection plots were established between 1968 and 1970 in closed canopy, high elevation forest (Alexander *et al.* 1982). Seed plots span an elevation gradient of 670 m and are separated by horizontal distances ranging from 159 to 8420 m. The uppermost plot occurs near treeline at ~3500 m. Mature *P. engelmannii* and *Abies lasiocarpa* predominate across all sites with minor components of *Pinus contorta* var. *latifolia* occurring at lower elevations. Increment core samples indicate that tree ages range from 200 to 400 years. Climate is characterized by cold temperatures, short growing seasons and high snowfall. Mean annual temperature during the 40-year study period was ~1.6 °C. Mean annual precipitation increases with elevation, ranging from 574 mm yr⁻¹ at 2770 m to

752 mm yr⁻¹ at 3230 m. Precipitation is relatively evenly distributed across seasons, but nearly two thirds of annual total precipitation falls as snow between the months of October and May.

Seed collection and growth increment sampling

Ten wire mesh seed traps (0.093 m² in area) were randomly located within each of the 13 plots. Trap locations have remained constant for the length of the study. Seeds were collected from traps once per year following snowmelt in the spring of the year after seed maturation and release from cones. Seed counts and viability were determined for *P. engelmannii* only. Heights and diameters of all plot trees with diameters ≥ 10 cm (at 1.37 m ground height) were measured at approximately 10 year intervals. Stand basal area (*BA*) in m² per hectare was computed for each plot and species based on diameter measurements. Tree diameters and *BA* for non-measurement years was interpolated using linear regression.

We collected tree core samples in the summer of 2011 to determine long term variability in annual radial growth. Approximately 15 canopy trees were sampled in each of the 13 seed plots. We subjectively selected dominant canopy trees proximate to seed trap locations. A minimum of two cores were extracted from every sample tree from opposite sides of the stem, parallel to the slope contour and within 30 cm of the root crown. Cores were bonded to wooden core mounts, surfaced using progressively finer grades of sandpaper until tracheid cells were clearly visible under magnification and cross-dated using skeleton plots to ensure correct ring dates with annual resolution (Speer 2010). We then measured all ring widths in each core to a precision of 0.001 mm using a Velmex measuring system with an A40 UniSlide. Ring widths were tested for measurement or dating errors using COFECHA (Grissino-Mayer 2001). Approximately 400 cores were processed and measured.

Climate analyses

We analyzed trends in climate based on standardized climate records acquired from two meteorological stations located at 2770 and 3230 m. These two stations were selected from among a complex of stations at Fraser because their associated climate records were essentially complete for the length of the study. We aggregated the daily time series of temperature and precipitation to monthly, seasonal, and annual values after first inspecting records for missing and extreme values. Details regarding climate data processing are described in the Appendix. Temporal trends in climate were examined using linear regression (McGuire *et al.* 2012).

We also used available station data to evaluate and compare two gridded climate datasets, PRISM (Daly *et al.* 2008) and TopoWx (Oyler *et al.* 2014). Based on goodness of fit (GOF) measures, TopoWx temperature and PRISM precipitation data were used in all modeling analyses (see Appendix S1.1 in Appendix).

Seed production analyses

We first examined the 13 chronologies of seed data for long term trends in seed production and evidence of masting behavior, including periodicity, bimodality, and spatial synchronization among plots. We first converted raw counts of total seed per trap for 10 traps in each of 13 plots to estimates of annual mean seed abundance per m² ground area in each plot. These density estimates of seed output were used in all analyses unless otherwise noted. We analyzed long term trends in seed abundance using general linear models with autocorrelation structures (Richardson *et al.* 2005). Linear methods were used to provide parsimonious fits to trends visually evident in scatterplots. Year and elevation were included as predictors.

We generated descriptive statistics and histograms to characterize the distributions of seed density data and identify potential periodic or bimodal behavior related to masting

processes. Autocorrelation functions (ACF) were also computed to test for serial correlation related to temporal trends or negative lagged effects related to the costs of reproduction (Kelly & Sork 2002; Knops *et al.* 2007). Spatial synchrony in seed production among plots was evaluated using Pearson product-moment correlations and correlograms. Preliminary trend analyses suggested that the time series of seed abundance had significant temporal structure and therefore violated assumptions of a purely random processes; specifically, that observations are mutually independent and identically distributed (Chatfield 2004). The Augmented Dickey-Fuller test also revealed statistically significant correlations between the mean and variance within each series, indicating non-stationary processes. Temporal structure or common long term trends related to broad-scale contemporaneous processes such as climate warming may cause spurious correlations among plots and obfuscate tests of spatial synchrony (Liebhold *et al.* 2004). However, data transformations and autoregressive modeling to remove trends may inadvertently dampen high frequency chronology variance related to masting processes or reproductive variability (Bjørnstad *et al.* 1999), consequently removing part of the signal of interest. We, therefore, evaluated synchrony among plots using two alternate data sets: untransformed seed rain data scaled by the basal area of spruce in each plot, and detrended, white noise residuals from a first order autoregressive moving average (ARMA) model. Before detrending, seed counts from each plot were log transformed to stabilize variances (Chatfield 2004). Matrices of pairwise plot correlation coefficients were calculated for each data set and non-parametric spline correlograms with bootstrapped confidence envelopes were computed to evaluate synchrony as a function of distance (Bjørnstad & Falck 2001).

Statistical models used to determine the climate drivers of seed rain

We constructed the following independent, non-linear regression models to investigate the role of climate across all phases of the reproductive cycle of *P. engelmannii*: (1) a maturation year model tested climate effects in the year that seeds mature and are dispersed; (2) a bud initiation model tested environmental effects during the year of reproductive bud initiation (one year prior to seed maturation); (3) a priming year model evaluated the importance of antecedent climate conditions (two years prior to seed maturation). A full model integrated the effects of climate across all years. Implicit in these models are tests of the two alternate hypotheses discussed in the introduction; specifically that environmental stress in the initiation year leads to tradeoffs and enhanced initiation of reproductive buds (Duff & Nolan 1958), and alternately, that antecedent climate conditions influence internal plant resources available for seed development.

We tested the effects of alternate climate predictors on seed rain in each model including average temperature and total precipitation for annual and seasonal (spring and summer) periods. Seasons were defined according to 3 month intervals beginning with December of the previous year. A period of vegetative shoot elongation (April to June; Harrison & Owens 1983) was also defined to facilitate tests of Duff & Nolan's (1958) hypothesis. We normalized or scaled individual climate variables by the corresponding overall mean of each site based on the assumption that seed production depends on relative variations in temperature and precipitation rather than absolute levels. This scaling procedure generates dimensionless indices of climate with unit means.

To explicitly evaluate the effect of tree growth on the development of reproductive buds during the bud initiation year, we used an index of growth as an additional predictor variable in the bud initiation model. Plot specific growth indices were quantified from ring width

measurements. Ring widths were first standardized using traditional dendrochronological methods, which included a power transformation to stabilize ring width variance (Cook & Peters 1997) and the computation of residuals from a fitted cubic spline function (50% cutoff frequency of 32 years) and autoregressive model to remove long term size and age related trends. Residuals were combined into chronologies or indices of radial growth for each site using a biweight robust mean, which minimizes effects of extreme values (Cook & Kairiukstis 1990). Standardization analyses were performed in ARSTAN (Cook 1985).

We used maximum likelihood methods in the construction of the regression models. The response variable for all models was mean annual seed abundance per square meter of ground area. *BA* of *P. engelmannii* varied significantly among plots and was included as a predictor. We used a mixed model design with a random plot effect. Each analysis required the estimation of 13 site-specific intercept terms (the random effects) and the parameters for at least 3 independent variables or effects:

$$\text{Seed rain} = \text{PotSeed} \times \text{Temperature effect} \times \text{Precipitation effect} \times \text{Basal area}$$

Intercept terms (PotSeed) represent site-specific maximum potential seed abundance produced under optimum climate conditions. Multiplicative predictor variables for the effects are scalar terms constrained to range from 0 to 1 that reduce maximum potential seed rain. We used

Gaussian functions to estimate both *BA* and climate effects:

$$\text{Climate (or BA) effect} = \exp\left[-0.5 \times \left(\frac{X-X_0}{X_1}\right)^2\right]$$

where *X* is the observed climate variable or *BA* for a given period, *X*₀ corresponds to the value of the independent variable at which maximum PotSeed occurs and *X*₁ describes the variance of the term. Gaussian functions are flexible and can fit data distributions that are unimodal, monotonically increasing or monotonically decreasing.

We used simulated annealing (Goffe *et al.* 1994) with 40,000 iterations to solve for maximum likelihood estimates of the regression coefficients. Simulated annealing is a global optimization algorithm that uses an iterative procedure to simultaneously search for parameter values that maximize the likelihood of observing the recorded seed trap counts. Model residuals were approximately normal, but heteroscedastic. Therefore, we used a modified normal probability density function (PDF) to estimate likelihood in which variance is a power function of the mean. The residual (ε_i) for the i^{th} observation becomes

$$\varepsilon_i = \alpha + X_i^\beta$$

where X_i is the predicted value for the i^{th} observation and α and β are estimated by annealing.

Tests for temporal autocorrelation confirmed that residuals were random. Bias and R^2 were used to quantify the GOF of alternate models. Bias represents the difference between the predicted response and the observed data and was quantified from the slope of the regression of observed on predicted seed abundance (Canham *et al.* 2006). Unbiased models will generate unit slopes in this regression. Consistent under-prediction or over-prediction will result in slopes greater or less than 1.0, respectively. Akaike information criterion corrected for small sample size (AIC_c) was used to select the most parsimonious models (Burnham & Anderson 2002). AIC_c provides a quantitative measure of model performance that balances model fit, as measured by log-likelihood, and model complexity, determined by the number of parameters in the model. All analyses were conducted in R (Version 3.2.3, R Core Team 2013). Likelihood models were constructed using the likelihood package version 1.6.

Tree growth analyses

We further explored potential tradeoffs between growth and reproduction using cross-correlation functions. We used the pre-whitened residuals of both radial growth and seed

abundance (methods previously described) in cross-correlation analyses to avoid spurious correlations attributed to temporal autocorrelation.

We also examined the response of tree radial growth to critical climate conditions identified by seed production models as important for the initiation of reproductive buds. We constructed regression models, again in a maximum likelihood framework, with radial growth as the response. These regression models were fitted with raw ring width measurements rather than the pre-whitened residuals for which portions of the climate signal have potential been removed. We incorporated a tree size predictor based on reconstructed diameters to explicitly account for the effects of increasing tree size on ring width:

$$\text{Radial growth} = \text{PotGrowth} \times \text{Temperature effect} \times \text{Precipitation effect} \times \text{Size effect}$$

Regression coefficients were computed using maximum likelihood with simulated annealing per above. We tested alternative climate predictors including lagged effects to identify the most parsimonious model. We hypothesized a direct relationship between growth and climate, and therefore did not normalize climate predictors as with the seed models. Residuals from growth models were approximately normal and had no autocorrelation.

Results

Climate trends

Analyses of instrumental data from Fraser indicate significant positive trends in temperature over the 40-year period of seed data collection (Fig. 1.1). Mean annual *Tmin* and *Tmax* increased by ~1.0 °C from the first half to the latter half of the study period according to paired t tests ($p < 0.001$). Instrumental data show that annual mean temperature in the last decade of the study period exceeded the previous 30-year mean by over 1.0 SD and that six of the warmest years in the 40-year record occurred between 1999 and 2008. Warming trends are

relatively consistent over the elevation range separating climate stations (~460 m). However, significant differences in temperature trends were detected across seasons (Table S1.1).

Maximum warming occurred in spring months for all sites, when rates of temperature change ranged from 0.6 to 1.0 °C / decade. Rates of temperature change were lowest in winter and summer months. No significant trends ($p = 0.1$) in annual or seasonal precipitation were detected.

Temporal and spatial patterns of seed production

Regression models revealed a significant positive trend in seed production of ~ 50 seeds m^{-2} decade⁻¹ for the 40-year study period (Table 1.1; Fig. 1.2). Elevation had a weak and non-significant effect. Independent linear models for the first and latter two decades of the study period suggest that positive trends in seed production began *ca.* 1990, concurrent with trends observed in the instrumental climate data. Positive trends were driven in part by an extreme seeding event in 2006. Increasing tree age over the course of the study is an unlikely driver of observed trends in seed output since mean tree age across all plots based on core samples collected in 2010 was 239 years. Only a few scattered individual trees were younger than 100 years. Forest Service stand inventory data support our age estimates (Alexander *et al.* 1982). In addition, these closed canopy stands were relatively stable over the study period as quantified by periodic censuses conducted by the Forest Service. Tree mortality and recruitment of reproductively mature trees into the canopy were relatively low.

Descriptive statistics (Table 1.2) and histograms (not shown) indicate strongly right-skewed distributions of seed abundance reflecting a prevalence of low seed years interrupted by infrequent episodes of high seed rain. Coefficients of variation (CV) ranged from 1.6 to 3.3, indicating high variability in seed production among years relative to other published data (Kelly

1994). Variability as measured by CV also increased significantly with elevation ($p < 0.001$), although mean seed abundance did not ($p = 0.7$). Time series data similarly reveal variable and irregular seed production patterns over time with notable years of intermediate seed abundance over the 40-year study period. In addition, evidence for bimodality was not observed in histograms or detected by kurtosis estimates, which were strongly positive. Although not definitive indicators of bimodality, large negative values of kurtosis are generally associated with bimodal distributions (DeCarlo 1997). ACFs (Fig. S1.1) indicate the presence of consistent, positive 3rd order autocorrelation across all plots (ranging from 0.01 to 0.42). ACFs also reveal low levels of negative 1st and 2nd order autocorrelation in seed chronologies across all plots (ranging from -0.22 to -0.06; Table 1.2), though most coefficients were non-significant or only marginally significant according to confidence limits (not shown) computed following Salas *et al.* (1980).

An examination of the time series plot of seed production subjectively indicates strong synchrony among sites (Fig. 1.2). Correlation analyses were conducted to quantify the degree of synchrony among sites. As discussed, we compared levels of correlation for the untransformed seed rain data with those using white noise residuals from an autoregressive model. The resulting overall mean correlation between seed plots was 0.88 for untransformed data and 0.86 for model residuals. Nearly equivalent results could be explained by the low levels of temporal autocorrelation present in the original seed series, as autoregressive modeling accounted for only ~5% of the variance in the original seed series. Spatial patterns in synchrony quantified by correlograms were also comparable between the transformed and untransformed seed rain data and illustrate that inter-plot correlation does not decay with distance within the 8-km extent of

the Fraser study area (Fig. 1.3). Similarly, a fitted spline function shows no significant departures from the overall mean synchrony level with distance (Fig. 1.3).

Climate effects on seed rain

The modeling framework used in this study identifies the relative importance of climate variation on seed rain for critical phases of the reproductive cycle. The best models generated predictions with low to moderate levels of bias (Table 1.3), ranging from 0.8 for a relatively poor fitting seed maturation model to 1.2 for the final full model. Therefore, the best full model, with a slope of 1.2, generally under-predicted observed seed abundance, though an examination of residual plots (not shown) reveals that very high seed years were consistently under-predicted and low or zero seed years were generally over-predicted.

The seed maturation model indicates that climate in the year of seed dispersal has a comparatively weak influence on seed abundance. The best seed maturation model explained approximately 14% of the variance in the seed rain data. Model selection using AIC excluded the effect of *BA* of *P. engelmannii* from the final best model. Scatterplots suggest that *BA* is only weakly correlated with seed production during years of high seed output, when large trees and/or dense stands with high biomass of *P. engelmannii* produce disproportionately more seeds (see Table 1.2 for ranges in plot BA over the 40 year study period). The seed maturation model shows that peak seed production only occurs when average summer temperatures in the year of seed maturation are ~10% higher than long term means for a given site (Fig. 1.4). Summer temperatures only slightly colder than normal in the year of seed maturation (~5% below mean levels) lead to low or no seed production. Notably, summer temperatures only varied by ~20% above or below the overall mean of each site within the 40-year study period.

The best bud initiation model, which integrated temperature effects from the seed maturation year (Table 1.3), provided a stronger fit to the seed rain data compared with the seed maturation model alone; R^2 increased to ~ 19% for this composite model. Precipitation during the period of shoot elongation had the strongest effect on seed output. Specifically, low levels of precipitation during the period of shoot growth in the bud initiation year were associated with high seed rain in the subsequent year (Fig. 1.4). Weak evidence for a temperature effect was also detected. Seed rain appears to be maximized when temperatures during shoot elongation are slightly above long-term means (~4% greater). However, shoot period temperature was highly correlated with corresponding precipitation ($r=-0.6$), and ultimately excluded from the final model based on AICc. The positive response to reduced spring precipitation appears, at first, to be consistent with Duff & Nolan's (1958) hypothesis, previously described in the introduction, that early spring drought stress may depress vegetative growth thereby facilitating the enhanced initiation of reproductive buds in late summer. However, the tree growth explanatory variable used in this model shows that seed output actually increases with increasing radial increment (Fig. 1.4). Similarly, cross-correlation functions (Fig. 1.5) show positive associations between tree growth in the initiation year and subsequent seed output for most plots. Tradeoffs between growth and reproduction, expected under Duff & Nolan's (1958) hypothesis, are therefore not evident in this dataset. Furthermore, our models of tree growth revealed, despite a weak climate signal in the tree rings (Table S1.2), a positive rather than negative response in radial growth to low precipitation during the period of shoot elongation (Fig. 1.6). Thus, radial growth and seed output appear to covary due to a congruent positive response to reduced precipitation in spring months. These results suggest that high radial growth in the bud initiation year, associated with

low spring precipitation, may reflect favorable conditions for carbon or nutrient gain that may facilitate enhanced seed development and maturation in the subsequent year.

The best priming year model, which also integrates temperature effects from the maturation year (Table 1.3), indicates that climate conditions two years prior to seed maturation have strong effects on seed rain, explaining ~40% of the variance in the fitted data. Seed rain appears to be maximized when spring precipitation two years prior to seed dispersal is ~50% below long-term means. Again, it appears that reduced spring precipitation is associated with the accumulation of plant reserves that subsequently enhance seed output.

Our best full model, which integrates the previous 3 sub-models, produced the strongest fit to the observational data based on AICc suggesting that conditions in all years of the reproductive cycle are cumulatively important for seed production, and that favorable conditions in any one year alone are insufficient for the production of abundant seed (Table 1.3).

Discussion

Reproductive dynamics

The reproductive biology of *P. engelmannii* at Fraser does not strictly fit into the classical masting concept as defined by Kelly (1994). Seed production was highly variable across years and strongly synchronized among sites, but mast events could not be unambiguously identified. Instead of a bimodal distribution of seed abundance, seed output varied continuously over time, with notable, intermediate levels of seed abundance evident (Fig. 1.2). These patterns agree with results from Koenig & Knops (2000), who found minimal evidence for bimodality in a review of seed production data for a range of northern hemisphere tree species. However, we did identify evidence, based on ACFs, for a weak periodic structure, reflecting at least moderate increases in seed output over 3 year intervals. Interestingly, Woodward *et al.* (1994) also detected a 3-year

cycle in the seed output of *A. lasiocarpa*, a conifer that regularly co-occurs with *P. engelmannii* in subalpine forests of North America.

Climate effects on seed rain

A primary goal of this study was to develop parsimonious mechanistic models of seed production that could be used to parameterize fecundity in a simulation model such as SORTIE (Pacala *et al.* 1996). We were more interested in understanding general mechanisms using readily interpretable analyses rather than modeling seed production at Fraser with the highest degree of fidelity to the observed seed rain record. We, therefore, purposefully avoided constructing overly complex models that might improve model fit at the expense of model generality. Similarly, we minimized intensive data management, such as log-transformations, which are commonly applied to seed count data (Koenig & Knops 2000), that might improve model fit but inhibit the interpretability of model results. Nevertheless, the best models fitted with raw seed data achieved a reasonably strong fit, explaining ~40% of the variability in observed seed abundance.

Model results do not unambiguously support the stress / tradeoff hypothesis of Duff & Nolan (1958). Low spring precipitation in the initiation year was found to be correlated with subsequent high seed rain a year later, as predicted by this hypothesis. However, evidence for tradeoffs between growth and reproduction, a critical element of this hypothesis, was lacking. Rather, diameter growth and seed production co-varied (Figs 4 and 5), due to coincident positive responses to low spring precipitation. In addition, average summer temperatures in the initiation year had no significant effect on either seed production or diameter growth. We hypothesize, therefore, that elevated spring precipitation, which predominantly occurs as snow at Fraser, reduces growing season length, impacting both diameter growth and late summer reproductive

bud initiation (Woodward *et al.* 1994). Deep, persistent snowpacks associated with high spring precipitation may persist well into the growing season at these elevations, maintaining low soil temperatures and consequently limiting plant physiological processes, even as air temperatures warm (Fritts 1976). Thus, evidence for drought or heat stress limiting growth processes and thereby facilitating the initiation and development of reproductive buds is limited.

A basic tenet of life history theory is that internal plant resources are finite and that high reproductive effort reduces nutrient or carbon reserves at the expense of other processes (Reznick 1985). Widespread negative correlations between radial growth and reproduction in trees support this assumption (Koenig & Knops 1998). The lack of evidence for visible tradeoffs in this study is not unprecedented, however (Speer 2001; Knops *et al.* 2007; Żywiec & Zielonka 2013). Our failure to identify expected tradeoffs may be attributed to within plant resource variability. Costs associated with reproductive bud development may be concentrated within branches and shoots, which we did not measure, rather than in the main stem (Hoch 2005; Sánchez-Humanes *et al.* 2011).

More evident is the influence of priming year climate on subsequent levels of seed rain. Among all phases of the reproductive cycle, climate conditions two years prior to seed fall had the strongest effects on indices of model fit. Spring precipitation that was ~50% below mean levels during the priming year correlated with high seed rain two years later. In support of these model results, negative, albeit weak, lagged autocorrelation coefficients suggest that reproductive output depends on the restoration of plant resources depleted by previous reproductive effort. We hypothesize once again that spring snowfall and snowpack depth affect growing season length, thereby limiting either nutrient acquisition from soils (Smaill *et al.* 2011) or net carbon gain through photosynthesis. Notably, Hoch *et al.* (2013) found that seed

production in oak and beech was not dependent on stored carbon reserves. Similarly, Richardson *et al.* (2005) found, using model selection, that net carbon in the priming year was not an important predictor of seed output for beech trees in New Zealand. These findings suggest that nutrient reserves, rather than carbon, may be determining reproductive dynamics in some species.

Model results also indicate that warm temperatures in the year of seed maturation are associated with high seed rain, although this is the weakest effect. The seed maturation model reveals that high seed rain is dependent on a relatively narrow range of concurrent average summer temperatures. Specifically, high seed rain is associated with summer temperatures that exceed long term means by between ~10 and 20%. Interestingly, summer temperatures that exceed this range are correlated with decreasing seed rain. It is generally assumed that growth processes in trees at high elevations are limited by temperature rather than precipitation (Brown & Shepperd 1995; Salzer & Kipfmüller 2005). Hypotheses explaining temperature limitation in high elevation trees include insufficient net photosynthesis or a direct thermal effect on meristematic activity (Hoch & Körner 2003). Elevated summer temperatures may, therefore, result in enhanced rates of tissue synthesis, including cone and seed development. Richardson *et al.* (2005) also found positive associations between warm temperatures, carbon availability and seed output in the maturation year. In contrast, Roland *et al.* (2014) identified negative effects associated with high summer temperatures on seed output in *Picea glauca*, which they attributed to the effects of drought stress on tree physiology. We may likewise be observing a negative moisture stress effect at this site as temperatures warm beyond a threshold level.

There is some evidence that *P. engelmannii* has acclimated to local climate variation among sites. The congruent Gaussian response to relative summer temperature previously

discussed, with seed rain maximized by summer temperatures approximately 10% above local site means, suggests that trees at different sites may have adapted to local climate regimes. Recall that climate varies substantially across the almost 700 m elevation gradient; average annual temperature decreased by over 2°C, mean annual precipitation increased by over 120 mm (mostly as snow), and growing season length, measured by the number of days with *Tmin* greater than 5°C, declined by an average of 12 days from valley bottom to upper elevation plots. In spite of this relatively steep climate gradient, statistically significant differences in mean seed rain among sites were not observed.

Trends in seed output

Significant temporal trends were detected for both temperature and seed production at Fraser. Analyses of instrumental data revealed significant positive trends in both *Tmin* and *Tmax*, particularly since the mid 1990s (Fig. 1.1). Concurrently, seed abundance has increased at Fraser over the latter half of the study period according to fitted multiple regression models (Fig. 1.2). Trends in both temperature and seed production were consistent across elevations, contrasting the positive elevation-dependent trends in seed production identified by Richardson *et al.* (2005) for beech. Positive trends associated with *P. engelmannii* are attributed to increases in both intermediate and large seed years. Particularly high seed rain was observed in 2002, 2003 and 2006, approximately corresponding to a period of severe drought and high temperatures across Colorado (Pielke *et al.* 2005). Climate records from Fraser indicate that 3 of the driest springs occurred in 2002, 2004, and 2006 and that mean summer temperatures in 2002, 2003, and 2006 were among the highest in the 40-year study period. Thus, anomalous climate conditions that were favorable for seed production resulted in elevated seed abundance during the most recent decade of the study period.

A recent model that uses inter-annual temperature variation to quantify seed output for a range of taxa predicts that global climate change will have negligible effects on overall patterns of seed production (Kelly *et al.* 2013). Trends in seed abundance and associated climate at Fraser appear to contradict this prediction. Significant climate driven changes in reproductive effort have also been documented for other tree species (Richardson *et al.* 2005; Redmond *et al.* 2012). Increases in tree age or changes in stand densities are unlikely drivers of observed increases in seed abundance at Fraser since all plots were comprised of mature, stable, closed-canopy forests with mean stand ages of approximately 200 years at the start of the study in 1970. Previous research suggests that seed production in *P. engelmannii* peaks in mature trees between the ages of 100 and 250 years (Alexander 1974). In addition, stand basal area was excluded as a predictor from the most parsimonious models of seed production indicating that changes in tree size or possible increases in the number of reproductively mature individuals over time were not significant factors influencing trends in seed output.

No system can sustain unlimited growth, and we expect that current trends in seed output at Fraser will be constrained by inherent physiological limits or external processes. Indeed, our model results identify a potential threshold temperature level in the summer of seed maturation, above which seed output is predicted to decline (Fig. 1.4). Temperature increases in the most recent decade already appear to be bumping up against this threshold, which is ~20% above long term mean summer temperature for a site. Constraining factors may include elevated respiration rates associated with higher temperatures that subsequently reduce plant carbon reserves. Alternatively, the compounding effects of reduced snowpack depth, earlier snowmelt and warmer summer temperatures may result in drought stress and an effective shortening of growing season length. In a related trend, late summer drought stress has been identified as a

potential cause for the weakening of the growth response in high elevation and northern latitude tree species to warming temperatures over recent decades (D'Arrigo *et al.* 2008).

Changes in the reproductive biology of *P. engelmannii* may have a range of impacts affecting the composition, functioning and trajectories of change in subalpine forests of the Rocky Mountains. Differential responses among tree species to climate change may alter the availability of seed propagules for regeneration by sympatric species following disturbance and thus affect the composition of future forests. For example, limited evidence exists that reproduction in *A. lasiocarpa* may respond negatively to increasing temperatures, potentially due to a requirement for cool summer temperatures during the priming year (Woodward *et al.* 1994). Thus, reproduction in *A. lasiocarpa* and *P. engelmannii*, which commonly co-occur in this region, may have inverse responses to climate change. Changes in seed production may also affect interconnected food webs through complex, poorly understood pathways (Ostfeld *et al.* 1996). Increases in seed abundance may directly benefit seed consumers, such as pine squirrels (*Tamiasciurus hudsonicus fremonti*), insects and other small mammals (Alexander 1974). However, feedback loops are also possible. More frequent and larger seed crops may effectively smooth reproductive variability and consequently compromise any evolved benefits of predator satiation, a postulated mechanism for the regulation of seed consumer populations that depends on synchronized, irregular seed output (Silvertown 1980). Long term population fitness in *P. engelmannii* may thereby be negatively impacted. On the other hand, elevated seed rain may enhance the resiliency of *P. engelmannii* populations in the face of increasing frequencies of fire and insect related tree mortality. Seeds from this species suffer high predation losses, germinate quickly under a range of conditions, and have a limited period of viability after release from cones (Johnson & Fryer 1996). Thus, in the absence of a persistent, viable seed bank, the

reproductive success of *P. engelmannii* may depend on the availability and dispersal of adequate seed from surviving cone-bearing trees, which, according to these analyses, may be moderately enhanced by current warming trends in climate.

Data Accessibility

Time series of seed abundance and tree ring width data: USDA Forest Service Research Data Archive doi: <http://dx.doi.org/10.2737/RDS-2016-0004> (Buechling *et al.* 2016)

Tables

Table 1.1. Temporal and altitudinal effects on seed production from general linear models with autocorrelation structures (lag effect).

Time Period	Variable	Effect Size (seed/m ²)
1970 – 1989	Year	0.95
	Elevation	0.01
	Lag Effect	-0.15*
1990 - 2010	Year	10.69*
	Elevation	0.18
	Lag Effect	-0.13*
1970 – 2010	Year	5.31***
	Elevation	0.09
	Lag Effect	-0.12**

Significance: * $p < 0.05$; ** $p < 0.01$; *** $p < 0.001$

Table 1.2. Statistics describing the distribution of annual seed rain (seed/m²) over the 40-year study period for 13 study sites. Confidence intervals (CI) for the CV and the first order autocorrelation coefficient (ACF.1) were computed using bootstrap sampling. Sites are designated by elevation and are ordered from low to high elevation. Ranges in stand basal area (BA) for all plots were interpolated from Forest Service inventory data.

Site Elevation (m)	BA (m ² /ha)	Mean	Median	Max	Min	SD	b2 ¹	CV	CI 95% (CV)	ACF.1	CI 95% (ACF.1)
2800	28.3, 34.2	132	34	1373	0	250	16.31	1.9	1.42, 2.66	-0.19	-0.40, 0.17
2807	37.4, 38.9	73	18	1027	0	168	26.68	2.29	1.66, 3.66	-0.13	-0.39, 0.08
2887	46.4, 54.8	34	9	232	0	56	7.26	1.63	1.29, 2.06	-0.22	-0.69, 0.14
2908	68.2, 73.3	56	17	816	0	134	26.7	2.39	1.72, 3.72	-0.12	-0.45, 0.02
2919	53.7, 61.6	187	61	1892	0	346	15.84	1.85	1.40, 2.57	-0.19	-0.61, 0.10
2964	36, 41.6	92	25	1163	0	194	23.97	2.1	1.52, 3.26	-0.12	-0.45, 0.02
2990	31.3, 35.1	129	36	1732	1	285	25.8	2.21	1.54, 3.40	-0.12	-0.45, 0.02
3038	32.4, 40.9	68	13	719	0	153	15.02	2.26	1.63, 3.01	-0.07	-0.35, 0.13
3054	35.4, 37.2	96	26	1267	0	213	23.7	2.21	1.62, 3.38	-0.13	-0.45, 0.01
3138	20.1, 26.3	70	15	1097	0	180	27.15	2.56	1.88, 4.03	-0.08	-0.36, 0.09
3322	20.4, 25.7	113	18	2041	0	325	31.79	2.87	2.06, 4.79	-0.09	-0.35, 0.01
3385	38.7, 43.6	156	19	3011	0	480	32.2	3.07	2.27, 5.21	-0.06	-0.25, 0.12
3474	42.2, 49.6	160	16	3363	0	536	32.76	3.36	2.50, 5.51	-0.06	-0.22, 0.14

¹ kurtosis = $\frac{(\sum(Xi-\bar{X})^4 / n)}{(\sum(Xi-\bar{X})^2 / n)^2}$ (DeCarlo 1997)

Table 1.3. Goodness of fit and model comparison measures for models of seed rain. Models test climate effects on seed output across 3 years: the seed maturation year; the bud initiation year, one year prior to seed maturation; and the priming year, two years prior to seed maturation. Full models integrate climate effects in all 3 years. Statistics are shown for the most parsimonious models selected by AICc (corrected for small sample size).

Model	Covariates	n	NP ¹	AICc	R ²	Bias
Seed Maturation	Tave ³ summer lag0	533	17	6289.5	0.140	0.81
Bud Initiation	Tave summer lag0	533	19	6253.6	0.189	0.91
Bud Initiation+Growth	ppt ² shoot period lag1	533	21	6216.9	0.191	0.88
	Tave summer lag0					
Priming	ppt shoot period lag1	533	19	6160.0	0.396	1.15
	radial growth lag1					
	Tave summer lag0					
Full	ppt spring lag2	533	21	6114.0	0.355	1.16
	Tave summer lag0					
	ppt shoot period lag1					
	ppt spring lag2					

¹ number of parameters

² precipitation

³ average temperature

Figures

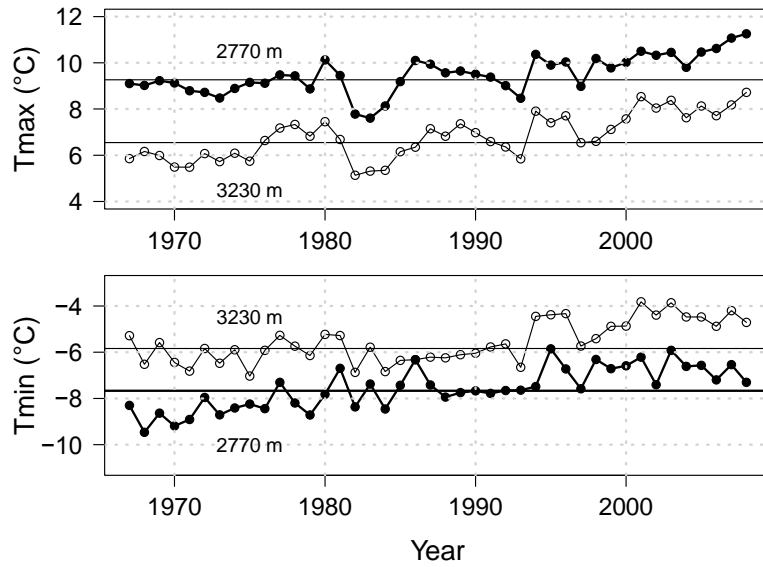


Figure 1.1. Time series of mean annual T_{max} and T_{min} at high elevation (3230 m) and low elevation (2770 m) climate stations at Fraser. Horizontal lines represent year 1970 to 2000 means (normals) and highlight generally enhanced warming rates at both elevations since the mid 1990s. These instrumental data indicate ubiquitous temperature inversions caused by cold air drainage, a widespread phenomenon in mountainous terrain (Nolan Doesken, Colorado State Climatologist, personal communication).

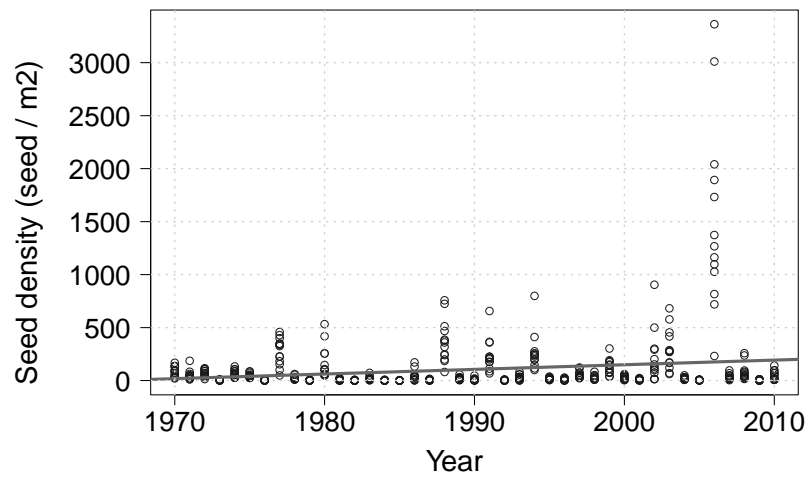


Figure 1.2. Time series of seed abundance per m² of ground area for 13 study sites. Synchronicity among sites for both high, low and intermediate levels of seed production is evident. The slope of the fitted regression line reflects an overall positive trend in seed output over the course of the study (~ 50 seeds/m²/decade).

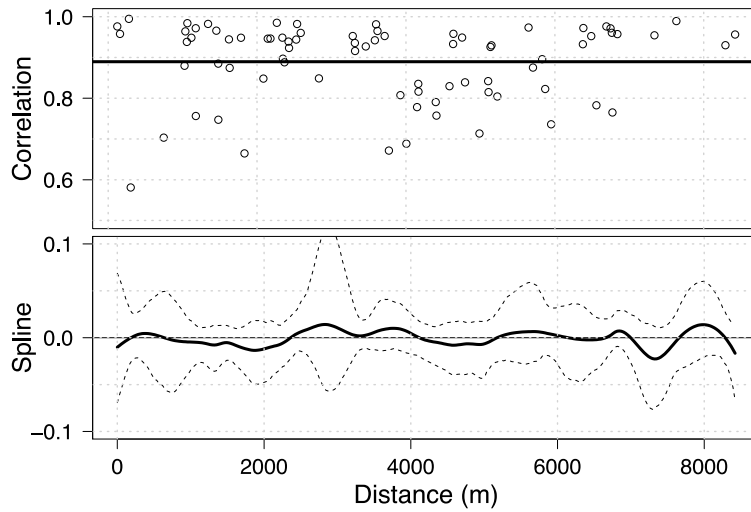


Figure 1.3. Correlograms computed from untransformed seed rain data illustrating spatial patterns of synchrony in rates of seed production. Upper figure shows all pairwise plot correlations plotted as a function of separating distance. The black horizontal line indicates the overall mean correlation (0.88). The spline correlogram in the lower plot is a continuous function estimating covariance as a function of distance separating seed-fall plots with corresponding confidence limits derived from bootstrap resampling (Bjørnstad & Falck 2001). The spline correlogram is centered so that the zero reference line denotes the overall mean level of synchrony across the study area.

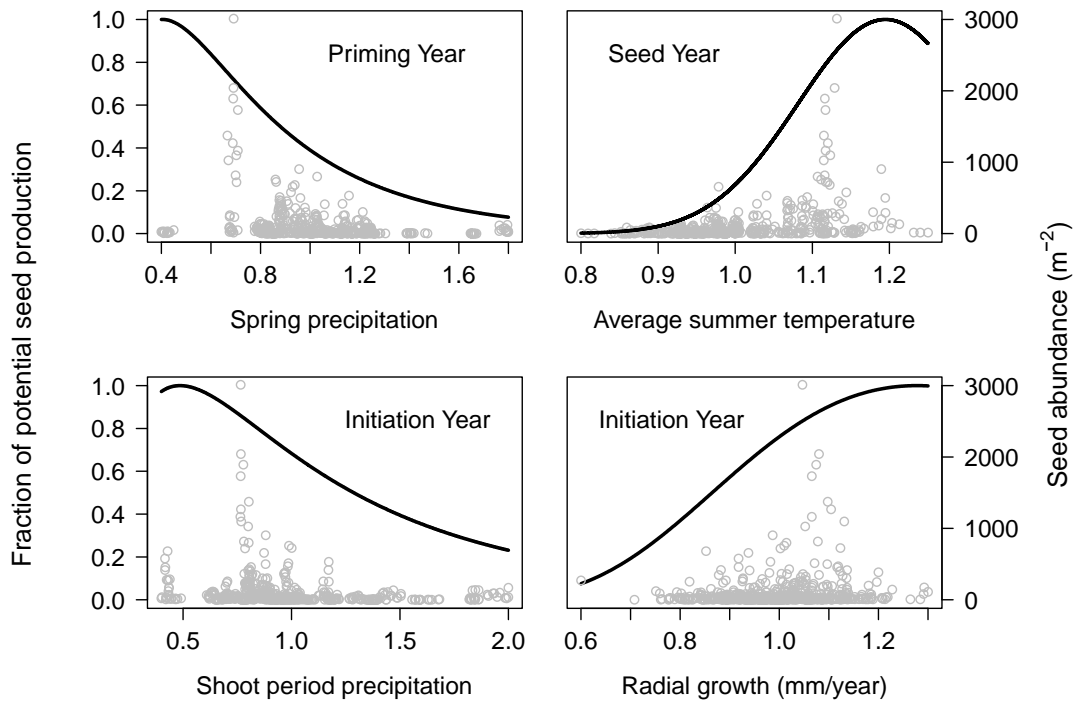


Figure 1.4. Fraction of modeled potential seed production (solid curves) and observed seed abundance per square meter of ground area (open circles) as a function of the 4 main predictors from the most parsimonious full model of seed production. Maximum potential seed output occurs when predictors are at their optimum levels for seed production. Each panel independently identifies the fractional decrease in potential seed output caused by the associated effect when all other predictors are held constant. Panels are arranged from upper left to lower right to correspond with the strength of the corresponding sub-model, based on AICc scores. Climate variables were normalized by the corresponding long-term mean of each site to produce dimensionless indices of climate. Climate values therefore indicate departures from the corresponding means (1.0) of each site. For example, spring precipitation values of 1.2 indicate that precipitation levels were 20% above long term means. Standardized radial growth values derived from ring width measurements similarly have unit means (see methods in text).

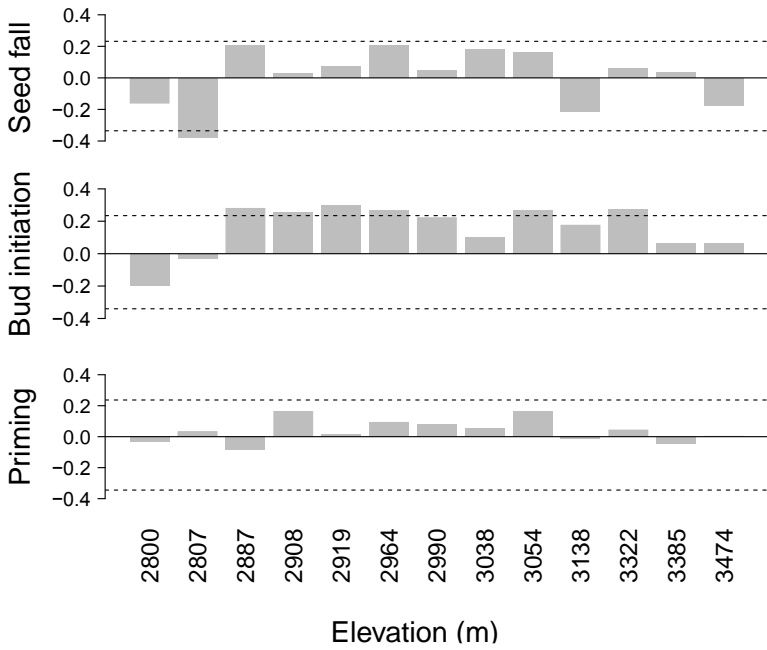


Figure 1.5. Cross-correlation functions between standardized radial growth indices and pre-whitened residuals of seed abundance for three periods in the reproductive cycle. Autoregressive models were used to generate pre-whitened residuals. Dashed lines delimit 95% confidence limits.

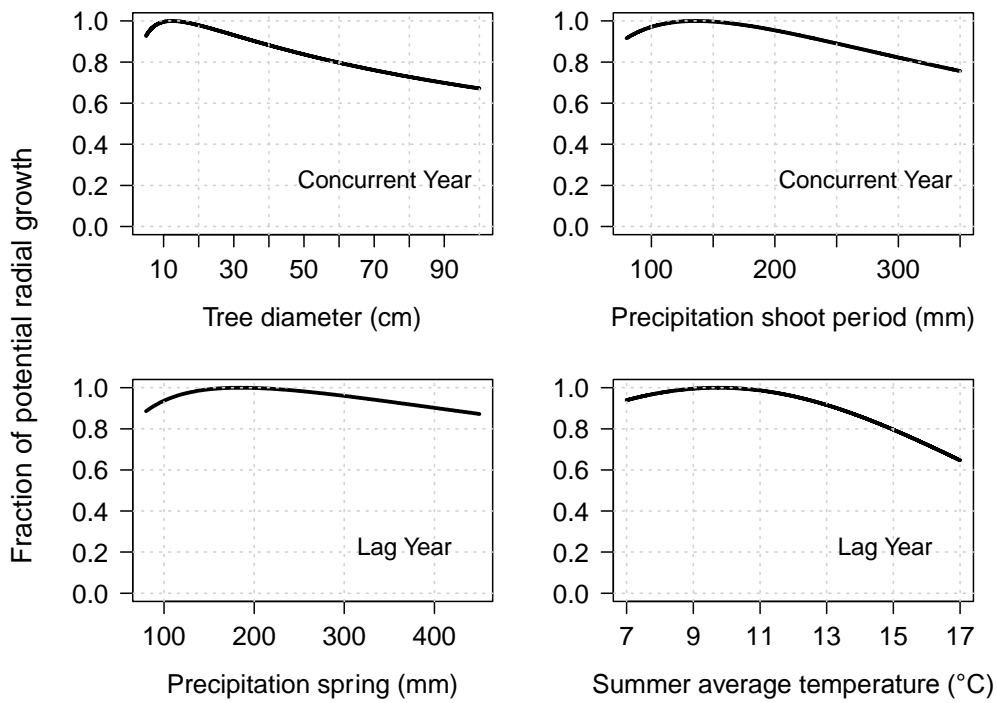


Figure 1.6. Fraction of maximum potential radial growth as a function of climate and tree size predictors from the most parsimonious likelihood model. Each panel independently identifies the fractional decrease in potential radial growth caused by the associated effect when other predictors are held constant. Climate predictors were not transformed. The upper two panels represent effects in the year concurrent with tree growth, while the lower two panels indicate effects in the year preceding ring width formation. Tree diameter was included to account for the effects of size and age on radial growth rates.

REFERENCES

- Alexander, R.R. (1974) Silviculture of central and southern Rocky Mountain forests: a summary of the status of our knowledge. Rocky Mountain Forest and Range Experiment Station, Fort Collins, CO. *USDA Forest Service Research Paper*, **RM-121**, 1-78.
- Alexander, R.R. & Watkins, R.K. (1977) The Fraser Experimental Forest, Colorado. Rocky Mountain Forest and Range Experiment Station, Fort Collins, CO. *USDA Forest Service General Technical Report*, **RM-40**, 1-35.
- Alexander, R.R., Watkins, R.K. & Edminster, C.B. (1982) Engelmann spruce seed production on the Fraser Experimental Forest, Colorado. Rocky Mountain Forest and Range Experiment Station, Fort Collins, CO. *USDA Forest Service Research Note*, **RM-419**, 1-6.
- Allen, C.D. & Breshears, D.D. (1998) Drought-induced shift of a forest–woodland ecotone: rapid landscape response to climate variation. *Proceedings of the National Academy of Sciences*, **95**, 14839-14842.
- Allen, C.D., Macalady, A.K., Chenchouni, H., Bachelet, D., McDowell, N., Vennetier, M., Kitzberger, T., Rigling, A., Breshears, D.D., Hogg, E.H., Gonzalez, P., Fensham, R., Zhang, Z., Castro, J., Demidova, N., Lim, J.H., Allard, G., Running, S.W., Semerci, A. & Cobb, N. (2010) A global overview of drought and heat-induced tree mortality reveals emerging climate change risks for forests. *Forest Ecology and Management*, **259**, 660-684.
- Allen, R.B., Mason, N.W., Richardson, S.J. & Platt, K.H. (2012) Synchronicity, periodicity and bimodality in inter-annual tree seed production along an elevation gradient. *Oikos*, **121**, 367-376.
- Angert, A.L., Crozier, L.G., Rissler, L.J., Gilman, S.E., Tewksbury, J.J. & Chunco, A.J. (2011) Do species' traits predict recent shifts at expanding range edges?. *Ecology Letters*, **14**, 677-689.
- Bjørnstad, O.N. & Falck, W. (2001) Nonparametric spatial covariance functions: estimation and testing. *Environmental and Ecological Statistics*, **8**, 53-70.
- Bjørnstad, O.N., Ims, R.A. & Lambin, X. (1999) Spatial population dynamics: analyzing patterns and processes of population synchrony. *Trends in Ecology & Evolution*, **14**, 427-432.
- Brown, P.M. & Shepperd, W.D. (1995) Engelmann spruce tree-ring chronologies from Fraser Experimental Forest, Colorado: Potential for a long-term temperature reconstruction in the Central Rocky Mountains. *Interior West global change workshop* (ed R.W. Tinus), p 23-26. U.S. Department of Agriculture, Forest Service, Rocky Mountain forest and Range Experiment Station, Fort Collins, CO, USA.

- Buechling, A., Martin, P.H., Canham, C.D., Shepperd, W.D., Battaglia, M.A. & Asherin, L. (2016) Seed and ring width data from 'Climate drivers of seed production in *Picea engelmannii* and response to warming temperatures in the southern Rocky Mountains'. Forest Service Research Data Archive, Fort Collins, CO, <http://dx.doi.org/10.2737/RDS-2016-0004>.
- Burnham, K.P. & Anderson, D.R. (2002) *Model Selection and Multimodel Inference: A Practical Information-theoretic Approach*, 2nd edn. Springer-Verlag, New York, NJ, USA.
- Canham, C.D., Papaik, M.J., Uriarte, M., McWilliams, W.H., Jenkins, J.C. & Twery, M.J. (2006) Neighborhood analyses of canopy tree competition along environmental gradients in New England forests. *Ecological Applications*, **16**, 540-554.
- Chatfield, C. (2004) *The Analysis of Time Series: An Introduction*. 6th edn. Chapman & Hall / CRC, New York, NY, USA.
- Cook, E.R. (1985) A time series analysis approach to tree-ring standardization. PhD thesis, University of Arizona, Tucson, AZ, USA.
- Cook, E.R. & Peters, K. (1997) Calculating unbiased tree-ring indices for the study of climatic and environmental change. *The Holocene*, **7**, 361-370.
- Cook, E.R. & Kairiukstis, L.A. (1990) Estimation of the mean chronology. *Methods of Dendrochronology: Applications in the Environmental Sciences* (eds E.R. Cook & L.A. Kairiukstis), pp. 123–132. Kluwer Academic Publishers, Boston, MA, USA.
- Daubenmire, R. (1960) A seven-year study of cone production as related to xylem layers and temperature in *Pinus ponderosa*. *American Midland Naturalist*, **64**, 187-193.
- Daly, C., Halbleib, M., Smith, J.I., Gibson, W.P., Doggett, M.K., Taylor, G.H., Curtis, J. & Pasteris, P.P. (2008) Physiographically sensitive mapping of climatological temperature and precipitation across the conterminous United States. *International journal of climatology*, **28**, 2031-2064.
- D'Arrigo, R., Wilson, R., Liepert, B. & Cherubini, P. (2008) On the 'divergence problem' in northern forests: a review of the tree-ring evidence and possible causes. *Global and Planetary Change*, **60**, 289-305.
- DeCarlo, L.T. (1997) On the meaning and use of kurtosis. *Psychological methods*, **2**(3), 292-307.
- Duff, G.H. & Nolan, N.J. (1958) Growth and morphogenesis in the Canadian Forest species: III. The time scale of morphogenesis at the stem apex of *Pinus Resinosa* AIT. *Canadian Journal of Botany*, **36**, 687-706.
- Fenner, M. (1998) The phenology of growth and reproduction in plants. *Perspectives in Plant Ecology, Evolution and Systematics*, **1**, 78-91.

- Forcella, F. (1981) Ovulate cone production in pinyon: negative exponential relationship with late summer temperature. *Ecology*, **62**, 488-491.
- Fritts, H.C. (1976) *Tree rings and climate*. Academic Press, New York, NY, USA.
- Goffe, W.L., Ferrier, G.D. & Rogers, J. (1994) Global optimization of statistical functions with simulated annealing. *Journal of Econometrics*, **60**, 65-99.
- Grissino-Mayer, H.D. (2001) Evaluating crossdating accuracy: a manual and tutorial for the computer program COFECHA. *Tree-ring research*, **57**, 205-221.
- Harrison, D.L. & Owens, J.N. (1983) Bud development in *Picea engelmannii*. I. Vegetative bud development, differentiation, and early development of reproductive buds. *Canadian Journal of Botany*, **61**, 2291-2301.
- Herrera, C.M., Jordano, P., Guitián, J. & Traveset, A. (1998) Annual variability in seed production by woody plants and the masting concept: reassessment of principles and relationship to pollination and seed dispersal. *The American Naturalist*, **152**, 576-594.
- Hoch, G. (2005) Fruit-bearing branchlets are carbon autonomous in mature broad-leaved temperate forest trees. *Plant, Cell & Environment*, **28**, 651-659.
- Hoch, G. & Körner, C. (2003) The carbon charging of pines at the climatic treeline: a global comparison. *Oecologia*, **135**, 10-21.
- Hoch, G., Siegwolf, R.T., Keel, S.G., Körner, C. & Han, Q. (2013) Fruit production in three masting tree species does not rely on stored carbon reserves. *Oecologia*, **171**, 653-662.
- Holmes, R. (1983) Computer-assisted quality control in tree-ring dating and measurement, *Tree-Ring Bulletin*, **43**, 69-75.
- Holmsgaard, E. & Olsen, H.C. (1966) Experimental induction of flowering in beech. *Forstl Forøgsvaes*, **30**, 1-17.
- Houle, G. (1999) Mast seeding in *Abies balsamea*, *Acer saccharum* and *Betula alleghaniensis* in an old growth, cold temperate forest of north-eastern North America. *Journal of Ecology*, **87**, 413-422.
- Hudson, P.J. & Cattadori, I.M. (1999) The Moran effect: a cause of population synchrony. *Trends in Ecology & Evolution*, **14**, 1-2.
- Janzen, D.H. (1976) Why bamboos wait so long to flower. *Annual Review of Ecology and Systematics*, **7**, 347-391.
- Johnson, E.A. & Fryer, G.I. (1996) Why Engelmann spruce does not have a persistent seed bank. *Canadian Journal of Forest Research*, **26**, 872-878.

- Kelly, D. (1994) The evolutionary ecology of mast seeding. *Trends in Ecology & Evolution*, **9**, 465-470.
- Kelly, D., Geldenhuis, A., James, A., Penelope Holland, E., Plank, M.J., Brockie, R.E., Cowan, P.E., Harper, G.A., Lee, W.G., Maitland, M.J., Mark, A.F., Mills, J.A., Wilson, P.R. & Byrom, A.E. (2013) Of mast and mean: differential-temperature cue makes mast seeding insensitive to climate change. *Ecology Letters*, **16**, 90-98.
- Kelly, D. & Sork, V.L. (2002) Mast seeding in perennial plants: why, how, where? *Annual Review of Ecology and Systematics*, **33**, 427-447.
- Koenig, W.D. & Knops, J.M. (1998) Scale of mast-seeding and tree-ring growth. *Nature*, **396**, 225-226.
- Koenig, W.D. & Knops, J.M. (2000) Patterns of annual seed production by northern hemisphere trees: a global perspective. *The American Naturalist*, **155**, 59-69.
- Koenig, W.D. & Knops, J.M. (2014) Environmental correlates of acorn production by four species of Minnesota oaks. *Population Ecology*, **56**, 63-71.
- Knops, J.M., Koenig, W.D. & Carmen, W.J. (2007) Negative correlation does not imply a tradeoff between growth and reproduction in California oaks. *Proceedings of the National Academy of Sciences*, **104**, 16982-16985.
- Liebhold, A., Koenig, W.D. & Bjørnstad, O.N. (2004) Spatial synchrony in population dynamics. *Annual Review of Ecology, Evolution, and Systematics*, **35**, 467-490.
- Littell, J.S., McKenzie, D., Peterson, D.L. & Westerling, A.L. (2009) Climate and wildfire area burned in western US ecoprovinces, 1916–2003. *Ecological Applications*, **19**, 1003-1021.
- Macalady, A.K. & Bugmann, H. (2014) Growth-mortality relationships in pinon pine (*Pinus edulis*) during severe droughts of the past century: shifting processes in space and time. *PLoS ONE*, **9**, e92770.
- Mann, M.E., Bradley, R.S. & Hughes, M.K. (1999) Northern hemisphere temperatures during the past millennium: inferences, uncertainties, and limitations. *Geophysical Research Letters*, **26**, 759-762.
- McGuire, C.R., Nufio, C.R., Bowers, M.D. & Guralnick, R.P. (2012) Elevation-dependent temperature trends in the Rocky Mountain Front Range: changes over a 56-and 20-year record. *PLoS ONE*, **7**, e44370.
- Ostfeld, R.S., Jones, C.G. & Wolff, J.O. (1996) Of mice and mast: Ecological connections in eastern deciduous forests. *Bioscience*, **46**, 323–330.

- Owens, J.N. & Blake, M.D. (1985) *Forest tree seed production, a review of the literature and recommendations for future research*. Canadian Forestry Service, Petawawa, Canada.
- Owens, J.N. (1995) Constraints to seed production: temperate and tropical forest trees. *Tree Physiology*, **15**, 477-484.
- Oyler, J.W., Ballantyne, A., Jencso, K., Sweet, M. & Running, S.W. (2014) Creating a topoclimatic daily air temperature dataset for the conterminous United States using homogenized station data and remotely sensed land skin temperature. *International Journal of Climatology*, **35**, 2258-2279.
- Pacala, S.W., Canham, C.D., Saponara, J., Silander Jr, J.A., Kobe, R.K. & Ribbens, E. (1996) Forest models defined by field measurements: estimation, error analysis and dynamics. *Ecological Monographs*, **66**, 1-43.
- Pepin, N., Bradley, R.S, Diaz H.F, Baraer, M., Caceres, E.B., Forsythe, N., Fowler, H., Greenwood, G., Hashmi, M.Z., Liu, X.D., Miller, J.R., Ning, L, Ohmura, A., Palazzi, E., Rangwala, I., Schoner, W., Severskiy, I., Shahgedanova, M., Wang, M.B., Williamson, S.N. & Yang, D.Q. (2015) Elevation-dependent warming in mountain regions of the world. *Nature Climate Change* **5**, 424–430.
- Piovesan, G. & Adams, J. M. (2001) Masting behaviour in beech: linking reproduction and climatic variation. *Canadian Journal of Botany*, **79**, 1039-1047.
- Pearse, I.S., Koenig, W.D. & Knops, J.M. (2014) Cues versus proximate drivers: testing the mechanism behind masting behavior. *Oikos*, **123**, 179-184.
- Pielke, R.A., Doesken, N., Bliss, O., Green, T., Chaffin, C., Salas, J.D., Woodhouse, C.A., Lukas, J.J. & Wolter, K. (2005) Drought 2002 in Colorado: an unprecedented drought or a routine drought? *Pure and Applied Geophysics*, **162**, 1455-1479.
- Raffa, K.F., Aukema, B.H., Bentz, B.J., Carroll, A.L., Hicke, J.A., Turner, M.G. & Romme, W.H. (2008) Cross-scale drivers of natural disturbances prone to anthropogenic amplification: the dynamics of bark beetle eruptions. *Bioscience*, **58**, 501-517.
- R Core Team (2013) R: A Language and Environment for Statistical Computing. R Foundation for Statistical Computing, Vienna, Austria. URL <http://www.R-project.org/>.
- Redmond, M.D., Forcella, F. & Barger, N.N. (2012) Declines in pinyon pine cone production associated with regional warming. *Ecosphere*, **3**, 1-14.
- Rees, M., Kelly, D. & Bjørnstad, O.N. (2002) Snow tussocks, chaos, and the evolution of mast seeding. *The American Naturalist*, **160**, 44-59.

Reznick, D. (1985) Costs of reproduction: an evaluation of the empirical evidence. *Oikos*, **44**, 257-267.

Richardson, S.J., Allen, R.B., Whitehead, D., Carswell, F.E., Ruscoe, W.A. & Platt, K.H. (2005) Climate and net carbon availability determine temporal patterns of seed production by *Nothofagus*. *Ecology*, **86**, 972-981.

Roland, C.A., Schmidt, J.H. & Johnstone, J.F. (2014) Climate sensitivity of reproduction in a mast-seeding boreal conifer across its distributional range from lowland to treeline forests. *Oecologia*, **174**, 665-677.

Ross, S.D. (1985) Promotion of flowering in potted *Picea engelmannii* (Perry) grafts: effects of heat, drought, gibberellin A4/7, and their timing. *Canadian Journal of Forest Research*, **15**, 618-624.

Salas, J.D., Delleur, J.W., Yevjevich, V.W. & Lane, W.L. (1980) *Applied Modeling of Hydrologic Time Series*. Water Resources Publication, Littleton, CO, USA.

Salzer, M.W. & Kipfmüller, K.F. (2005) Reconstructed temperature and precipitation on a millennial timescale from tree-rings in the southern Colorado Plateau, USA. *Climatic Change*, **70**, 465-487.

Schauber, E.M., Kelly, D., Turchin, P., Simon, C., Lee, W.G., Allen, R.B., Payton, J., Wilson, P.R., Cowan, P.E. & Brockie, R.E. (2002) Masting by eighteen New Zealand plant species: the role of temperature as a synchronizing cue. *Ecology*, **83**, 1214-1225.

Sánchez-Humanes, B., Sork, V.L. & Espelta, J.M. (2011) Trade-offs between vegetative growth and acorn production in *Quercus lobata* during a mast year: the relevance of crop size and hierarchical level within the canopy. *Oecologia*, **166**, 101-110.

Selås, V., Piovesan, G., Adams, J.M. & Bernabei, M. (2002) Climatic factors controlling reproduction and growth of Norway spruce in southern Norway. *Canadian Journal of Forest Research*, **32**, 217-225.

Silvertown, J.W. (1980) The evolutionary ecology of mast seeding in trees. *Biological Journal of the Linnean Society*, **14**, 235-250.

Smaill, S.J., Clinton, P.W., Allen, R.B. & Davis, M.R. (2011) Climate cues and resources interact to determine seed production by a masting species. *Journal of Ecology*, **99**, 870-877.

Speer, J.H. (2001) Oak mast history from dendrochronology: a new technique demonstrated in the southern Appalachian region. PhD thesis, University of Tennessee, Knoxville, TN, USA.

Speer, J.H. (2010) *Fundamentals of Tree-ring Research*. University of Arizona Press, Tucson, AZ, USA.

Van Mantgem, P.J., Stephenson, N.L., Byrne, J.C., Daniels, L.D., Franklin, J.F., Fulé, P.Z., Harmon, M.E., Larson, A.J., Smith, J.M., Taylor, A.H. & Veblen, T.T. (2009) Widespread increase of tree mortality rates in the western United States. *Science*, **323**, 521-524.

Woodward, A., Silsbee, D.G., Schreiner, E.G. & Means, J.E. (1994) Influence of climate on radial growth and cone production in subalpine fir (*Abies lasiocarpa*) and mountain hemlock (*Tsuga mertensiana*). *Canadian Journal of Forest Research*, **24**, 1133-1143.

Żywiec, M. & Zielonka, T. (2013) Does a heavy fruit crop reduce the tree ring increment? Results from a 12-year study in a subalpine zone. *Trees*, **27**, 1365-1373.

CHAPTER 2 CLIMATE AND COMPETITION EFFECTS ON TREE GROWTH IN ROCKY MOUNTAIN FORESTS²

Synopsis

Climate is widely assumed to influence physiological and demographic processes in trees, and hence forest composition, biomass and range limits. Growth in trees is an important barometer of climate change impacts on forests as growth is highly correlated with other demographic processes including tree mortality and fecundity. We investigated the main drivers of diameter growth for five common tree species occurring in the Rocky Mountains of the western United States using non-linear regression methods. We quantified growth at the individual tree level from tree core samples collected across broad environmental gradients. We estimated the effects of both climate variation and biotic interactions on growth processes and tested for evidence that disjunct populations of a species respond differentially to climate. Relationships between tree growth and climate varied by species and location. Growth in all species responded positively to increases in annual moisture up to a threshold level. Modest linear responses to temperature, both positive and negative, were observed at many sites. However, model results also revealed evidence for differentiated responses to local site conditions in all species. In severe environments in particular, growth responses varied non-linearly with temperature. For example, in northerly cold locations pronounced positive growth responses to increasing temperatures were observed. In warmer southerly climates, growth responses were unimodal, declining markedly above a threshold temperature level. Net effects from biotic interactions on diameter growth were negative for all

² This research was originally published in the *Journal of Ecology*: Buechling A., Martin P.H. & Canham C.D. (2017) Climate and competition effects on tree growth in Rocky Mountain forests. *Journal of Ecology*, doi: <http://dx.doi.org/10.1111/1365-2745.12782>.

study species. Evidence for facilitative effects was not detected. For some species, competitive effects more strongly influenced growth performance than climate. Competitive interactions also modified growth responses to climate to some degree. These analyses suggest that climate change will have complex, species specific effects on tree growth in the Rocky Mountains due to non-linear responses to climate, differentiated growth processes that vary by location and complex species interactions that impact growth and potentially modify responses to climate. Thus, robust model simulations of future growth responses to climate trends may need to integrate realistic scenarios of neighborhood effects as well as variability in tree performance attributed to differentiated populations.

Introduction

Modern trends in climate, especially rates of warming and shifting precipitation regimes, may be unprecedented in the past two millennia (Jones & Mann 2004). Associated environmental changes are expected to exceed the physiological tolerances and adaptive capacity of many plant taxa (Hansen *et al.* 2001). Radial growth in trees is an important barometer of climate change impacts on the performance of tree species and the dynamics of forest communities, as growth is highly correlated with other demographic processes including tree mortality (Martin *et al.* 2010) and fecundity (Martin & Canham 2010). Demographic processes of birth, growth, dispersal and mortality and interspecific differences in these vital rates shape the relative abundance of tree species in forests (Pacala *et al.* 1996) and determine the distribution of populations across landscapes. Climate driven changes in vital rates lead to local extinction and colonization events that aggregate across populations to shape trajectories of change in species ranges (Hansen *et al.* 2001). Recent large-scale studies investigating evidence for range shifts in tree species, however, have revealed inconsistent and idiosyncratic responses to contemporary

climate trends (Zhu *et al.* 2012), suggesting that range shifts may lag changes in the demographic rates that determine species migrations (Littell *et al.* 2008). For instance, evidence has been detected for increased growth rates among tree taxa occurring at high elevations (Bunn *et al.* 2005), which may presage range expansion in some of these areas. Such patterns indicate that understanding an organism's climate niche and sensitivity to climate change requires rigorous empirical quantification of the demographic processes that constitute its niche, data that is currently lacking in predictive models of global change (McMahon *et al.* 2011).

Growth processes in trees can be investigated using regression methods, as temporal series of radial growth record the effects of past environmental variation with annual resolution. Dendrochronology, a commonly used framework for analyzing tree ring series, has a long history in climate research for the reconstruction of past climates (Graumlich 1993; Büntgen *et al.* 2013). Related methods have been used to quantify climatic drivers of growth (Littell *et al.* 2008), to infer functional responses to disturbance (Alfaro-Sánchez *et al.* 2016), and to forecast growth responses to future climate (Williams *et al.* 2010). Traditional dendrochronological techniques typically involve substantial data transformations to generate stationary time series of ring widths. These data transformations are designed to remove temporal autocorrelation and to dampen ring width variance attributed to non-climatic effects, including tree allometry and stand dynamics, thereby enhancing a target climate signal (Blasing *et al.* 1983). Thus, regression models based on standardized chronologies of growth cannot be used to assess the absolute effects of climate on growth rates, nor to assess the relative strength of climate versus other factors on growth processes (but see Ettinger & HilleRisLambers 2013). However, a growing body of evidence indicates that biotic interactions, by substantially moderating tree growth, may influence associated responses to climate variation in important

ways (Kunstler *et al.* 2011; Coomes *et al.* 2014; Rollinson *et al.* 2016). For example, differences in the competitive environments of individual trees may partially explain idiosyncratic growth responses to warming trends in boreal forests of Alaska (Wilmking *et al.* 2004). Positive facilitative interactions between tree species experiencing physiological stress have also been detected (e.g. Gazol & Camarero 2016; Thurm *et al.* 2016). Thus, robust analyses of growth responses to climate may require an alternate statistical framework that can explicitly integrate both climate factors and biotic effects (Clark *et al.* 2011).

Additional factors potentially influencing growth processes include genetic variation and adaptation to local conditions among distant populations of plant species. Previous studies have revealed evidence for population-level differentiated responses to local climate for some tree species (Rehfeldt *et al.* 1999). Differentiated populations, which may develop via either genetic adaptation or phenotypic acclimation, have unique climate optima and tolerances, and hence divergent responses to changing environmental conditions. Failure to account for differentiated processes may obfuscate empirical relationships between plant performance and climate and potentially bias predictions of growth under future climates (O'Neill *et al.* 2008; Angert *et al.* 2011).

In this study, we investigated the main drivers of radial growth for five common tree species in the Rocky Mountains of the western United States using non-linear regression methods. We quantified growth at the individual tree level from tree core samples collected across large spatial scales and environmental gradients. We estimated the effects of temperature, precipitation and biotic interactions on growth processes. Measures of forest stand density were used to assess the nature and relative strength of biotic or neighborhood effects. Models were

formulated to explicitly test for evidence of differentiated growth responses to local climate regimes.

The direct effects of climate on growth processes in individual trees have been previously found to be modest in some forest systems (e.g. Coomes *et al.* 2014; Canham & Murphy 2016). However, we expect that growth processes may be influenced by complex interactions between climate variation, neighborhood structure, and differentiated populations. Specifically, given the recognized importance of biotic interactions in mediating plant responses to environmental change (Brooker 2006), we hypothesize that neighborhood effects may strongly influence growth responses to climate for these species, and that in some environments differential responses to the presence of neighbors may alter growth hierarchies between species. We further expect that across the broad environmental gradients that characterize Rocky Mountain forests, disjunct populations of the same species vary in their responses to climate and that growth potential at a given location may be negatively correlated with extremes in climate.

Materials and methods

Study area

We collected tree ring data from five sites distributed across a latitudinal gradient from the southern terminus of the Rockies in New Mexico to the Canadian border in the north (Fig. S2.1 in Appendix). Sites include from south to north: (1) Lincoln National Forest (LNF) in southern New Mexico (32.84° N, 105.7° W), (2) San Isabel National Forest (SNF) in southern Colorado (38.04° N, 105.11° W), (3) Roosevelt National Forest (RNF) in northern Colorado (40.71° N, 105.58° W), (4) Bighorn National Forest (BNF) in northern Wyoming (44.53° N, 107.35° W) and (5) Glacier National Park (GNP) in northern Montana (48.7° N, 113.71° W). Forests span elevations from ~1850 to over 3600 m in southern sites and between ~1300 and

3050 m at northern sites. The five study sites encompass a wide range of climates. In general, annual temperature decreases and precipitation increases from south to north across the study area. Mean annual temperatures range from ~4.9°C (1.8 to 9.8°C) in southern sites to ~3.3°C (1.9 to 5.2°C) in the north. Average annual precipitation is ~661 mm (457 to 926 mm) in the south and ~923 mm (519 to 1341 mm) in the north. We selected five common tree species for growth sampling: *Abies lasiocarpa* (Hook.) Nutt. (subalpine fir), *Picea engelmannii* Parry ex Engelm. (Engelmann spruce), *Pinus contorta* Douglas ex Loudon (lodgepole pine), *Pinus ponderosa* Lawson & C. Lawson (ponderosa pine) and *Pseudotsuga menziesii* (Mirb.) Franco (Douglas-fir).

Growth data

Geospatial analyses were used to design a stratified random distribution of plot locations for sample data collection. Plot locations were dispersed over environmental gradients hypothesized to affect both climate and forest stand structure, and hence associated growth responses. Specifically, we used the National Elevation Dataset (1 arc-second spatial resolution) from the U.S. Geological Survey to produce raster datasets representing elevation, terrain aspect, and an index of soil moisture (Parker 1982) for the study region using spatial tools in ArcGIS (Version 10.3; ESRI 2011). We then generated a random distribution of plot locations across these surfaces for each study species, constrained by the range of a species' distribution within each of the 5 study sites. We used a vegetation type raster dataset from LANDFIRE (<http://www.landfire.gov/>) to delimit the geographic range of each species.

Focal species were sampled at a minimum of 3 study sites. We excluded plots located in stands with recent tree mortality or disturbance. A single adult target tree from the dominant canopy layer was sampled at each plot location. Saplings (<10 cm diameter at breast height)

were not sampled. Trees with obvious external damage were excluded. We collected at least 2 increment cores per target tree at a height of 30 cm above the root crown. We collected additional samples (up to 4 cores per tree) if the shape of the stem was strongly asymmetric or if the quality of a sample core was uncertain. A mean of 2.4 cores were collected per tree in this study. Cores were extracted as low as possible on the stem to maximize the time depth of each ring width series for cross-dating purposes and to obtain age estimates as close to the germination year as possible. We measured the diameter of each target tree at breast height (DBH; 1.3 m) and the distance to and DBH of all neighboring trees within a 15 m radius of the target tree.

Final sample sizes varied by species, ranging from 131 to 179 sample trees across the study region as a whole (Table 2.1). Sites with less than 5 sample trees were excluded from modeling analyses. After excluding those data, mean samples sizes within individual study sites ranged from 45 (38-54) for *P. menziesii*, 43 (39-51) for *P. ponderosa*, 42 (13-55) for *P. engelmannii*, 36 (22-58) for *A. lasiocarpa*, and 36 (13-50) for *P. contorta* (see Fig. S2.2). Sample trees covered broad environmental gradients (Appendix S2.1; Table S2.1; Fig. S2.3). Over 1,900 tree core samples were lab processed to obtain annual measures of radial growth (RG). Cores were mounted, sanded until tracheid cells were clearly visible under magnification, and visually cross-dated using the entire series length to ensure correct ring dates (Speer 2010). We then measured ring widths for the most recent 20 years in each core (1992 to 2011) to a precision of 0.001 mm using a Velmex measuring system. We limited measurements to a 20-year window for which we assumed that stand composition and neighborhood effects were relatively invariant, based on the selection of forest stands with minimal evidence of recent disturbance. Ring widths

were examined for measurement and dating errors using COFECHA (Grissino-Mayer 2001). Multiple cores from the same tree were averaged to produce a single time series of annual RG.

Growth models

We constructed independent regression models for each species using likelihood methods of parameter estimation. The response variable for all models was annual RG (mm/year). We used raw annual measurements of RG from individual trees to fit growth models, contrasting the common practice in dendrochronological studies of detrending and averaging individual time series of growth into composite mean indices of growth for a site. These data transformations effectively homogenize data variability between individual trees (Fritts 1976; Cook 1987), which may obfuscate temporal or spatial trends and limit inferential ability in certain applications (Wilmking *et al.* 2004; Carrer 2011).

Time series of ring widths from trees are generally serially or temporally autocorrelated; meaning that data from individual years are not strictly independent. Autocorrelated data structures result in inflated estimates of degrees of freedom and biased underestimates of variance. Temporal autocorrelation may be related to a range of factors including inherent negative trends associated with increasing stem circumferences in aging trees, and extrinsic factors such as disturbance events and changes in stand structure (Fritts 1976). However, techniques commonly used to reduce autocorrelation, such as autoregressive modeling (Chatfield 2004), may dampen signal variance related to climate and thus further bias associated ecological inferences. RG may alternately be averaged over multiple year periods to remove autocorrelation, but smoothing ring width variability in this way may again result in the loss of information regarding the target climate signal. In this study, geometric trends in the ring width series were modeled using a size effect, derived from tree DBH. We incorporated prior year

climate variables to account for potential antecedent effects that could cause a lagged effect on growth processes. Given our sampling design (see above), we also assumed that forest stand structure, neighborhood tree densities and the associated strength of biotic interactions remained constant within the relatively narrow 20-year window of analysis. Additionally, we argue that likelihood estimation is robust to issues of autocorrelation, as these methods do not rely on measures of degrees of freedom for hypothesis testing, parameter estimation or model comparison. Furthermore, the resulting residuals from all best fitting models were randomly distributed according to tests for autocorrelation (residual plots shown in Fig. S2.4 & S2.5).

A fundamental assumption in dendrochronological research is that RG responses to climate are time invariant within a species and thus age-independent, after accounting for trends associated with increasing tree size and forest stand dynamics (Carrer & Urbinati 2004; Esper *et al.* 2008). However, preliminary analyses (not shown) in this study revealed possible relationships between tree age and growth rates. Thus, we constructed alternate models to explicitly test for age effects and thereby account for any age-related trends in the ring width series, as described below.

A series of alternate hierarchical models were developed for each species. Full models estimated size, age, neighborhood and climate effects as factors in a multiplicative non-linear framework:

$$RG = PRG[\text{site}] \times \text{Size} \times \text{Age} \times \text{Neighborhood} \times \text{Temperature} \times \text{Precipitation} \quad [1]$$

PRG represents potential or expected RG for a hypothetical free-growing tree and was estimated uniquely for each study site. Tree size, age, neighborhood and climate effects are scalar modifiers that proportionally reduce or increase potential growth. We minimized assumptions

concerning the shape of the relationships between response and effect terms, so we tested relatively flexible functional forms, such as lognormal or Gaussian, that can fit monotonically increasing, decreasing, or unimodal data distributions. Both size and age effects were fit with a lognormal function:

$$\text{Size or age effect} = \exp\left[-0.5 \times \left(\frac{\ln\left(\frac{\text{DBH or age}}{\delta}\right)}{\sigma}\right)^2\right] \quad [2]$$

where δ represents the modal value of DBH or age corresponding to potential growth (PRG) and σ describes the breadth of the function.

An individual tree modeling approach facilitates the explicit estimation of neighborhood effects on growth processes. We used a distance-dependent measure of forest stand structure, an index of neighborhood crowding (NCI), to quantify neighborhood effects (Canham *et al.* 2004). NCI was parameterized from our field data and depends on the density, species composition and size of neighboring trees within each 15 m radius plot:

$$\text{NCI} = \sum_{i=1}^s \sum_{j=1}^n \lambda_i \frac{(\text{DBH}_{ij})^\alpha}{(\text{distance}_{ij})^\beta} \quad [3]$$

Subscripts i and j denote the species identity of a given neighbor and the corresponding number of stems of that species, respectively. Thus, the magnitude of the neighborhood effect on a target tree varies as a direct function of the DBH of a given neighbor and inversely with the distance of that neighbor from a target tree. The shape of the neighborhood effect is determined by the exponents α and β . To constrain model complexity, we assumed that α and β were constant for all neighbor species. However, we did test for potential differences between neighbor species in their overall effect on a target tree by incorporating species specific NCI coefficients (λ_i) in Equation 3.

We estimated target tree responses to NCI using a flexible exponential function:

$$\text{Neighborhood response} = e^{\pm C \times \text{DBH}^\gamma \times \text{NCI}} \quad [4]$$

The exponential decay parameter (C) governs the shape of the response; positive values fit monotonically increasing responses to NCI and reflect beneficial or facilitative interactions with neighbors; negative exponents track declining growth responses and reflect net negative or competitive effects on growth. We also allowed this function to vary with the DBH of the target tree to evaluate whether sensitivity to crowding depends on tree size. The exponent γ governs any size-dependent variation in response to neighbors. Specifically, negative values of γ indicate that growth in larger diameter target trees is less affected by crowding than growth in smaller trees. Conversely, for positive values of γ , sensitivity to crowding increases with increasing tree size.

Relationships between climate and tree growth have been investigated using a wide range of climate metrics, varying by study, species and location. There is no *a priori* theory or consensus for selecting appropriate model form (Cook *et al.* 1987). Relationships between leaf level responses to short-term climate variation identified in the ecophysiological literature do not readily elucidate the most important climate drivers of average diameter growth, which depends on long-term climate variability integrated over a year or more. In this study, we investigated climate-growth relationships using annual mean temperature and annual total precipitation. This *a priori* selection mitigates widely recognized statistical issues related to the *a posteriori* selection of predictors based on goodness of fit comparisons between a multitude of possible permutations of temperature and precipitation that may be parameterized for any given species. In addition, annual climate values were highly correlated with seasonal means. Spearman correlations between annual mean temperature and various seasonal temperature means ranged

from 0.87 to 0.96. Correlations between precipitation variables were slightly lower, ranging from 0.55 to 0.81. We did test model performance based on a limited selection of objectively defined seasonal climate predictors, but associated model fits were weaker for most species compared with annual models (see Appendix S2.2 & Table S2.2).

Climate variables were derived from PRISM, a model that generates spatially continuous estimates of monthly temperature and precipitation for the United States (Daly *et al.* 2008). We extracted PRISM data (30 arc-second or ~800 m resolution) for target tree locations using a weighted interpolation of adjacent pixel values. Annual precipitation sums and temperature means were derived from the extracted monthly data. Annual periods were defined according to a U.S. Geological Survey hydrological year that spans a 12 month period from October 1st of the previous year to September 30th of the current year. Precipitation effects were fit with lognormal functions for all species. Temperature effects were estimated using Gaussian functions:

$$\text{Temperature effect} = \exp\left[-0.5 \times \left(\frac{(t - \text{temp. } a)}{\text{temp. } b}\right)^2\right] \quad [5]$$

where t is observed temperature, and $\text{temp. } a$ and $\text{temp. } b$ describe the mode and variance of the function, respectively.

We also tested for evidence of adaptation or acclimation to both temperature and precipitation at each study site by modifying climate functions (Gaussian for temperature and lognormal for precipitation) so that a unique mode and variance was estimated for each climate variable at each site. Differentiated climate functions quantify unique, site-specific growth responses to corresponding climate regimes that differ across the study region.

Model specification and evaluation

A series of alternate models based on Equation 1 were produced to evaluate the relative importance of climate and crowding effects. Simulated annealing, a global optimization

algorithm, was used to solve for maximum likelihood estimates of regression parameters (Goffe *et al.* 1994). Model residuals were approximately normal, but heteroscedastic. Thus, we used a modified normal probability density function, for which variance was computed as a linear function of the mean, to estimate likelihood. Bias and proportion of variance explained (R^2) were used to quantify the goodness of fit (GOF) of alternate models. Bias was quantified from the slope of the linear regression of observed versus predicted RG. Akaike information criterion corrected for small sample size (AIC_c) was used to select the most parsimonious models (Burnham & Anderson 2002). Analyses were conducted in R (Version 3.2.3; R Core Team 2013). Likelihood models were constructed using likelihood package version 1.6.

Results

The most parsimonious models for all species included site, tree age, temperature, precipitation and neighborhood effects (Table 2.2). Age functions accounted for consistent negative trends in the growth data associated with increasing tree age (Fig. S2.6) and substantially improved the statistical fit of all models in terms of AIC_c. Size functions were excluded from final models based on parsimony (low AIC_c values), potentially due in part to modest correlations between size and age parameters for trees in this study (0.36 to 0.5 depending on species). The explanatory power of the final full models varied among species with R^2 values ranging from 0.37 for *A. lasiocarpa* to 0.74 for *P. ponderosa*. All models for all species produced unbiased predictions of RG (Table 2.2).

Growth responses to climate were site dependent for all species. Differences in the amplitude of RG responses to both temperature and precipitation (Fig. S2.7) were governed by site-specific estimates of PRG (Eqn. 1), and may reflect differences in local edaphic conditions or underlying geology. For most species, the shapes of RG responses to temperature, when

averaged across all sites, were effectively flat, increasing linearly with very low positive slopes in both the year concurrent with growth and in the previous year (Fig. 2.1A & 2.1C). Only *P. ponderosa* exhibited negative non-linear trends in RG with increasing annual temperature. However, the strongest full models for all species also included site-differentiated temperature functions (Table 2.2), indicating that not only the amplitudes, but the shapes of RG responses to climate varied by location within the study region. In particular, at climatically extreme sites relative to the study region as a whole, patterns of RG diverged markedly and non-linearly (Fig. 2.2). For example, at the most southerly and warmest study site, Lincoln NF, RG declined rapidly at high temperature for *P. ponderosa* and *P. engelmannii* and moderately for *A. lasiocarpa*. In contrast, *A. lasiocarpa* and *P. contorta* exhibited site-specific positive RG responses to temperature at Glacier, which is the most northerly site in the study region. RG trends at Glacier may reflect an integrated response to both temperature and precipitation, since, although temperature is not extreme at this site, annual precipitation sums at Glacier exceed total precipitation in the driest study sites by more than a factor of two, and most of this precipitation occurs as winter snow (Table S2.1).

Growth responses to precipitation generally assumed Gaussian shapes. All species responded positively to higher levels of annual precipitation in the drier portions of their precipitation ranges (Fig. 2.1B & 2.1D), particularly in the year concurrent with growth. However, above a threshold moisture level in the growth year, RG in all species except *P. ponderosa* declined with increasing annual precipitation. Threshold levels of precipitation associated with maximum RG ranged from a low of ~665 mm/year for *P. contorta* to a high of ~854 mm/year for *P. menziesii* (Fig. 2.1B). Notably, we found little evidence for differentiation

to local precipitation regimes, as determined by model comparison statistics (AICc). Only one species, *P. menziesii*, exhibited unique site-specific responses to precipitation (Table 2.2).

Neighborhood effects were important for all species and retained in all best-fitting full models of growth based on AICc (Table 2.2). For two species, *A. lasiocarpa* and *P. contorta*, models that estimated neighborhood effects only (Neighborhood models in Table 2.2) provided a statistically stronger fit to the growth observations than models that estimated climate effects alone (Climate models in Table 2.2). Optimization routines fitted RG responses to NCI with negative exponential functions for all species, unambiguously demonstrating that RG in all species declined with increased levels of crowding from neighboring trees (Fig. S2.8). Negative responses in target tree growth varied with the size, distance to, and number of neighboring trees in a plot. A comparison of mixed versus equivalent neighborhood models based on AICc indicated that simpler models that treated all neighboring species as equivalent competitors were consistently stronger for all focal species (Table 2.2). Thus, RG responses were not sensitive to the species composition of corresponding neighborhoods.

The five study species differed in their sensitivity to neighborhood effects. In general, the two most shade intolerant species, *P. contorta* and *P. ponderosa*, were the most affected by variation in neighborhood conditions (Fig. S2.8). Species differences depend on multiple interacting factors. For example, the proximity of neighboring trees had strong negative effects on growth processes in *P. contorta* and *P. ponderosa* (Fig. 2.3). In contrast, distance had only minor effects on the 3 shade tolerant species, *A. lasiocarpa*, *P. engelmannii* and *P. menziesii*. Responses to crowding for most species were directly proportional to the DBH of neighboring trees, as determined by α values (Eqn. 3) approximately equal to 1.0 (Table S2.3). Target tree size further modified these patterns; smaller diameter trees in the species *A. lasiocarpa*, *P.*

engelmannii and *P. contorta* were more sensitive to neighborhood effects than larger diameter trees. The converse was true for *P. ponderosa* and *P. menziesii*.

Modest evidence was detected that varying levels of neighborhood crowding influence growth responses in focal species to climate variation, potentially leading to altered performance hierarchies among species. For example, when neighborhood crowding effects (NCI) are low, RG in *P. engelmannii* consistently surpasses growth rates in *A. lasiocarpa* across the full precipitation breadth of *P. engelmannii* (Fig. 2.4). In contrast, at high NCI, RG in *A. lasiocarpa* exceeds growth in *P. engelmannii* at both low and high limits of annual precipitation. More substantial growth reversals associated with changing stand densities occur between *P. engelmannii* and *P. menziesii*, but currently, these species overlap within only limited portions of the study region.

Discussion

Tree species in this study occupy extremely broad ecological gradients. The thermal niche alone spans more than 10°C in mean annual temperature for all focal species. A similarly wide fundamental niche has been estimated for *P. contorta* in British Columbia, which Rehfeldt (1999) postulated is an expression of a high degree of adaptability among individuals and populations. Given these broad distributions, we argue that comprehensive census data is requisite for the robust estimation of factors that shape demographic processes in these species and for detecting differences among populations in their responses to external controls. A lack of bias in the parameter estimates of our models reflects well distributed field samples that capture a broad range of ecological conditions. We further argue that the multiplicative modeling framework used in this study facilitates an understanding of the interactions between factors that influence growth and thereby more unequivocally elucidate the effects of individual variables.

Full models in our analyses, identified based on principles of parsimony, integrated current and antecedent climate, neighborhood effects, site factors, and age trends, and explained a relatively high proportion of RG variance for these species.

Responses to climate were complex, non-linear and varied substantially between species. All species except *P. ponderosa* exhibited unimodal or threshold responses to moisture. Non-linear relationships with precipitation have been identified in previous analyses based on individual tree modeling methods (Coomes *et al.* 2014; Rollinson *et al.* 2016), as well as in some studies using more traditional dendrochronological approaches (e.g. Miyamoto *et al.* 2010). Potential growth in our study system was thus constrained at many locations by moisture availability and responded positively up to a species specific threshold limit. These thresholds were generally exceeded in the northern parts of the study area (Glacier NP), suggesting tree growth could increase with increasing aridity in the northern Rockies. *Pinus ponderosa* typically occupies the warmest and driest environments in the region, which generally occur at the lowest elevations and at more southerly latitudes. Growth in this species responded positively to moisture increases without reaching a threshold limit. Similar but asymptotic responses to moisture have been detected in drought-tolerant Mediterranean tree species (Fernández-de-Uña *et al.* 2015).

Growth responses to temperature in this study were generally more complex than responses to precipitation. Minor and approximately linear relationships with temperature were observed for most species when data from all sites were combined into a single growth function (Fig. 2.1), or when equivalent responses to climate are assumed for all populations (Fig. S2.7). Relatively modest thermal effects on tree growth or biomass accumulation in closed canopy forests have been observed in other studies (Ettinger & HilleRisLambers 2013; Coomes *et al.*

2014; Canham & Murphy 2016). However, in this study, more complex models that allowed the mode and breadth of the temperature function to vary depending on location revealed substantial site-specific differences in RG responses to temperature for all species. Thus, growth processes in this system appear to be tuned or differentiated to local temperature regimes through processes of either physiological acclimation (Cunningham & Read 2002) or evolutionary adaptation. Regardless of the mechanism, differentiated populations may be expected to respond in idiosyncratic ways to projected rates of future warming.

The reciprocal transplant literature indicates that differentiated responses to climate and other environmental conditions is common in plant taxa generally (Leimu & Fischer 2008). For a range of tree species, common garden studies investigating growth responses in seedlings and saplings have documented extensive evidence for population specialization (Rehfeldt *et al.* 1999). Evidence is more limited for adult trees. However, Chen *et al.* (2010) identified unique site specific growth responses in *P. menziesii* in western North America which they attributed to local adaptation. Our study shows that similar patterns of differentiation to local temperature occur in adult-sized trees for a wide range of species, despite the challenge of detecting differentiated growth processes in adult trees in mountainous environments (i.e. due to the low, innate growth potential and growth variability of trees at high elevations). Caution in this interpretation is warranted, however, as some of the locally differentiated responses to temperature in this study may be driven by anomalous temperature variability at extreme sites that is not replicated at other locations (Fig. 2.2).

Model results revealed persistent, net negative responses in individual tree growth to crowding for all species across a wide range of neighborhood conditions, supporting fundamental ecological theories that competition between individuals is a main factor in the

population ecology of trees (Harper 1964). For two species, *P. contorta* and *A. lasiocarpa*, negative crowding effects were more important than climate. According to our analyses, these two high-elevation, cold-tolerant species have a comparatively low innate growth potential and are relatively less sensitive to climate variation compared with the other focal species in this study (Fig. 2.1). A lack of support for facilitative processes in this study may be attributed to the comprehensive scope of the sampling design. Much of the evidence for facilitation has been detected using experimental approaches restricted to a limited range of environments and over short study periods (Brooker *et al.* 2008, Maestre *et al.* 2009). Typically, facilitative processes in forests have been associated with periods of severe abiotic stress, such as episodic drought occurrence (Gazol & Camarero 2016; Thurm *et al.* 2016), or in strongly resource limited environments (Callaway 1998). In contrast, we designed our field sampling to encompass broad ecological gradients. Unproductive environments, such as treeline, constituted only a minority of all sample sites (~6 percent). Our model results, therefore, reflect a net response to neighborhood conditions across the full distribution of these species, over which competitive effects, on average, strongly outweigh any facilitative processes that may be transient or restricted to particular environmental conditions. Using a Bayesian model of individual tree growth, Kunstler *et al.* (2011) similarly found no evidence for facilitative effects among 16 tree species sampled across broad ecological gradients in France. Additionally, some authors have hypothesized that positive interactions between individuals may have more prominent effects on plant survival than on growth (Goldberg & Novoplansky 1997).

Perhaps unexpectedly, competitive responses to crowding in all focal species did not depend on the species composition of the neighborhood. Ecological equivalence in terms of competitive effects on growth contradicts assumptions inherent in theories of competition (e.g.

Puettmann & Reich 1995), and results from previous studies (Canham *et al.* 2004; Uriarte *et al.* 2004a; Coates *et al.* 2009). A generalized response to neighboring trees may be driven by similar resource requirements among coexisting species (Uriarte *et al.* 2004b). Alternately, the lack of support for taxonomic differences in competitive effects may be attributed to inherent modeling or sampling limitations in this study. Previous analyses that have revealed species specific effects in adult trees have explicitly parameterized both above-ground shading effects and below-ground root competition (Canham *et al.* 2004; Coates *et al.* 2009). Here we merged these processes into a single, integrated index of neighborhood effects, which may have obfuscated differences between species. Previous authors have also suggested that very large sample sizes are required, in terms of sample trees occurring in a wide range of competitive environments, to distinguish differential competitive effects (Uriarte *et al.* 2004b; Coates *et al.* 2009).

Despite the equivalence of neighboring species in their competitive effects on a target tree, all focal species differed considerably in their sensitivity to crowding. Species specific responses to neighborhood crowding varied according to a range of interacting factors, including the size, proximity and number of trees in a neighborhood. The functional shapes of these responses were non-linear for all species, consistent with results from other analyses of neighborhood dynamics (Uriarte *et al.* 2004a; Canham *et al.* 2006; Fernández-de-Uña *et al.* 2015). Competitive interactions are potentially further modified by variation in soil resources (Boyden *et al.* 2005) or changes in climate (Kunstler *et al.* 2011). The complex nature of these interactions precludes a consistent ranking of species according to competitive ability. Nevertheless, shade tolerant species (*P. engelmannii*, *A. lasiocarpa* and *P. menziesii*) were relatively less sensitive to crowding effects compared with other species (Fig. S2.8). These results suggest that analyses that approximate neighborhood effects with simpler indices, such as

stand basal area, or that use linear methods to estimate associated responses, may not fully describe the variability of these processes or capture differences between species in their sensitivity to crowding.

The multiplicative structure of our models inherently accounts for interactions between climate and crowding effects, contrasting linear additive methods that estimate these effects independently. Competition in our models thus modifies the innate growth potential of a species associated with particular climate conditions. Furthermore, evidence from these analyses suggests that the asymmetric nature of species interactions influences growth responses to climate among species in individualistic ways, potentially altering growth hierarchies among sympatric taxa (Fig. 2.4). Competition driven altered growth hierarchies were most apparent for *P. engelmannii* and *P. menziesii*, whose ranges overlap predominantly at mid elevations in this study system. *P. engelmannii* is more sensitive to crowding by neighbors than *P. menziesii* and thus responds more strongly to different permutations of competition and climate conditions. Similar results demonstrating interactions between climate and competition were observed for tree species in eastern North America (Rollinson *et al.* 2016). Future analyses are needed to determine if the maximum potential growth response to climate, determined by the mode of the corresponding function, shifts under different levels of competition. Accounting for interactions between climate and competitive effects may be critical for developing unbiased predictions of forest response to environmental change.

We tested both age and size effects in our models to account for associated trends in RG, thereby facilitating more robust estimates of climate and neighborhood effects. Traditional growth studies have generally used relative growth rates to account for age or size related trends that may potentially obscure climatic effects. Other methods based on spatially explicit,

individual-based modeling approaches have frequently parameterized size effects only (Kunstler *et al.* 2011; Coomes *et al.* 2014; Rollinson *et al.* 2016; Canham & Murphy 2016). Model results in this study indicate that growth in all species was strongly age dependent, declining exponentially with increasing age (Fig. S2.6A). Size effects were not significant in the most parsimonious full models. Mechanisms determining potential relationships between age and growth at the individual tree level remain unclear. Current hypotheses describe processes that cause progressive increases in physiological stress over time, including continuous increases in respiration demand in accumulating tissues and hydraulic limitations associated with increasing stem height (Ryan *et al.* 2004). Age and size may be confounded in some of these hypotheses. While the objective of this study was not to elucidate mechanisms driving any age related changes in tree growth, our analyses do indicate that age effects should be considered in similar analyses to control for confounding trends that are inherent in temporal series of RG measurements. Additionally, age related differences in tree growth responses to climate have been detected in some previous studies (Carrer & Urbinati 2004; Mamet & Kershaw 2013). Age effects, where significant, may interact with other site level effects, including locally differentiated growth processes, to further modify or amplify differences between disjunct populations in their responses to climate change.

We argue that impacts to Rocky Mountain forests related to projected changes in future climate will likely be complex and context specific. The most consistent expected climate trend – sustained temperature increases – may have notably inconsistent impacts on the growth performance of species in this system due to species specific, non-linear responses to climate, differentiated growth processes that vary by location, and complex species interactions that strongly influence maximum growth potential for a given species and in some instances may

alter growth hierarchies between species. Future climate change will have additional and significant indirect effects on tree growth by influencing changes in stand structure, through altered disturbance regimes and rates of tree mortality, which may in turn modify competitive processes and subsequent responses to climate. Variation in tree size and age, which are strongly linked to local stand histories, may further interact with these complex processes. Thus, model predictions that tree growth will decline or increase uniformly in this system (e.g. Williams *et al.* 2010) may be unrealistic.

Our results support previous assertions that linear additive methods do not capture climate thresholds and may generate biased predictions of growth responses to climate when extrapolated beyond the observed range of the covariates used to calibrate a particular model (Loehle 2009; Gea-Izquierdo *et al.* 2013). We suggest that robust estimates of future impacts to forest trees may require the parameterization of mechanistic models that fully simulate vegetation dynamics by integrating non-linear demographic rates, climate variation, potential fertilization effects associated with atmospheric nitrogen deposition or CO₂ enrichment, and environmental disturbance processes for multiple interacting species.

Data Accessibility

Annual tree growth measurements and neighborhood data available from the Dryad Digital Repository: <http://dx.doi.org/10.5061/dryad.fv322> (Buechling *et al.* 2017).

Tables

Table 2.1. Physical and environmental attributes (mean and ranges) of sampled trees.

Variable	Species				
	<i>A. lasiocarpa</i>	<i>P. engelmannii</i>	<i>P. contorta</i>	<i>P. ponderosa</i>	<i>P. menziesii</i>
Acronym	ABLA	PIEN	PICO	PIPO	PSME
¹ N	151	173	143	131	179
DBH (cm)	26.2 (10.2, 69)	35.0 (13, 83.8)	24.8 (12.9, 60)	38.7 (12.8, 96)	37.7 (13.4, 90)
Age (years)	119 (33, 321)	136 (35, 521)	129 (35, 482)	115 (24, 281)	120 (26, 366)
Radial growth (mm/year)	1.1 (0.1, 4.7)	1.4 (0.01, 6.2)	0.8 (0.05, 3.4)	1.4 (0, 11.7)	1.6 (0, 11.7)
Elevation (m)	2412 (1324, 3386)	2520 (1300, 3618)	2385 (1315, 3245)	2311 (1327, 3004)	2260 (1310, 3367)
Aspect (°)	180 (1, 360)	181 (1, 360)	168 (9, 360)	174 (2, 360)	179 (2, 360)
Slope (%)	36 (10, 88)	37 (10, 88)	32 (10, 88)	41 (7, 88)	44 (8, 88)
² P annual (mm/year)	939 (219, 2777)	902 (220, 2777)	870 (196, 2584)	558 (168, 1030)	784 (167, 2128)
³ T annual (°C)	2.7 (-2.7, 8)	3 (-3, 9.5)	3 (-2.8, 7.1)	7.5 (1.2, 13.6)	5.5 (-1.3, 11.3)
⁴ Neighborhood density	73 (5, 253)	70 (2, 228)	88 (22, 253)	35 (0, 135)	54 (0, 256)

¹ Sample size (number of target trees)

² Average annual total precipitation

³ Mean annual temperature

⁴ Count of neighboring trees within 15 m of the target tree

Table 2.2. Model comparison statistics including delta AICc (model AICc – best model AICc) and R^2 (in brackets) for models predicting RG for the 20-year period between 1992 and 2011. The modeling framework is hierarchical and evaluates the relative effects of site, size, age, climate, competition, and local differentiation to climate. Climate models estimate the effects of concurrent years' temperature and precipitation on growth (1 year model), as well as the additive effects of concurrent and prior years' temperature and precipitation on RG (2 year model). Neighborhood models estimate RG responses to crowding (NCI) in the absence of climate terms. Neighborhood models were alternately formulated to test whether crowding effects depend on the species composition of a neighborhood (mixed versus equal). Full models integrate climate (2 year) and neighborhood effects. Climate, neighborhood and full models include size, age and site effects, unless otherwise indicated. Species specific crowding indices from mixed neighborhood models were excluded from all full models by AICc. Full models were further modified to test for the importance of locally differentiated (LD) growth responses to temperature (T) and precipitation (P).

Model	ABLA	PIEN	PICO	PIPO	PSME
Site	1357.2 (0.05)	2645.5 (0.08)	2286.6 (0.07)	3669.6 (0.04)	2211.1 (0.16)
Size Site	1282.4 (0.07)	2511.7 (0.11)	2081.7 (0.13)	2889.0 (0.21)	1911.7 (0.24)
Size Age Site	187.8 (0.33)	824.6 (0.35)	694.9 (0.41)	582.6 (0.68)	734.6 (0.41)
Climate (1 year)	151.6 (0.36)	862.6 (0.32)	528.4 (0.45)	459.9 (0.57)	¹ 238.5 (0.39)
Climate (2 year)	166.1 (0.35)	572.4 (0.39)	460.0 (0.46)	156.9 (0.73)	¹ 175.9 (0.39)
Neighborhood (equal)	78.3 (0.37)	675.6 (0.40)	170.0 (0.46)	537.4 (0.62)	¹ 576.4 (0.43)
Neighborhood (mixed)	195.7 (0.35)	834.1 (0.34)	665.8 (0.43)	597.2 (0.68)	¹ 589.3 (0.36)
Full (equal comp)	71.7 (0.36)	70.1 (0.48)	82.8 (0.48)	2.3 (0.75)	¹ 43.2 (0.42)
LD Full (T)	¹ 0.0 (0.37)	¹ 0.0 (0.48)	¹ 0.0 (0.50)	0.0 (0.74)	¹ 41.0 (0.41)
LD Full (T & P)	¹ 56.4 (0.36)	1078.2 (0.44)	27.6 (0.50)	¹ 142.3 (0.64)	¹ 0.0 (0.43)

Parameters for Best Models (delta AICc = 0)

Model	ABLA	PIEN	PICO	PIPO	PSME
² NP	37	32	32	25	44
³ N	3020	3400	2860	2580	3579
⁴ Bias	1.014	1.001	1.013	1.031	1.016

¹ Size effect excluded by AICc

² NP = number of parameters

³ N = sample size (number of target trees * number of years)

⁴ Bias = slope of observed versus predicted

Figures

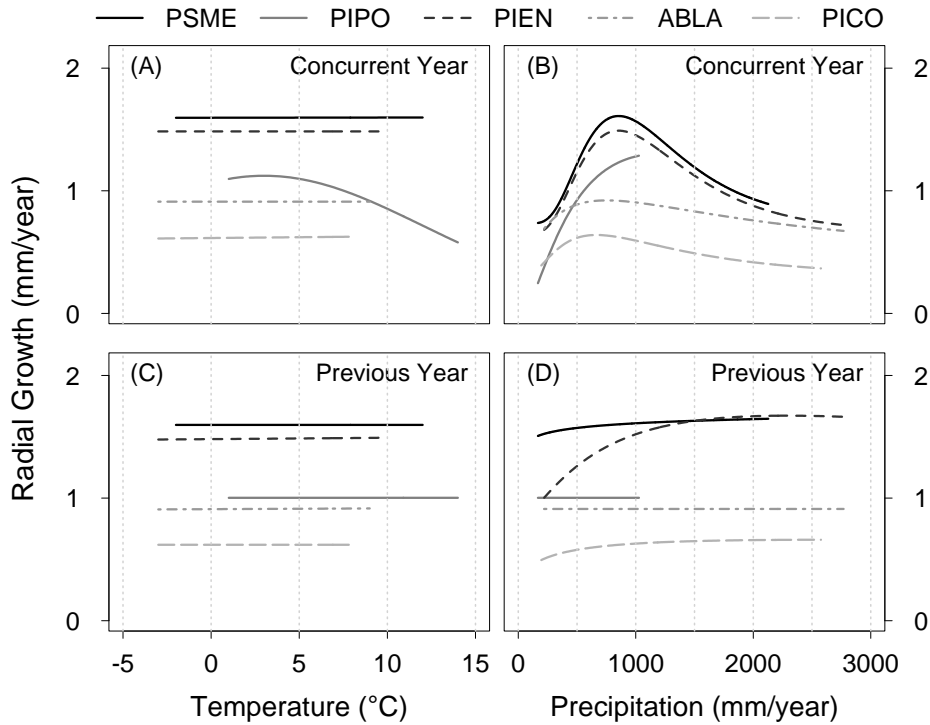


Figure 2.1. Growth responses (mm/year) by species for an average aged 30 cm diameter tree to concurrent and prior year mean annual temperature and annual total precipitation. Responses are based on parameters from the best fitting full models of growth and are averaged across sites. For the temperature panels, precipitation is held constant at the overall mean level for a species. Temperature is held constant in the precipitation panels. Competition is also held constant at the mean level for a species. The climate breadth of each response curve represents the observed climate range of each species. Species acronyms are defined in Table 2.1.

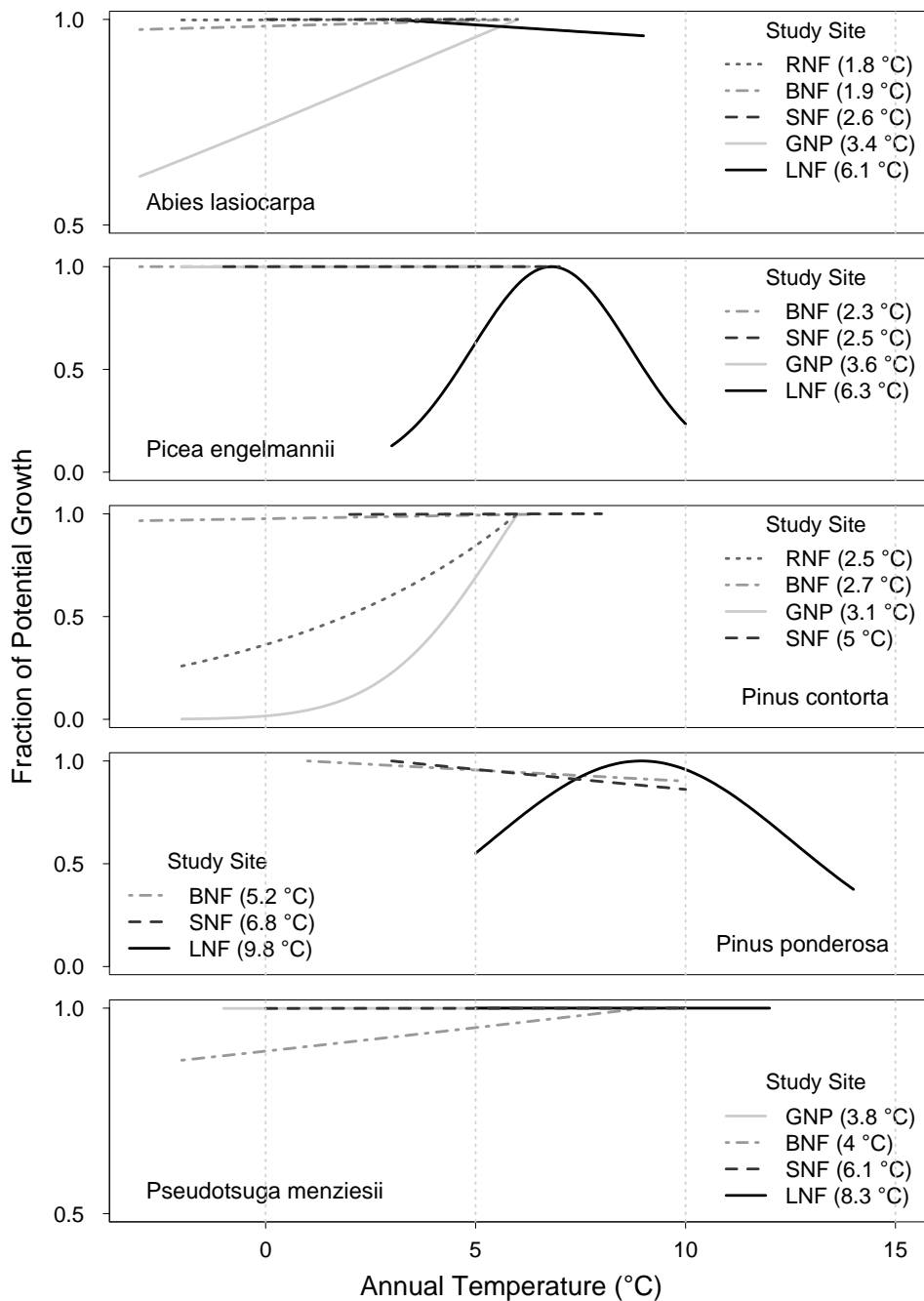


Figure 2.2. Site differentiated growth responses to annual temperature based on parameters from the best fitting full models. Response curves represent the site-specific fractional reduction in potential growth due to variation in temperature. The breadth of each site curve reflects the temperature ranges associated with field samples from that site. Sites are abbreviated as: BNF – Bighorn National Forest; GNP – Glacier National Park; LNF – Lincoln National Forest; RNF – Roosevelt National Forest; SNF – San Isabel National Forest. Site-specific mean annual temperatures are listed in parentheses.

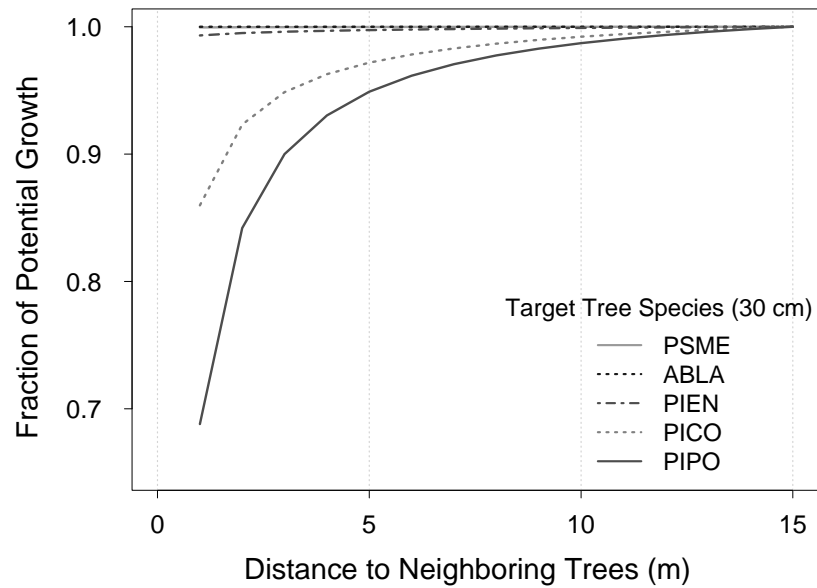


Figure 2.3. Radial growth responses to variation in the location of neighboring trees. Response curves represent the fractional reduction in potential growth for a 30 cm target tree at mean climate for a given species. Competition effects were quantified for hypothetical tree neighborhoods comprised of 5 trees (30 cm DBH) located at equal distances from a target tree. Separation distances between the 5-tree neighborhoods and the target tree were varied from 1 to 15 m to produce the response curves.

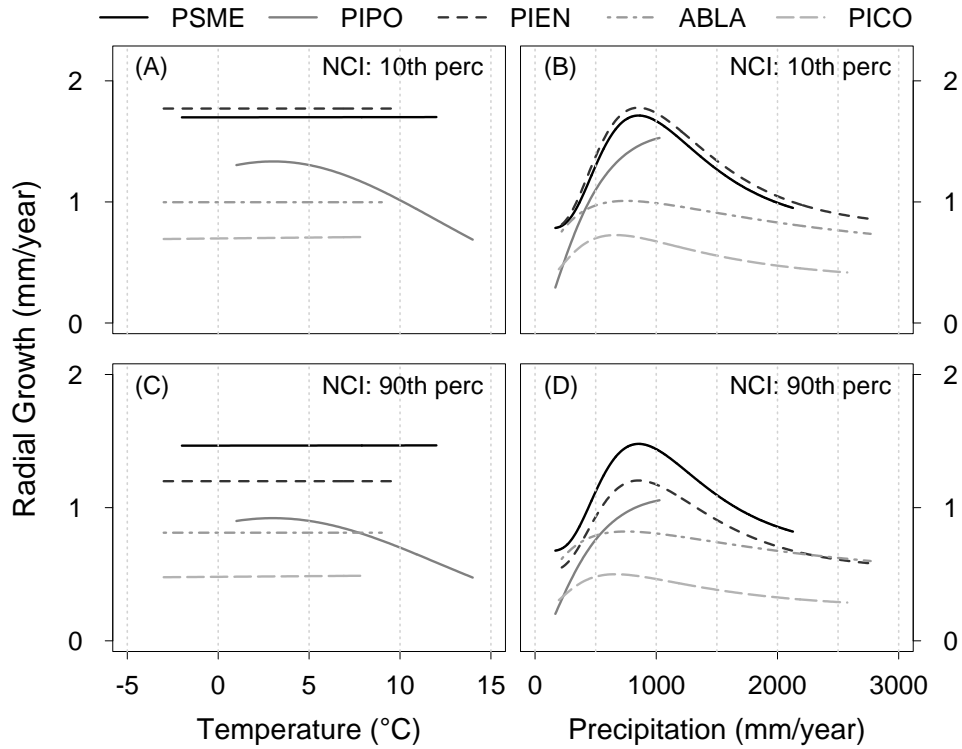


Figure 2.4. Growth responses (mm/year) by species for an average aged 30 cm diameter tree to concurrent year mean annual temperature and precipitation for two levels of NCI (10th and 90th percentile levels). Responses are from the most parsimonious full model of radial growth for each species. For the temperature panels, precipitation is held constant at the overall mean level for a species. Similarly, temperature is held constant in the precipitation panels.

REFERENCES

- Alfaro-Sánchez, R., Camarero, J.J., Sánchez-Salguero, R., Sangüesa-Barreda, G. & De Las Heras, J. (2016) Post-fire Aleppo pine growth, C and N isotope composition depend on site dryness. *Trees*, **30**, 581-595.
- Angert, A.L., Crozier, L.G., Rissler, L.J., Gilman, S.E., Tewksbury, J.J. & Chuncó, A.J. (2011) Do species' traits predict recent shifts at expanding range edges? *Ecology Letters*, **14**, 677-689.
- Blasing, T.J., Duvick, D.N. & Cook, E.R. (1983) Filtering the effects of competition from ring-width series. *Tree-Ring Bulletin*, **43**, 19-30.
- Boyden, S., Binkley, D. & Senock, R. (2005) Competition and facilitation between Eucalyptus and nitrogen-fixing *Falcataria* in relation to soil fertility. *Ecology*, **86**, 992-1001.
- Brooker, R.W. (2006) Plant-plant interactions and environmental change. *New Phytologist*, **17**, 271-284.
- Brooker, R.W., Maestre, F.T., Callaway, R.M., Lortie, C.L., Cavieres, L.A., Kunstler, G., Liancourt, P., Tielbörger, K., Travis, J.M., Anthelme, F. & Armas, C. (2008) Facilitation in plant communities: the past, the present, and the future. *Journal of Ecology*, **96**, 18-34.
- Buechling, A., Martin, P.H. & Canham, C.D. (2017) Data from "Climate and competition effects on tree growth in Rocky Mountain forests". *Dryad Digital Repository*, doi:10.5061/dryad.fv322.
- Bunn, A.G., Graumlich, L.J. & Urban, D.L. (2005) Trends in twentieth-century tree growth at high elevations in the Sierra Nevada and White Mountains, USA. *The Holocene*, **15**, 481-488.
- Büntgen, U., Kyncl, T., Ginzler, C., Jacks, D.S., Esper, J., Tegel, W., Heussner, K.U. & Kyncl, J. (2013) Filling the Eastern European gap in millennium-long temperature reconstructions. *Proceedings of the National Academy of Sciences*, **110**, 1773-1778.
- Burnham, K.P. & Anderson, D.R. (2002) *Model Selection and Multimodel Inference: A Practical Information-theoretic Approach*, 2nd edn. Springer-Verlag, New York, NJ, USA.
- Callaway, R.M. (1998) Competition and facilitation on elevation gradients in subalpine forests of the northern Rocky Mountains, USA. *Oikos*, **82**, 561-573.
- Canham, C.D., LePage, P.T. & Coates, K.D. (2004) A neighborhood analysis of canopy tree competition: effects of shading versus crowding. *Canadian Journal of Forest Research*, **34**, 778-787.
- Canham, C.D. & Murphy, L. (2016) The demography of tree species response to climate: sapling and canopy tree growth. *Ecosphere*, **7**, e01474. 10.1002/ecs2.1474.

- Canham, C.D., Papaik, M.J., Uriarte, M., McWilliams, W.H., Jenkins, J.C. & Twery, M.J. (2006) Neighborhood analyses of canopy tree competition along environmental gradients in New England forests. *Ecological Applications*, **16**, 540-554.
- Carrer, M. (2011) Individualistic and time-varying tree-ring growth to climate sensitivity. *PLoS One*, **6**, e22813.
- Carrer M. & Urbinati, C. (2004) Age-dependent tree-ring growth responses to climate in *Larix decidua* and *Pinus cembra*. *Ecology*, **85**, 730–740.
- Chatfield, C. (2004) *The Analysis of Time Series: An Introduction*, 6th Edn. Chapman & Hall/CRC, New York, NY, USA.
- Chen, P.Y., Welsh, C. & Hamann, A. (2010) Geographic variation in growth response of Douglas-fir to interannual climate variability and projected climate change. *Global Change Biology*, **16**, 3374-3385.
- Clark, J.S., Bell, D.M., Hersh, M.H. & Nichols, L. (2011) Climate change vulnerability of forest biodiversity: climate and competition tracking of demographic rates. *Global Change Biology*, **17**, 1834-1849.
- Coates, K.D., Canham, C.D. & LePage, P.T. (2009) Above versus below ground competitive effects and responses of a guild of temperate tree species. *Journal of Ecology*, **97**, 118-130.
- Cook, E.R. (1987) The decomposition of tree-ring series for environmental studies. *Tree-Ring Bulletin*, **47**, 37-59.
- Cook, E.R., Johnson, A.H. & Blasing, T.J. (1987) Forest decline: modeling the effect of climate in tree rings. *Tree Physiology*, **3**, 27-40.
- Coomes, D.A., Flores, O., Holdaway, R., Jucker, T., Lines, E.R. & Vanderwel, M.C. (2014) Wood production response to climate change will depend critically on forest composition and structure. *Global Change Biology*, **20**, 3632-3645.
- Cunningham, S. & Read, J. (2002) Comparison of temperate and tropical rainforest tree species: photosynthetic responses to growth temperature. *Oecologia*, **133**, 112-119.
- Daly, C., Halbleib, M., Smith, J.I., Gibson, W.P., Doggett, M.K., Taylor, G.H., Curtis, J. & Pasteris, P.P. (2008) Physiographically sensitive mapping of climatological temperature and precipitation across the conterminous United States. *International Journal of Climatology*, **28**, 2031-2064.
- Esper, J., Niederer, R., Bebi, P. & Frank, D. (2008) Climate signal age effects—evidence from young and old trees in the Swiss Engadin. *Forest Ecology and Management*, **255**, 3783-3789.

ESRI (2011) *ArcGIS Desktop: Release 10*. Environmental Systems Research Institute, Redlands, CA, USA.

Ettinger, A.K. & HilleRisLambers, J. (2013) Climate isn't everything: competitive interactions and variation by life stage will also affect range shifts in a warming world. *American Journal of Botany*, **100**, 1344-1355.

Fernández-de-Uña, L., Cañellas, I. & Gea-Izquierdo, G. (2015) Stand competition determines how different tree species will cope with a warming climate. *PLoS One*, **10**, p.e0122255.

Fritts, H.C. (1976) *Tree rings and climate*. Academic Press, New York, NY, USA.

Gazol, A. & Camarero, J.J. (2016) Functional diversity enhances silver fir growth resilience to an extreme drought. *Journal of Ecology*, **104**, 1063-1075.

Gea-Izquierdo, G., Fernández-de-Uña, L. & Cañellas, I. (2013) Growth projections reveal local vulnerability of Mediterranean oaks with rising temperatures. *Forest Ecology and Management*, **305**, 282-293.

Goldberg, D. & Novoplansky, A. (1997) On the relative importance of competition in unproductive environments. *Journal of Ecology*, **85**, 409-418.

Goffe, W.L., Ferrier, G.D. & Rogers, J. (1994) Global optimization of statistical functions with simulated annealing. *Journal of Econometrics*, **60**, 65-99.

Graumlich, L.J. (1993) A 1000-year record of temperature and precipitation in the Sierra Nevada. *Quaternary Research*, **39**, 249-255.

Grissino-Mayer, H.D. (2001) Evaluating crossdating accuracy: a manual and tutorial for the computer program COFECHA. *Tree-ring Research*, **57**, 205-221.

Hansen, A.J., Neilson, R.P., Dale, V.H., Flather, C.H., Iverson, L.R., Currie, D.J., Shafer, S., Cook, R. & Bartlein, P.J. (2001) Global change in forests: responses of species, communities, and biomes interactions between climate change and land use are projected to cause large shifts in biodiversity. *BioScience*, **51**, 765-779.

Harper, J.L. (1964) The individual in the population. *The Journal of Animal Ecology*, **52**, 149-158.

Jones, P.D. & Mann, M.E. (2004) Climate over past millennia. *Reviews of Geophysics*, **42**, RG2002, doi: 10.1029/2003RG000143.

Kunstler, G., Albert, C.H., Courbaud, B., Lavergne, S., Thuiller, W., Vieilledent, G., Zimmermann, N.E. & Coomes, D.A. (2011) Effects of competition on tree radial growth vary in importance but not in intensity along climatic gradients. *Journal of Ecology*, **99**, 300-312.

- Leimu, R. & Fischer, M. (2008) A meta-analysis of local adaptation in plants. *PLoS One*, **3**, e4010.
- Loehle, C. (2009) A mathematical analysis of the divergence problem in dendroclimatology. *Climatic Change*, **94**, 233-245.
- Littell, J.S., Peterson, D.L. & Tjoelker, M. (2008) Douglas-fir growth in mountain ecosystems: water limits tree growth from stand to region. *Ecological Monographs*, **78**, 349-368.
- Maestre, F.T., Callaway, R.M., Valladares, F. & Lortie, C.J. (2009) Refining the stress-gradient hypothesis for competition and facilitation in plant communities. *Journal of Ecology*, **97**, 199-205.
- Mamet, S.D. & Kershaw, G.P. (2013) Age-dependency, climate, and environmental controls of recent tree growth trends at subarctic and alpine treelines. *Dendrochronologia*, **31**, 75-87.
- Martin, P.H. & Canham, C.D. (2010) Dispersal and recruitment limitation in native versus exotic tree species: life-history strategies and Janzen-Connell effects. *Oikos*, **119**, 807-824.
- Martin, P.H., Canham, C.D. & Kobe, R.K. (2010) Divergence from the growth-survival trade-off and extreme high growth rates drive patterns of exotic tree invasions in closed-canopy forests. *Journal of Ecology*, **98**, 778-789.
- McMahon, S.M., Harrison, S.P., Armbruster, W.S., Bartlein, P.J., Beale, C.M., Edwards, M.E., Kattge, J., Midgley, G., Morin, X. & Prentice, I.C. (2011) Improving assessment and modelling of climate change impacts on global terrestrial biodiversity. *Trends in Ecology & Evolution*, **26**, 249-259.
- Miyamoto, Y., Griesbauer, H.P. & Green, D.S. (2010) Growth responses of three coexisting conifer species to climate across wide geographic and climate ranges in Yukon and British Columbia. *Forest Ecology and Management*, **259**, 514-523.
- O'Neill, G.A., Hamann, A. & Wang, T. (2008) Accounting for population variation improves estimates of the impact of climate change on species' growth and distribution. *Journal of Applied Ecology*, **45**, 1040-1049.
- Pacala, S.W., Canham, C.D., Saponara, J., Silander Jr, J.A., Kobe, R.K. & Ribbens, E. (1996) Forest models defined by field measurements: estimation, error analysis and dynamics. *Ecological monographs*, **66**, 1-43.
- Parker, A.J. (1982) The topographic relative moisture index: an approach to soil-moisture assessment in mountain terrain. *Physical Geography*, **3**, 160-168.
- Puettmann, K.J. & Reich, P.B. (1995) The differential sensitivity of red pine and quaking aspen to competition. *Canadian Journal of Forest Research*, **25**, 1731-1737.

R Core Team (2013) R: A language and environment for statistical computing. R Foundation for Statistical Computing, Vienna, Austria. URL <http://www.R-project.org/>.

Rehfeldt, G.E., Ying, C.C., Spittlehouse, D.L. & Hamilton Jr, D.A. (1999) Genetic responses to climate in *Pinus contorta*: niche breadth, climate change, and reforestation. *Ecological Monographs*, **69**, 375-407.

Rollinson, C.R., Kaye, M.W. & Canham, C.D. (2016) Interspecific variation in growth responses to climate and competition of five eastern tree species. *Ecology*, **97**, 1003–1011.

Ryan, M.G., Binkley, D., Fownes, J.H., Giardina, C.P. & Senock, R.S. (2004) An experimental test of the causes of forest growth decline with stand age. *Ecological Monographs*, **74**, 393-414.
Speer, J.H. (2010) *Fundamentals of tree-ring research*. University of Arizona Press, Tucson, Arizona.

Thurm, E.A., Uhl, E. & Pretzsch, H. (2016) Mixture reduces climate sensitivity of Douglas-fir stem growth. *Forest Ecology and Management*, **376**, 205-220.

Uriarte, M., Canham, C.D., Thompson, J. & Zimmerman, J.K. (2004a) A neighborhood analysis of tree growth and survival in a hurricane-driven tropical forest. *Ecological Monographs*, **74**, 591-614.

Uriarte, M., Condit, R., Canham, C.D. & Hubbell, S.P. (2004b) A spatially explicit model of sapling growth in a tropical forest: does the identity of neighbours matter? *Journal of Ecology*, **92**, 348-360.

Williams, A.P., Allen, C.D., Millar, C.I., Swetnam, T.W., Michaelsen, J., Still, C.J. & Leavitt, S.W. (2010) Forest responses to increasing aridity and warmth in the southwestern United States. *Proceedings of the National Academy of Sciences*, **107**, 21289-21294.

Wilmking, M., Juday, G.P., Barber, V.A. & Zald, H.S. (2004) Recent climate warming forces contrasting growth responses of white spruce at treeline in Alaska through temperature thresholds. *Global Change Biology*, **10**, 1724-1736.

Zhu, K., Woodall, C.W. & Clark, J.S. (2012) Failure to migrate: lack of tree range expansion in response to climate change. *Global Change Biology*, **18**, 1042-1052.

CHAPTER 3 A TEMPERATURE HISTORY FROM HIGH ELEVATION TREE SPECIES IN THE SOUTHERN ROCKY MOUNTAINS OF WESTERN NORTH AMERICA³

Synopsis

Historical temperature reconstructions are used to quantify the inherent internal variability of the climate system and allocate effects associated with external factors including anthropogenic carbon loading of the atmosphere. Continued debate concerning the degree of temperature variance within particular historical intervals highlights the need for additional regional scale temperature reconstructions. Here we use samples of radial growth from multiple high elevation tree species to reconstruct past temperatures for a relatively narrow study region in the southern Rocky Mountains of the western United States. We augmented archived data records with recent field samples to capture anomalous trends in modern temperature. We compared model performance using alternate standardization methods. Based on a hypothesis that non-linear relationships between tree growth and temperature potentially underlie a weakening or diverging response to modern climate trends, we explicitly evaluated the robustness of linear models. Model results revealed evidence for differentiated growth processes among populations within a species. Temperature reconstructions delineated distinct warm and cold intervals over the previous millennium relative to the overall historical mean. Estimated trends are congruent with recent, hemispheric scale reconstructions, but diverge somewhat with regard to the amplitude of past temperature variability.

³ In preparation for submission to the journal *Climate Change* with co-author P.H. Martin: Buechling, A. & Martin, P.H. (In prep). A temperature history from high elevation tree species in the southern Rocky Mountains. *Climate Change*.

Introduction

Anticipating the consequences of climate change requires robust estimates of future climate states. Paleodata critically inform the development and evaluation of both climate system and ecological response models (Williams & Jackson 2007). Temporal changes in climate are influenced by broad-scale external effects on the energy budget of the planet, driven by changes in solar insolation and atmospheric chemistry for example. Climate states are further characterized by an inherent natural variability driven by interactions between internal climate system components (Schurer *et al.* 2013). Thus, robust simulations of future climate depend on reliable estimates of both external forcings and this internal climate variability. The quantification of external forcing mechanisms from contemporary meteorological observations is constrained by limited temporal depth and a perturbation of the modern system by anthropogenic effects (Edwards *et al.* 2005). Thus, the refinement of climate simulation models that attempt to partition internal climate variability and various forcing mechanisms, and quantify corresponding climate system responses to those different mechanisms, depend on reliable reconstructions of past climate at regional and global scales (Free & Robock 1999; Hegerl *et al.* 2006; Schurer *et al.* 2013). These reconstructions are derived from various biotic and abiotic materials, such as ice cores, corals, sedimentary deposits, and tree rings that serve as proxies for corresponding climate conditions present during their formation (Jones *et al.* 2009). Spatial networks of proxy records are statistically composited to estimate climate parameters, particularly temperature, over large geographical scales. Although general trends in Holocene temperature are well established for the northern hemisphere, persistent discrepancies are evident between proxy reconstructions regarding the amplitude and timing of particular warm and cold intervals (Ljungqvist 2010; Marcott *et al.* 2013; Wilson *et al.* 2016). For example, estimates from proxy reconstructions for

the breadth of late Holocene temperature variability vary from 0.2 to 1.0 °C among studies (Ljungqvist 2010; Frank *et al.* 2010). Discrepancies in reconstructed temperatures have important implications for the magnitude, detection and attribution of forcing mechanisms, and the associated sensitivity of the climate system to continued increases in anthropogenic greenhouse gases (Edwards *et al.* 2007). The lack of congruence among studies may be partially attributed to inadequate geographical replication and limited temporal depth of available proxy records (Esper 2009). In particular, many existing reconstructions are based on calibration data that predate the steep warming trends that have been observed since ~1990. Associated models may thus under-estimate temperature conditions for historical periods with comparable mean climate (Wilson *et al.* 2007; Ljungqvist 2010).

Statistical analyses that attempt to reconstruct past temperatures depend strongly on assumptions that the processes which generated a particular proxy record are stable through time and that relationships between proxy formation and climate are linear (Ljungqvist *et al.* 2012). However, evidence for apparently non-stationary growth processes in trees has been identified in some dendroclimatic studies from different regions (e.g. Jacoby & D'Arrigo 1995; Jacoby *et al.* 2000; Lloyd & Fastie 2002; Wilson & Luckman 2003). Specifically, radial growth (RG) in some conifer species at some high latitude sites has deviated from an expected positive linear response to increasing warmth in the latter half of the 20th century. Documented declines in temperature sensitivity and even shifts from positive to negative growth responses have been widely discussed in the dendroclimatic literature and are commonly referred to as divergence phenomena (D'Arrigo *et al.* 2008). Various hypotheses have been postulated to account for divergent growth processes, including warming related drought effects on growth that dampens an otherwise positive linear response to temperature (Lloyd & Fastie 2002; Wilmking *et al.*

2004), changes in growing season length associated with variation in the seasonality of precipitation (Vaganov *et al.* 1999), differing responses to daily maximum and nightly minimum temperatures amplified by diverging temporal trends in these parameters (Wilson & Luckman 2003; Way & Oren 2010), and anthropogenic pollution-related effects on atmospheric ozone and solar insolation (D'Arrigo *et al.* 2008). Loehle (2009) argued that observations of a divergence from expected growth reflects inherently non-linear RG responses to climate. Temperature thresholds for divergent growth responses identified in some dendroclimatic studies (D'Arrigo *et al.* 2004; Wilmking *et al.* 2004) support this hypothesis. Recent studies using spatially explicit, individual-based modeling approaches have described unimodal or asymptotic RG responses to climate for a range of species (Kunstler *et al.* 2011; Coomes *et al.* 2014; Canham & Murphy 2016; Buechling *et al.* 2017). Those analyses used multivariate techniques to estimate RG responses to temperature while explicitly quantifying and controlling for the interacting effects of precipitation and competition; however, those studies also parameterized growth functions with data distributed across broad climatic gradients. Dendroclimatic studies, in contrast, are generally based on samples collected at subjectively selected, thermally extreme environments, such as high-elevation treeline, where temperature is assumed to be most limiting to growth (Hoch & Körner 2003) and where growth responses are hypothesized to be linear in shape (Fritts 1976). However, if assumptions of linearity are not robust across all or even most treeline sites, linear models may generate biased predictions of historical temperature variation by failing to capture climate thresholds and other non-linear growth-climate relationships (Loehle 2009).

In this study, we used samples of radial growth from multiple high elevation tree species to reconstruct past temperature variability for a relatively small area in the southern Rocky Mountains of the western United States. Historical temperatures have been estimated previously

for northern portions of the Rocky Mountain ecoregion by Kipfmueller (2008) and Luckman and Wilson (2005), while a comparable reconstruction for the southern portion of the Rockies has not been developed to our knowledge. We used data principally from *Picea engelmannii* Parry ex Engelm. (Engelmann spruce), as previous analyses have shown a high degree of fidelity between RG in this species and temperature records (Brown & Shepperd 1995). We supplemented archived RG measurements from various locations and from different authors with recent field samples in an effort to extend the temporal depth of associated collections and capture modern, apparently anomalous warming trends. As the statistical treatment of tree growth data has been specifically identified as a potential source of uncertainty in climate reconstructions (Marcott *et al.* 2013), we compared model performance using alternate standardization methods. To test that assumptions of linearity are satisfied, we developed individual-based regression models in a likelihood framework to explicitly evaluate the shape of RG responses to temperature. We also estimated the magnitude of precipitation effects on growth, to confirm that reconstructions are robust to any potential modulating and confounding warming-induced drought processes that could bias model predictions (Loehle 2009).

Materials and methods

Study area

Selected sites for both field sampling and archived ring width (RW) data were located within a relatively constrained region centered on the continental divide in the central to southern portions of the Rocky Mountains in the western United States (Fig. 3.1). Sample sites are distributed from Almagre Mountain in central Colorado (38.77° N, 104.98° W) to the Medicine Bow Range (41.5° N, 106.24° W) in southern Wyoming. All sites are proximate to high elevation tree line, ranging in elevation from ~3100 to 3570 m (Table 3.1). Climate is

comparatively uniform in terms of temperature, with annual mean temperature varying from ~0.8 to 1.7 °C depending on location (Table 3.1). Precipitation is more variable ranging from ~650 to 1140 mm annually across sites. Radial growth (RG) measurements for 3 tree species were analyzed, including *Pinus aristata* Engelm. (bristlecone pine), *Pinus flexilis* James (limber pine), and *Picea engelmannii* Parry ex Engelm. (Engelmann spruce).

Growth data

Field data collection was restricted to *P. engelmannii*. We sampled *P. engelmannii* at 6 locations with archived RW records and at another 6 locations with no known existing data. Archived records for an additional 15 sites for 3 species, *P. engelmannii*, *P. aristata*, and *P. flexilis*, were acquired for analysis, but were not resurveyed (Fig. 3.1 & Table 3.1). Resurvey sites for *P. engelmannii* were selected based on accessibility and the quality of the associated location information. Archived datasets were obtained from the International Tree Ring Data Bank (<https://data.noaa.gov/dataset/international-tree-ring-data-bank-itrd>).

We subjectively selected individual adult *P. engelmannii* trees from the dominant canopy layer for sampling at each target location. Trees with obvious external damage or in areas recently exposed to disturbance were excluded. Large diameter trees and individuals occupying rocky substrates near treeline were preferentially targeted. We collected 1 to 2 increment cores per sample tree at a height of 30 cm above the root crown. We collected additional samples (up to 4 cores per tree) if the shape of the stem was strongly asymmetric or if the quality of a sample core was uncertain. Cores were extracted as low as possible on the stem to maximize the time depth of each RG series for cross-dating purposes and to obtain age estimates as close to the germination year as possible.

Approximately 350 trees were sampled across 12 sites over two field seasons. Associated cores were mounted, sanded until tracheid cells were clearly visible under magnification, and visually cross-dated using the entire series length to ensure correct annual dating (Speer 2010). We then measured ring widths to a precision of 0.001 mm using a Velmex measuring system. The resulting RG series were examined for measurement and dating errors using COFECHA (Grissino-Mayer 2001). Multiple measurement series from the same tree were averaged to produce a single time series of annual growth.

After combining field and archived RG datasets, final sample sizes across the study region as a whole ranged from 138 trees for *P. aristata*, 591 trees for *P. engelmannii*, and 126 trees for *P. flexilis* (Table 3.2). Mean samples sizes within individual study sites ranged from 28 (10-40) for *P. aristata*, 33 (16-66) for *P. engelmannii*, and 32 (27-40) for *P. flexilis*.

The raw measurements of RG were subsequently transformed into approximately stationary time series using two alternate methods; regional curve standardization (RCS; Briffa *et al.* 1992; Esper *et al.* 2003) and normalized basal area increment (BAI). RCS is a commonly used statistical technique in dendroclimatology designed to remove short term trends in RG variance attributed to biological factors, including age, size and disturbance effects, while simultaneously retaining long term secular trends and spectral properties hypothesized to be driven by climate (Briffa *et al.* 1992). This method involves the computation of growth anomalies for each year in each series based on associated ring width deviation from an empirically derived biological growth function, which estimates expected growth based on individual tree age (Esper *et al.* 2002). Anomalies from the expected growth function are assumed to be caused by climate (Esper *et al.* 2003). In this study, we fit a rigid spline function to all age aligned RG series to estimate the regional growth function. Since we acquired archival

RG measurements in this study with unknown pith or origin ages, we assumed that the oldest measurement year recorded represents the germination date of the corresponding tree. We subsequently scaled actual growth by expected growth to produce a standardized index of RG for use in regression analyses. We also computed an alternate index of RG by transforming linear ring width measurements into estimates of BAI. Basal area estimates account for size or geometric trends inherent in linear measures of RG. We scaled basal area estimates with the corresponding mean BAI of each sample to normalize data among trees occupying dissimilar environments.

Climate data

Unlike in European countries, climate data collection at high elevations (>2400 m) in the Rocky Mountain region has been inconsistent over time and reliable continuous climate records prior to ~1960 are sparse in our study area (Nolan Doesken, Colorado State Climatologist, personal communication). Thus, we used gridded climate data from PRISM (Daly *et al.* 2008) to develop climate variables for response analyses and model fitting. PRISM is a regression model that generates spatially continuous estimates of daily temperature and precipitation for the United States at high spatial resolution (30 arcsec or ~800 m pixel size). Gridded climate data have been used previously to calibrate models of historical climate (e.g. Luckman & Wilson 2005).

A prior study evaluated the performance of PRISM by comparing gridded model output with independent high elevation weather station data collected on an ecological gradient in the Fraser Experimental Forest in central Colorado (see details in Buechling *et al.* 2016), which encompasses two of our sample sites (Fool and Lexen). Goodness of fit analyses between PRISM and meteorological records revealed high model accuracy despite ubiquitous temperature inversions caused by cold air drainage that could potentially bias model predictions. Estimates of

mean absolute error ranged from ~0.8 to 2.0 °C depending on season, but were only ~1.0 °C for growing season months (Fig. S3.1 in Appendix).

We extracted PRISM data (30 arc-second or ~800 m resolution) for sample locations using a weighted interpolation of adjacent pixel values. Data were aggregated into various permutations of seasonal means. Annual periods were defined according to a U.S. Geological Survey hydrological year that spans a 12 month period from October 1st of the previous year to September 30th of the current year. A regional composite climate series was derived by averaging local PRISM climate values across all sample sites.

Growth - climate relationships

We investigated the strength, continuity, and shape of relationships between RG and climate for each species using correlation analyses and regression models. Pearson correlation coefficients were calculated between the standardized RG indices and various permutations of seasonal climate to identify an optimum temperature response variable for use in predictive models of historical temperature. Moving window correlations were used to evaluate the temporal stability of growth-climate relationships. We also explicitly modeled relationships between temperature and RG to ensure that assumptions of linearity are valid. Specifically, we developed multiple regression models to estimate RG responses to climate based on alternate functional forms for the climate covariates, including non-linear functions. These regression models were constructed in a likelihood, multiplicative framework with the following covariates:

$$RG = PRG[\text{site}] \times \text{Size} \times \text{Age} \times \text{Temperature} \times \text{Precipitation} \quad [\text{Eqn. 1}]$$

We used untransformed linear measurements of RG in mm/year for individual trees as the response variable. PRG represents potential or expected RG for a hypothetical free-growing tree and was estimated uniquely for each sample site. Tree size, age, and climate effects are scalar

modifiers that proportionally reduce or increase potential growth. Size, age, and precipitation effects were fit with lognormal functions:

$$\text{Effect} = \exp\left[-0.5 \times \left(\frac{\ln\left(\frac{x}{\delta}\right)}{\sigma}\right)^2\right] \quad [\text{Eqn. 2}]$$

where x corresponds to the fitted value of size, age or precipitation, δ represents the modal value of the effect corresponding to maximum potential growth (PRG) and σ describes the breadth of the function. Size effects were parameterized with tree diameter (cm) in the year of growth.

Temperature effects were initially estimated using a Gaussian function:

$$\text{Temperature effect} = \exp\left[-0.5 \times \left(\frac{(t - \text{temp.a})}{\text{temp.b}}\right)^2\right] \quad [\text{Eqn. 3}]$$

where t is observed temperature, and temp.a and temp.b describe the mode and variance of the function, respectively. Gaussian functions have flexible shapes that can fit monotonically increasing, decreasing, or unimodal data distributions. However, we also tested strictly linear forms for the temperature effect:

$$\text{Temperature effect} = \text{temp.a} * t + \text{temp.b} \quad [\text{Eqn. 4}]$$

In this case, temp.a and temp.b represent the slope and intercept of the function respectively.

Previous studies have detected evidence for locally differentiated climate responses based on physiological acclimation or genetic adaptation among disjunct populations of the same species (Buechling *et al.* 2017). Thus we tested for evidence of adaptation or acclimation to both temperature and precipitation at each study site by modifying climate functions so that a unique mode and variance was estimated for each climate variable at each sample site. Differentiated climate functions quantify unique, site-specific growth responses to corresponding climate regimes that differ across the study region.

Temperature reconstruction

Regression models were developed to predict historical temperatures based on relationships with RG. Following traditional methods, we used composite mean chronologies of growth as covariates. These mean chronologies were computed by averaging the standardized indices of growth for individual sample trees, previously discussed, using a biweight robust mean to minimize outliers. We filtered sites used in the composite chronologies by the strength of their response or correlation with climate. Specifically, we calculated a threshold correlation, based on the mean correlation among all sites between standardized growth indices and local site-specific temperature. Only data from sites that exceeded this threshold were used to calculate composite mean growth indices.

We again constructed regression models using likelihood methods. Alternate models were tested based on different permutations of model covariates and standardized RG indices. A single composite regional chronology and associated covariate were calculated by averaging data from all species and sites, after screening for threshold responses to temperature. We also investigated the importance of locally differentiated growth processes. We used hierarchical cluster analyses with a complete linkage algorithm to classify and group populations with congruent RG responses to climate. A total of 3 distinct clusters were identified. Growth indices from clustered populations were averaged into distinct composite chronologies and used to parameterize independent model covariates. For comparative purposes, we also conducted principle component analyses (PCA) to quantify independent, low dimensional, uncorrelated predictors representing site-specific divergent RG responses. We used the first 3 principle component scores (PCs) from a PCA of normalized BAI, which captured over 90% of the variance in the original RG series, as covariates in an alternative regression model.

Thus, full multiplicative models with a seasonal temperature response (T in °C) had the following form:

$$T = \text{POT} \times \prod_{i=1}^n (\text{RG}_0 + \text{RG}_1)_i \quad [\text{Eqn. 5}]$$

where POT is a potential response term (°C), RG_0 and RG_1 are standardized indices of growth for the i th cluster (or PC) for the year concurrent with the temperature prediction and one year lagged forward respectively, and n represents the total number of population clusters (or PCs) used in the model. In the case where $n=1$, a single composite regional mean RG index was computed from all screened sites. Lagged parameters were tested based on an assumption that prior year climate may influence current year growth (Fritts 1976). Each RG term was estimated using a linear function, as in Eqn. 4.

Model specification

We used simulated annealing with 20,000 iterations to solve for maximum likelihood estimates of all model parameters (Goffe *et al.* 1994). Bias, proportion of variance explained (R^2), and root mean square error (RMSE) were used to quantify the goodness of fit of alternate likelihood models. Bias was quantified from the slope of the linear regression of observed versus predicted temperature. Akaike information criterion corrected for small sample size (AIC_c) was used to select the most parsimonious models (Burnham & Anderson 2002).

All analyses were conducted in R (Version 3.2.3; R Core Team 2013). Correlation analyses were conducted using the package treeclim version 2.0.0. RG standardization and mean chronologies were built using the package dplR version 1.6.4. PCA was performed using the function prcomp in the stats package version 3.3.2. Likelihood models were constructed using the likelihood package version 1.6.

Results and Discussion

Evidence for non-stationary or diverging relationships between RG and temperature, driven by co-varying factors or non-linear growth responses, was not strong in these datasets. Results from individual based models, for example, indicate that RG responses to temperature are linear in shape for treeline populations in this region. Specifically, the most parsimonious growth models for all species were based on linear temperature functions (Fig. 3.2 & Fig. S3.2; Table 3.3). Models using flexible Gaussian functions were consistently less robust in terms of AICc. Further, results from a moving 30-year correlation analysis with local site temperatures did not reveal an unequivocal reduction in correlation between RG and rising temperatures in recent decades (Fig. S3.3), which when present may reflect non-stationary processes (D'Arrigo *et al.* 2008). Rather, correlations vary substantially throughout the 20th century, the period of modern instrumental records, and are not synchronized between sites. We argue that these patterns reflect the presence of substantial non-climatic noise in the growth data for these species as well as a relatively limited temporal depth and insufficient sample sizes to explicitly explain these relationships. Furthermore, potentially non-stationary biases in the PRISM data (Fig. S3.1) may also influence the temporal stability of correlations (Wilson *et al.* 2007).

The multiplicative framework of our models allowed relationships between RG and temperature to be quantified while controlling for precipitation variability (Fig. S3.2). The most parsimonious models for all species estimated both temperature and precipitation effects, indicating that these species are sensitive to both factors (Table 3.3). Models based on temperature alone were consistently weaker than more complex models incorporating multiple climate parameters (Table 3.3). The shape of the precipitation effect was essentially flat for *P. engelmannii*, Gaussian for *P. aristata*, and approximately linear and moderately positive for *P.*

flexilis (Fig. 3.2 & S3.2). Correlations analyses generally support these model estimates, indicating weak relationships between RG and both annual and growing season precipitation for both *P. engelmannii* and *P. aristata* ($r < 0.1$; Fig. S3.4) and slightly stronger correlations for *P. flexilis* ($r \sim 0.2$). Moderate evidence for a substantive influence of precipitation on RG for these populations, despite their upper treeline location, indicates that moisture effects have the potential to bias reconstruction models of historical temperature (Loehle 2009). Drought effects may be important (Wilmking *et al.* 2004), but high annual precipitation also has the potential to effect growth rates in *P. aristata* and *P. flexilis* and for some populations of *P. engelmannii* (Fig. S3.2). To maximize the fidelity of RG responses to temperature and minimize prediction bias associated with the confounding effects of moisture availability, all PIFL populations were excluded from model calibration analyses due to relatively high correlations ($>$ overall mean for all species) with annual precipitation.

Scientific and policy debates concerning global climate change have generally been framed in terms of trends in mean annual temperature. Similarly, general circulation models simulate long-term trends in climate. However, various permutations of growing season temperature provided stronger correlations with RG than annual climate composites in these datasets (Fig. S3.5), despite high mean correlations between annual and seasonal temperature ($r \sim 0.81$). In some cases, individual monthly temperatures were more strongly correlated with RG than seasonal means (Fig. S3.5), but monthly variables are less representative of annual conditions, and aggregated growing season or annual temperatures have been more commonly used in previous climate reconstructions (e.g. Ljungqvist 2010; Wilson *et al.* 2016). We ran preliminary calibration models with a July temperature response, but model performance in terms of AICc and R^2 was weaker than comparable seasonal based models (data not shown). We

therefore used June to August mean temperature as the target response variable in temperature models, and hence assume that any decoupling of annual and seasonal climate trends over time is minor.

Various statistical measures were calculated to evaluate and compare the strength of alternate reconstruction models (Table 3.4). Model performance in this study is partly constrained by limitations in the temporal length of available calibration data. Gridded PRISM datasets span years from 1895 to 2010, but data available for model fitting are further reduced and limited to the maximum period of overlap between the component covariates in a given model. Unequal calibration sample sizes precludes a direct comparison of all models based on parsimony alone, as quantified by AICc. AICc values do indicate that reconstruction models that included both current and forward lagged standardized RG terms (2 year models) were consistently stronger than models that parametrized either concurrent or lagged RG covariates only (Table 3.4). AICc values further suggest that the two standardization methods used in this study, RCS and normalized BAI produce models with similar levels of parsimony.

Evidence for differentiated growth responses to temperature among disjunct populations of *P. engelmannii* was identified by likelihood analyses (Fig. S3.2; Table 3.3). In support of these results, hierarchical cluster analyses revealed two distinct groups or clusters of *P. engelmannii* populations based on their unique, divergent growth responses to climate (Fig. S3.6). Thus, models that incorporated discrete covariates representing these site specific growth responses (cluster models) generated predictions with greater fidelity to the calibration data (higher R^2 and lower RMSE) compared with models that averaged growth indices from all populations into single composite covariates (regional models; see Table 3.4). Further, composite regional models generated unbiased, but significantly autocorrelated residuals, suggesting that

associated reconstructions did not capture long term trends in temperature variability (Wilson *et al.* 2016). In particular, the smoothed reconstruction from the regional model based on RCS exhibits an essentially flat long term trend (Fig. 3.3B). We argue that the process of merging diverging growth responses from different species and differentiated populations into composite covariates dampens predicted long term trends and variability in the associated reconstructions.

Model parsimony and fit statistics indicate that the most robust reconstructions were generated by models with three cluster terms (Table 3.4). RMSE for these models was limited to $\sim 0.6^{\circ}\text{C}$, which is less than the standard deviation of the PRISM calibration data ($\sim 0.91^{\circ}\text{C}$). Further, corresponding model residuals were unbiased, normally distributed, and random. The fit of the PC model was marginally less robust compared with cluster models, which may be a reflection of a more constrained data fitting range (Table 3.4). Cluster reconstructions based on RCS and BAI were indistinguishable based on uncertainty statistics. Associated predictions for the calibration period were also similar (Fig. 3.4), though models based on BAI more closely approximate temperature trends evident in the most recent two decades of the study period (Fig. 3.3 & 3.4). However, between ~ 1500 and ~ 1800 , the RCS based model generated substantially warmer temperatures compared with other models. Prior to 1495, both the RCS and BAI models rely on data from *P. aristata* only and associated reconstructions converge over this interval. We suggest that sample sizes and age distributions within individual clusters may be insufficient for estimating and fitting robust regional curves for standardization purposes (Esper *et al.* 2016), leading to biased model results. Thus, all subsequent summaries and discussion are based on results from the three cluster BAI model.

Reconstructed temperatures for this study area exhibit substantial variability over decadal time scales (Table 3.5), but also track longer term trends consistent with previous reconstructions

(Fig. 3.5). In particular, the pre-industrial era is characterized by a prolonged period of elevated temperatures in the early portions of the record, commonly denoted as a Medieval Warm Period (MWP; e.g. Crowley & Lowery 2000), followed by an interval of cooler mean conditions, generally referred to as the Little Ice Age (LIA; e.g. Free & Robock 1999). The precise timing of these periods in the northern hemisphere has been variously defined, depending on proxy source and reconstruction method (Wilson *et al.* 2016), with substantial spatial and geographical variation within local records (Christiansen & Ljungqvist 2012; Trouet *et al.* 2013). In general, warmer conditions associated with the MWP have been found to range from between ~900 and 1300 AD across the northern hemisphere, while subsequent cooler conditions associated with the LIA persist in most reconstructed records until ~1850 or 1900 AD (Ljungqvist 2010). In northern Colorado, climate appears to have shifted from a warmer to colder state late in the 12 century (Fig. 3.5), which approximately agrees with other regional records from northern portions of the Rocky Mountains (Luckman & Wilson 2005) and from the Colorado Plateau (Salzer & Kipfmueller 2005), as well as with recent hemispheric scale reconstructions (Christiansen & Ljungqvist 2012; Wilson *et al.* 2016). Thus, four of the five warmest climate normals (30-year averages) in this record occurred prior to the end of the 12th century, while the five coldest normals occurred subsequently (Table 3.6). Interestingly, the second coldest 30-year period, 1666-1695, coincides with occurrences of some of the most extensive forest fires documented for this region (Kipfmueller & Baker 2000; Buechling & Baker 2004; Sibold *et al.* 2006), although these large fire events are superimposed on a longer term trend of reduced biomass burning during the Little Ice Age period (Marlon *et al.* 2012; Higuera *et al.* 2014). Cool climate conditions associated with the LIA return to a warmer state in Northern Colorado beginning in the late 1700s (Fig. 3.5). The second warmest climate normal of the pre-industrial period is

estimated to have occurred between 1776 and 1815 (Table 3.6). The end of LIA conditions in this record predate corresponding warming trends identified in other reconstructions (Fig. 3.5), but are congruent with rising solar insolation between 1750 and 1850 (Eddy 1977; Fig. 3.6).

Despite a high degree of congruence among studies concerning the general temporal extent of warm and cold intervals in the historical record, the amplitude of climatic variability associated with these periods remains uncertain (Crowley & Lowery 2000; Jones *et al.* 2009; Frank *et al.* 2010; Ljungqvist 2010). In this study, historical climate conditions in northern Colorado were characterized by substantial decadal scale variability (Table 3.5). Model results reveal a maximum temperature amplitude of $\sim 0.45^{\circ}\text{C}$ between the warmest and coldest 30-year intervals prior to the period of modern industrialization. Based on a 100-year moving window analysis, the maximum difference between the warmest and coldest century was $\sim 0.42^{\circ}\text{C}$. These results are comparable to but somewhat lower than previous amplitude estimates derived from networks of proxy datasets covering the northern hemisphere (Mann *et al.* 2008; Ljungqvist 2010; Wilson *et al.* 2016), which approach $\sim 1.0^{\circ}\text{C}$ on a decadal scale. Although, the overall record of modeled temperatures for northern Colorado correlates moderately well with selected hemispheric scale reconstructions (Fig. 3.5), particular intervals within both the MWP and LIA were estimated to be less extreme in this analysis. For example, the decade centered on the year 1700 was estimated to be substantially colder in the hemispheric reconstructions of Wilson *et al.* (2016) and Christiansen & Ljungqvist (2012), as well as in the regional model for British Columbia from Luckman and Wilson (2005). Although, differences between reconstructions may reflect local climatic variability, methodological limitations may also contribute to biased temperature estimates in this study. Limited samples sizes for recent years and across extreme temperature gradients may have constrained our ability to detect non-linear relationships

between RG and temperature that could potentially dampen variance estimates associated with extrapolated data (Loehle 2009). Additionally, a nominal warm bias in the PRISM data (Fig. S3.1) could affect model calibration and associated temperature estimates, particularly with respect to the degree of cooling during the LIA. Instrumental data uncertainty has previously been identified as a potential source of prediction error (Esper *et al.* 2016). A positive bias in the fitting data could also explain a more pronounced warming trend estimated for the mid to late 19th century in this record compared with other reconstructions (Fig. 3.5). Alternately, local or regional model results may reflect associated climatic variability not discernable in large-scale hemispheric studies, which, by combining proxy datasets from multiple sources effectively smooth local-scale variability (Ljungqvist 2010; Wilson *et al.* 2016).

Predicted mean temperatures for northern Colorado during the modern era exceed historical pre-industrial temperature means over the entire length of this reconstruction record based on a decadal-scale temporal resolution (Fig. 3.3; Table 3.5). Maximum reconstructed temperatures for the most recent decades in this study agree closely with predicted mean temperatures for the northern hemisphere from Wilson *et al.* (2016; Fig. 3.5), but do underestimate corresponding values in the PRISM record (Fig. 3.4). We argue that limited calibration data coverage for the most recent period beginning ~1995 (Fig. 3.3C), when temperatures in Colorado began increasing substantially (Rangwala & Miller 2012), constrain the ability of this model to reproduce extreme events. Large estimated support intervals (Fig. 3.3A) for this period are similarly driven by comparatively small sample sizes. Limited sample replication has been previously identified as a major impediment to prediction performance (Wilson *et al.* 2016).

Climate trends associated with the LIA and MWP correlate only moderately strongly with various forcing mechanisms in this study (Fig. 3.6). For example, Pearson correlations

between atmospheric CO₂ and temperature, when smoothed with a 50 year spline and lagged by 50 years, were ~0.31. Pearson correlations between spline transformed temperature and solar irradiance series were ~0.43. Previous studies using superposed epoch analyses have identified significant relationships between volcanic activity and depressed temperatures (Lough & Fritts 1987; Kipfmueller 2006). However, robust analyses investigating the influence of external forcing mechanisms on climate variability require the use of coupled atmosphere-ocean general circulation models (GCMs). For example, GCM simulations have determined that temperature trends during the LIA were significantly shaped by variations in solar output and volcanic aerosols, as well as changes in atmospheric greenhouse gas concentrations (Free & Robock 1999; Schurer *et al.* 2013). Further efforts to refine historical reconstructions of temperature are required to more precisely quantify these forcings and thus better forecast future climate responses to anthropogenic CO₂ emissions.

Tables

Table 3.1. Site attributes associated records of radial growth used in temperature reconstructions, including mean elevation (Elev), mean aspect (Asp), 30-year (1980-2010) annual temperature (Temp) and precipitation (Prec) means (based on PRISM), and latitude (Lat) and longitude (Long) coordinates. A total of six archived ring width datasets were updated with additional samples collected in 2011 and 2014. Six new sites were sampled in 2014. References are provided for archived datasets. Sites arranged by species and from low to high elevation within species. Species include *Pinus aristata* (PIAR), *Picea engelmannii* (PIEN), and *Pinus flexilis* (PIFL).

Site	Species	Elev (m)	Asp (°)	Temp (°C)	Prec (mm)	Lat (°N)	Long (°W)	Reference
Almagre L	PIAR	3535	NA	0.99	657	38.77	104.97	LaMarche & Harlan 1968a
Evans	PIAR	3535	NA	0.26	729	39.63	105.58	LaMarche & Harlan 1968b
Goliath	PIAR	3535	NA	0.26	728	39.63	105.58	Graybill 1983b
Almagre G	PIAR	3536	NA	0.75	666	38.77	104.98	Graybill 1983a
Windy	PIAR	3570	NA	0.04	759	39.32	106.08	Graybill 1985
³ Rocky	PIEN	3099	302	0.50	922	41.472	106.24	
Cameron	PIEN	3100	NA	0.58	925	40.55	105.83	Bigler & Veblen 2003
Medicine	PIEN	3150	NA	0.64	1144	41.381	106.337	Briffa & Schweingruber 1983a
¹ Sand	PIEN	3170	360	-0.20	1052	41.451	106.273	Brown <i>et al.</i> 1999
³ Brooklyn	PIEN	3218	80	-0.05	950	41.37	106.234	
¹ Jeff Lake	PIEN	3296	300	-0.79	1110	41.399	106.279	Earle 1990
¹ Rainbow	PIEN	3320	160	0.53	998	40.024	105.589	Kienast 1982
¹ Lexen	PIEN	3370	358	1.06	683	39.89	105.935	Brown & Shepperd 1995
Niwot Ridge	PIEN	3400	NA	1.67	878	40.05	105.55	Schweingruber 1982
³ Crags	PIEN	3411	264	-0.05	663	38.868	105.094	
Milner Pass	PIEN	3413	NA	-0.47	973	40.42	105.8	Graybill 1987b
³ Vasquez	PIEN	3431	315	0.02	838	39.815	105.838	
³ Berthoud	PIEN	3460	240	-0.51	996	39.795	105.776	
² Fool	PIEN	3474	300	1.10	704	39.863	105.862	Brown & Shepperd 1995
Timberline	PIEN	3505	NA	0.82	915	40.37	105.67	Graybill 1987e
³ Goliath	PIEN	3566	100	0.28	744	39.641	105.593	
Pike	PIEN	3600	NA	-0.11	694	38.876	105.068	Briffa & Schweingruber 1983b

Site	Species	Elev (m)	Asp (°)	Temp (°C)	Prec (mm)	Lat (°N)	Long (°W)	Reference
¹ Brainard	PIEN	3700	340	0.52	997	40.07	105.578	Hansen-Bristow 1979
Island	PIFL	3200	NA	0.76	976	40.03	105.58	Woodhouse 1989
Frosty	PIFL	3218	NA	0.99	657	38.77	104.97	Graybill 1987a
Niwot Ridge	PIFL	3400	NA	1.67	878	40.05	105.55	Graybill 1987c
Rainbow	PIFL	3352	NA	1.38	855	40.4	105.67	Graybill 1987d

¹ Updated in 2014

² Updated in 2011

³ New site sampled in 2014

Table 3.2. Mean site statistics for annual linear measurements of radial growth (RG) including mean Spearman correlation between trees (R), mean Spearman correlation with a composite chronology (Rho), first order autocorrelation coefficient (AR1), expressed population signal (EPS), and the oldest year with an EPS > 0.85 (EPS85).

Site	Species	Period (years)	¹ N	RG mean (mm)	RG SD	Series length (years)	² R	³ Rho	AR1	⁴ EPS	EPS85
Almagre G	PIAR	560-1983	40	0.41	0.17	576	0.35	0.56	0.80	0.86	1084
Almagre L	PIAR	1-1968	28	0.43	0.18	444	0.42	0.60	0.79	0.79	1119
Evans	PIAR	977-1968	10	0.50	0.18	464	0.60	0.52	0.73	0.63	1369
Goliath	PIAR	525-1983	31	0.35	0.16	634	0.39	0.56	0.80	0.81	1084
Windy	PIAR	1050-1985	29	0.46	0.19	491	0.33	0.56	0.79	0.82	1386
Berthoud	PIEN	1350-2013	30	0.82	0.32	365	0.41	0.65	0.86	0.93	1714
Brainard	PIEN	1137-2013	45	0.66	0.28	344	0.26	0.53	0.83	0.85	1664
Brooklyn	PIEN	1528-2008	20	0.72	0.36	342	0.36	0.64	0.82	0.74	1809
Cameron	PIEN	1552-2003	16	0.04	0.02	399	NA	0.51	0.86	0.74	NA
Crags	PIEN	1547-2013	24	0.67	0.28	330	0.32	0.64	0.83	0.86	1664
Fool	PIEN	1224-2010	57	0.64	0.25	349	0.36	0.60	0.82	0.91	1261
Goliath	PIEN	1574-2013	17	0.88	0.34	248	0.29	0.64	0.83	0.75	1814
Jeff Lake	PIEN	1421-2013	66	0.85	0.38	310	0.28	0.63	0.82	0.91	1614
Lexen	PIEN	1395-2013	54	0.63	0.26	404	0.28	0.59	0.81	0.90	1464
Medicine Bow	PIEN	1401-1983	27	1.01	0.39	276	0.45	0.64	0.82	0.92	1434
Milner	PIEN	1668-1988	23	0.79	0.33	277	0.36	0.61	0.85	0.94	1688
Niwot	PIEN	1694-1982	22	0.52	0.19	213	0.46	0.62	0.73	0.92	1733
Pike	PIEN	1530-1983	24	0.52	0.22	301	0.41	0.66	0.80	0.88	1584

Site	Species	Period (years)	¹ N	RG mean (mm)	RG SD	Series length (years)	² R	³ Rho	AR1	⁴ EPS	EPS85
Rainbow	PIEN	1575-2013	19	0.69	0.34	272	0.28	0.55	0.83	0.81	1814
Rocky	PIEN	1465-2013	41	0.37	0.18	458	0.32	0.63	0.85	0.92	1514
Sand	PIEN	1197-2013	59	0.87	0.39	347	0.39	0.64	0.80	0.94	1364
Timberline	PIEN	1503-1987	23	0.48	0.21	316	0.42	0.62	0.81	0.81	1538
Vasquez	PIEN	1510-2013	24	0.71	0.33	383	0.42	0.58	0.86	0.91	1514
Frosty	PIFL	1313-1987	29	0.29	0.15	546	0.42	0.66	0.78	0.94	1338
Island	PIFL	1169-1989	40	0.36	0.21	502	0.37	0.56	0.84	0.93	1340
Niwot	PIFL	1322-1987	27	0.47	0.21	338	0.32	0.55	0.84	0.79	1588
Rainbow	PIFL	1063-1987	30	0.41	0.18	358	0.37	0.54	0.81	0.79	1288

¹ Number of sample trees

² Mean Spearman correlation based on a 100 year running window

³ Mean Spearman correlation between each time series and a composite chronology built from all the other series (leave-one-out principle)

⁴ $EPS = n * R / ((n - 1) * R + 1)$ where n = average number of trees for each year

Table 3.3. Model comparison statistics including Δ AICc (model AICc – best model AICc) and R^2 (in brackets) for models predicting RG for the full period (1895-2012) across all sites. The modeling framework is hierarchical and evaluates the relative effects of size, age, site, and climate. Temperature models estimated concurrent year temperature effects only. Climate models estimated the effects of concurrent years' temperature and precipitation on growth (1 year model), as well as the additive effects of concurrent and prior years' temperature and precipitation on RG (2 year model). All temperature effects were fit with both Gaussian (Gau T) and linear (lin T) functions. All climate models include size, age and site effects. Climate models were further modified to test for the importance of locally differentiated (LD) growth responses to temperature (T) and to both temperature and precipitation (T & P) based on linear T functions. The strongest models (Δ AICc = 0) are indicated with bolded delta text.

Model	<i>P. aristata</i>	<i>P. engelmannii</i>	<i>P. flexilis</i>
Size	3086.5 (0.00)	42516.9 (0.07)	4306.9 (0.03)
Age	2516.5 (0.03)	29597.8 (0.21)	1913.7 (0.17)
Size Age Site	686.4 (0.21)	1934.1 (0.41)	72.7 (0.33)
Temperature (lin)	671.5 (0.22)	1648.7 (0.41)	38.22 (0.33)
Climate (1 year; Gau T)	652.8 (0.22)	1587.1 (0.42)	17.7 (0.33)
Climate (1 year; lin T)	607.4 (0.22)	1373.7 (0.42)	6.6 (0.33)
Climate (2 year; Gau T)	580.3 (0.22)	1025.4 (0.42)	24.2 (0.33)
Climate (2 year; lin T)	0 (0.28)	253.2 (0.42)	0 (0.34)
LD Climate (T)	20.2 (0.28)	207.6 (0.42)	21.3 (0.34)
LD Climate (T & P)	99.2 (0.28)	0 (0.42)	33.9 (0.34)
¹ NP	19	168	18
² N	7649	58241	8937
³ Bias	1.005	1.004	1.006

¹ NP = number of parameters in best model

² N = sample size (number of target trees * number of years)

³ Bias = slope of observed versus predicted RG for best model

Table 3.4. Model comparison statistics including AICc and variance explained in the calibration data (R^2) for alternate regression models predicting growing season mean temperature (June-August). Alternate explanatory variables are based on different permutations of clustered populations and standardized RG indices (BAI and RW). Sample size (N) indicates the number of years of growth data used to calibrate a model and is constrained by the maximum period of overlap of component growth series. Population clusters were derived from hierarchical cluster analyses of site-specific growth indices and were used in a multiplicative framework to predict temperature. Three clusters were identified: two clusters were comprised of distinct *P. engelmannii* (PIEN) populations and a third cluster was comprised of *P. aristata* (PIAR) only. The two-cluster models excluded *P. aristata* populations. The one-cluster or regional models averaged RG from all screened populations from both species into a single composite covariate. The principle component (PC) model integrated scores from the first 3 variables of a PCA of BAI as independent covariates. Two-year models integrated both concurrent and lagged years RG, while one-year models used concurrent year RG only (see Eqn 5).

Variable	Cluster Model				Regional Model		PC Model
	⁴ BAI	⁵ RW	BAI	BAI	BAI	RW	⁶ PC
No clusters/ PCs	3	3	2	2	1	1	3
Species	PIEN / PIAR	PIEN /PIAR	PIEN	PIEN	PIAR / PIEN	PIAR / PIEN	PIEN / PIAR
Years	2	2	2	1	2	2	2
AICc	176.6	176.7	263.8	270.2	260.6	261.9	161.2
R^2	0.33	0.33	0.26	0.15	0.22	0.21	0.30
RMSE	0.57	0.57	0.68	0.73	0.70	0.71	0.62
N (years)	87	87	117	117	117	117	71
¹ Bias	1.000	1.000	1.000	1.001	1.000	1.000	0.998
² NP	12	12	10	6	6	6	12
³ Box- Ljung	p > 0.05	p > 0.05	p < 0.001	p < 0.001	p < 0.001	p < 0.001	p > 0.05

¹ Bias = slope of observed versus predicted RG

² NP = number of model parameters

³ Ljung-Box (portmanteau) test for independence of residuals (Null hypothesis test of independence)

⁴ Normalized basal area increment (mm^2)

⁵ Linear ring width (mm) standardized by the RCS method

⁶ Principle component scores from a PCA of normalized BAI

Table 3.5. Comparison of pre-industrial (921-1850) and modern (1851-2010) estimated temperature variability. Bracketed values are standard deviations (z scores) from 1400-1850 mean conditions. Amplitude of temperature variability is calculated as the difference between the maximum and minimum estimated temperatures for a given period (Ljungqvist 2010).

Variable	Annual		30-Year Normal	
	Pre-industrial	Modern	Pre-industrial	Modern
Mean	9.15 (0.22)	9.82 (3.31)	9.16 (0.35)	9.82 (6.09)
SD	0.26	0.40	0.16	0.11
Maximum	10.67 (7.23)	10.85 (8.07)	9.68 (4.89)	10.01 (7.71)
Minimum	8.38 (-3.35)	8.96 (-0.66)	8.91 (-1.84)	9.55 (3.72)
Amplitude	2.28	1.89	0.78	0.46

Table 3.6. Warmest and coldest non-overlapping 30-year periods (normals) in the pre-industrial era (921-1850). Anomalies are calculated as standard deviations (z scores) relative to both a 1400-1850 reference period and the most recent 30 years in the reconstruction (1981-2010).

Warm Periods				Cold Periods			
Period	Mean T (°C)	Anomaly (1400-1850)	Anomaly (1981-2010)	Period	Mean T (°C)	Anomaly (1400-1850)	Anomaly (1981-2010)
1096-1125	9.40	2.16	-1.40	1336-1365	8.95	-1.37	-2.50
1786-1815	9.38	1.99	-1.45	1666-1695	8.98	-1.20	-2.45
946-975	9.37	1.97	-1.49	1306-1335	8.98	-1.16	-2.43
1156-1185	9.28	1.87	-1.71	1456-1485	8.98	-1.13	-2.43
1036-1065	9.27	1.16	-1.73	1486-1515	8.99	-1.11	-2.42

Figures

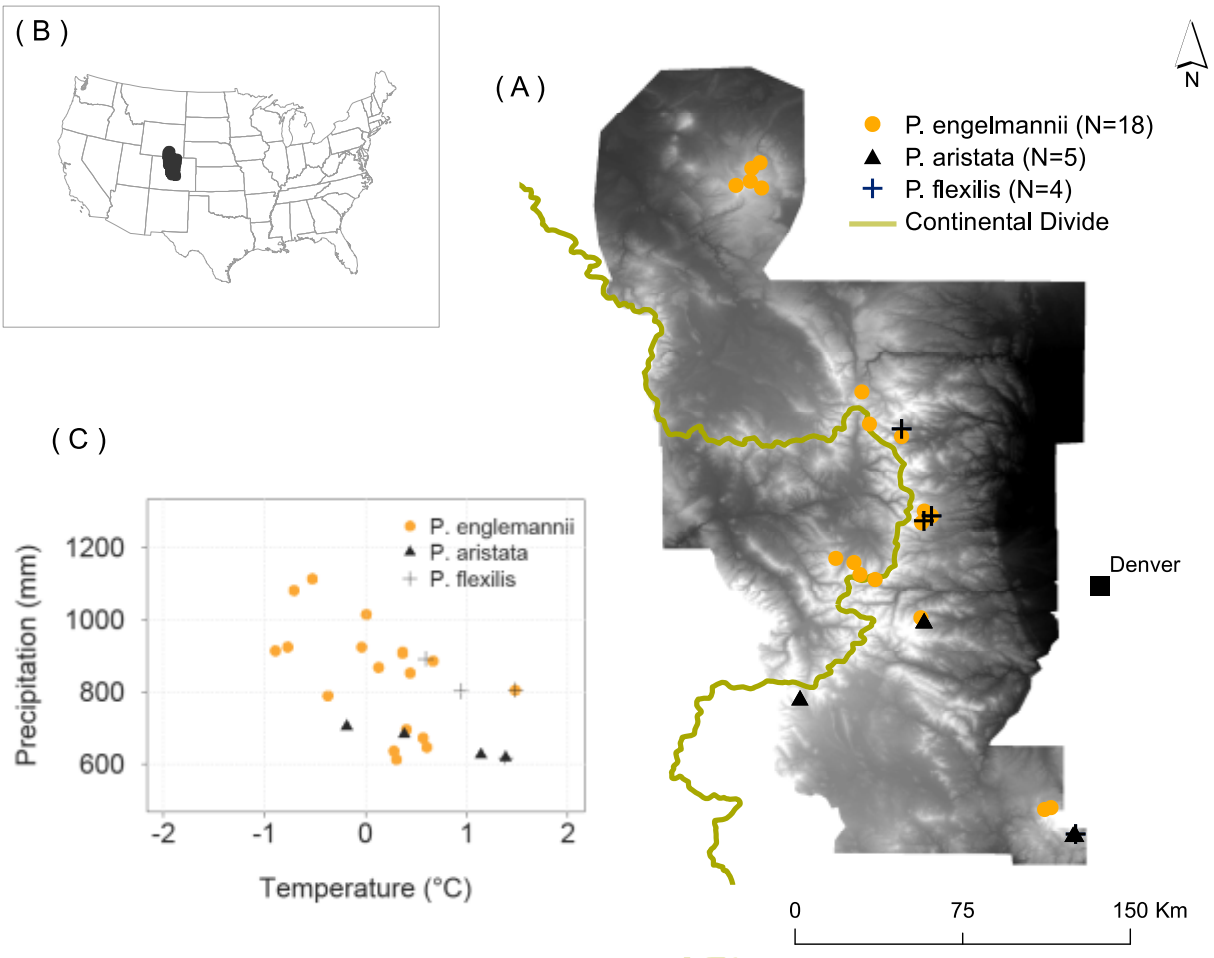


Figure 3.1. Distribution of sample sites in northern Colorado and southern Wyoming. Panel A shows the geographical distribution of sample locations against a background Digital Elevation Model. N values designate sample sizes (sites) for each species. Panel B shows the relative location of the study area within the United States. Panel C shows the distribution of sample sites across gradients of annual temperature and precipitation (30 year annual means).

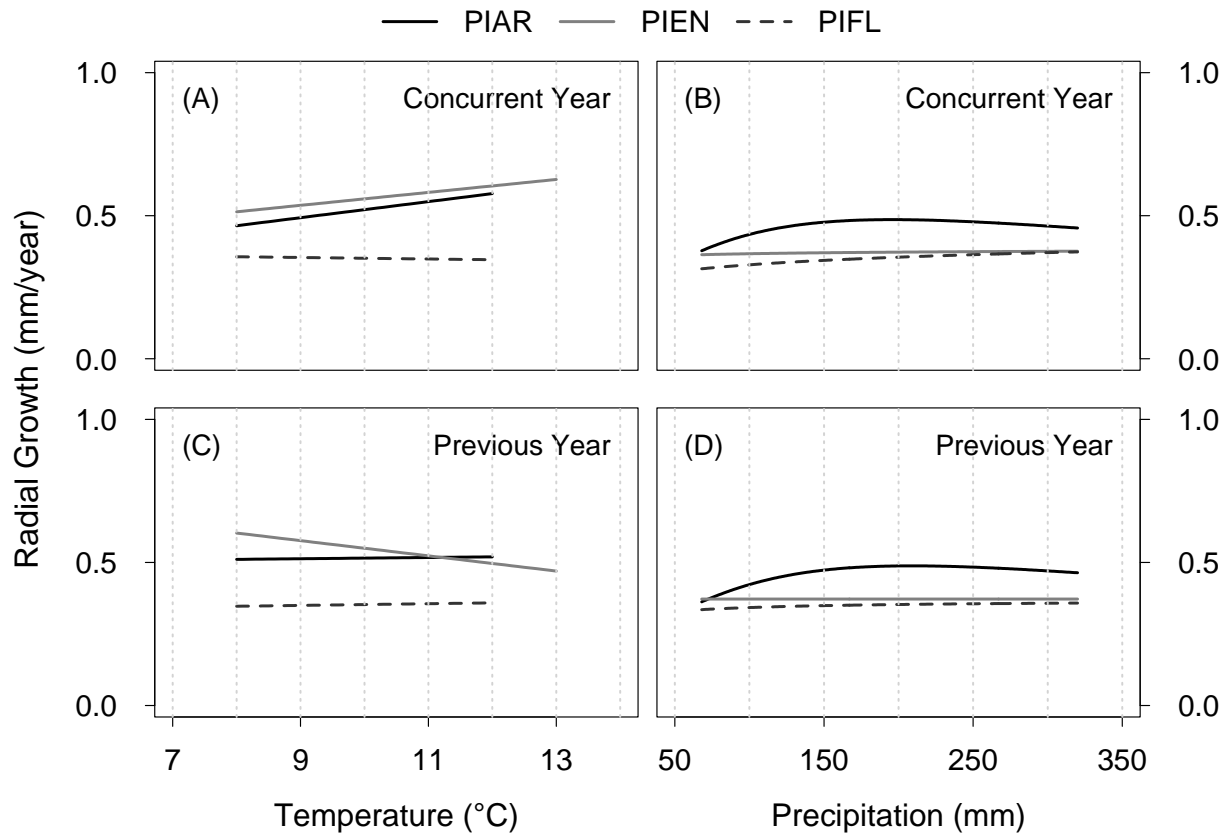


Figure 3.2. Growth responses (mm/year) by species for an average aged 30 cm diameter tree to concurrent and prior year mean summer temperature and total summer precipitation. Responses are based on parameters from the best fitting full models of growth and are averaged across sites. For the temperature panels, precipitation is held constant at the overall mean level for a species. Temperature is held constant in the precipitation panels. Competition is also held constant at the mean level for a species. The climate breadth of each response curve represents the observed climate range of each species. Species acronyms are defined in Table 3.1.

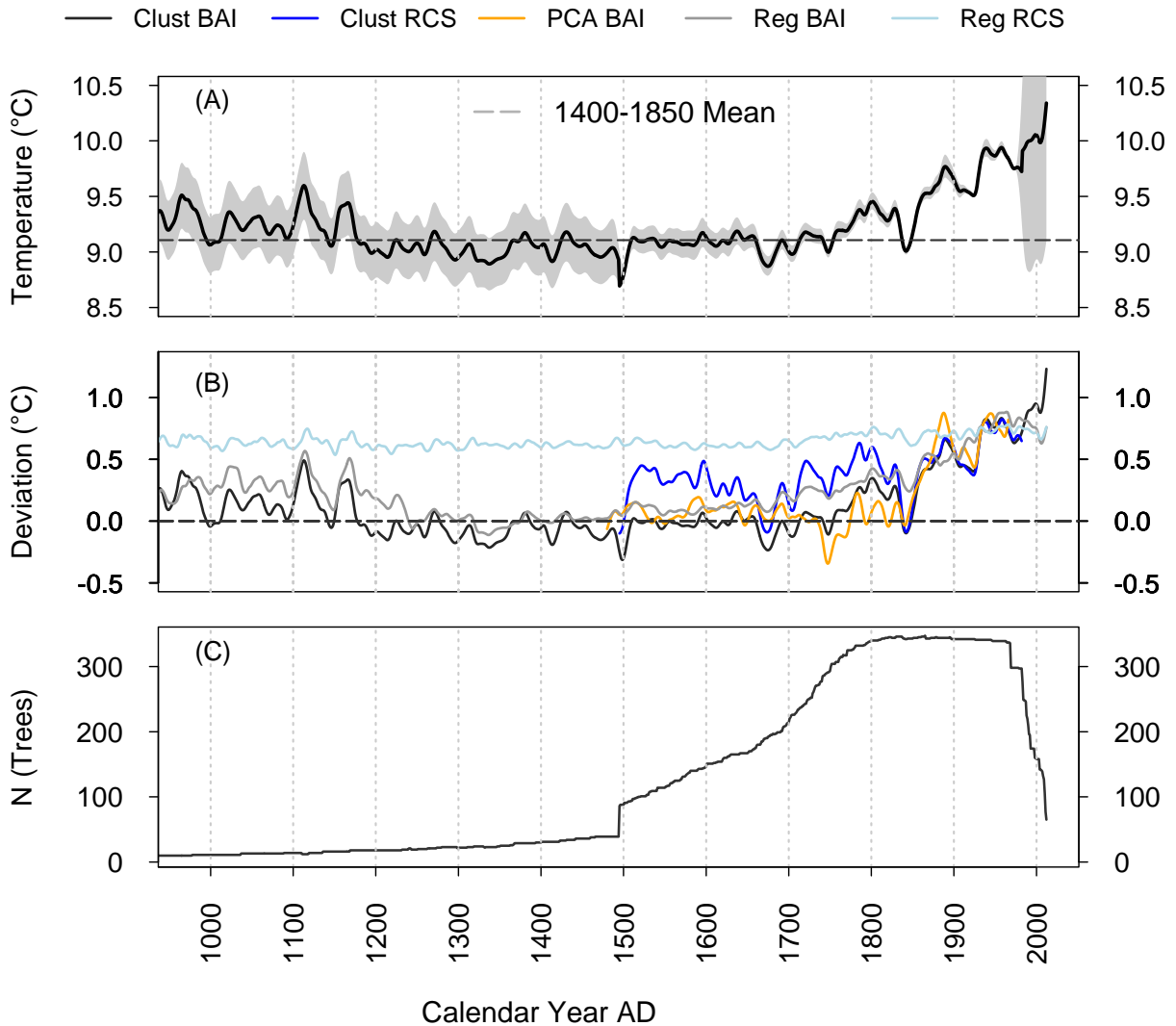


Figure 3.3. Reconstructed mean growing season temperature from alternate regression models. All models have been smoothed with a 20 year spline. Panel A shows temperatures from a cluster model based on normalized BAI with 3 species groups (Clust BAI model). Reconstructed temperatures prior to 1495 are derived from an independent model based exclusively on RG indices from *P. aristata*. Shading represents predicted temperature uncertainty, based on two unit support intervals which are approximately analogous to 95% confidence limits. Panel B shows predicted temperature deviations from the 1400-1850 mean for 5 alternate models, including the 3-cluster model from panel A, a 3-cluster model based on ring widths standardized with a regional curve (Clust RCS), a model using the first 3 terms from a PCA of normalized BAI, a composite regional chronology based on normalized BAI (Reg BAI), and a composite regional chronology based on RCS. Panel C indicates corresponding sample sizes in terms of individual trees. Reconstructions were subset to a minimum of 10 trees.

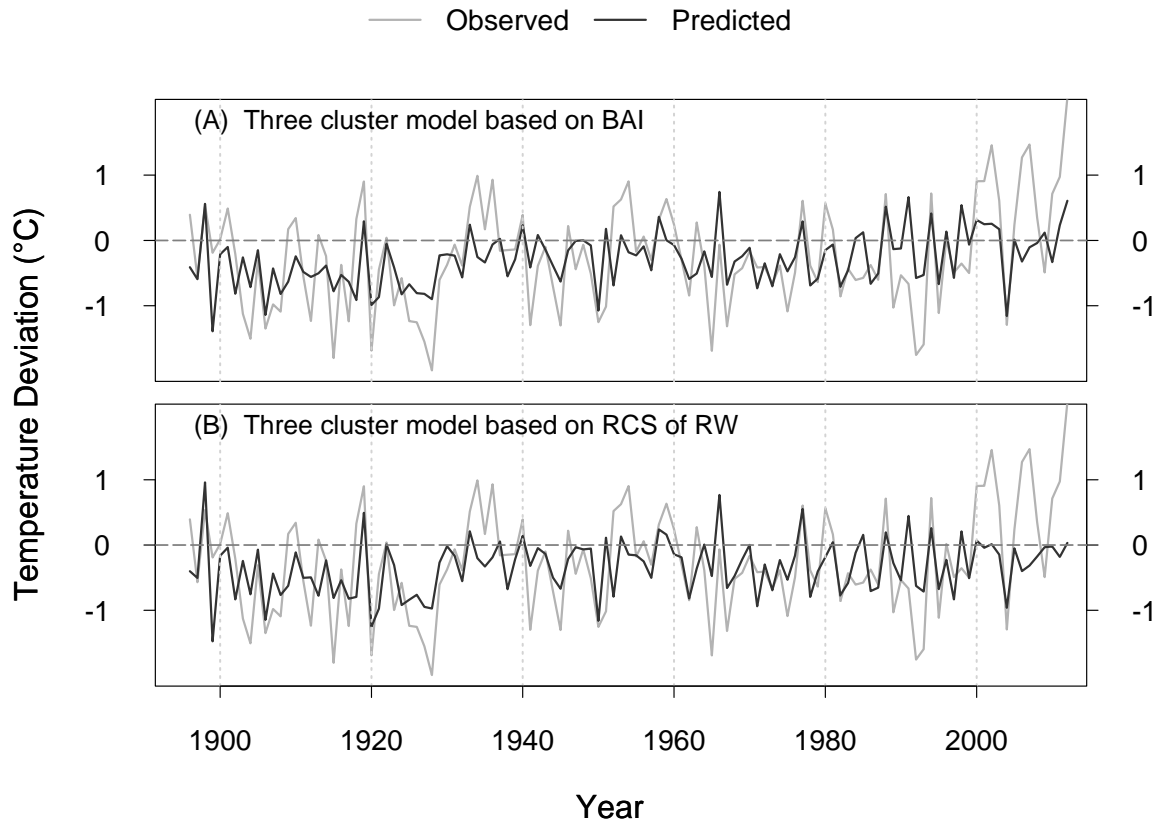


Figure 3.4. Observed and predicted temperatures ($^{\circ}\text{C}$) for the calibration period (1895-2010). Temperature series have been relativized to the 1895-2010 mean temperature. Panel A: Predictions from a 3 cluster model (3 species groups) in which radial growth was transformed into an index of normalized BAI. Panel B: Temperature estimates from an equivalent 3 cluster model based on a linear index of radial growth standardized using the RCS method.

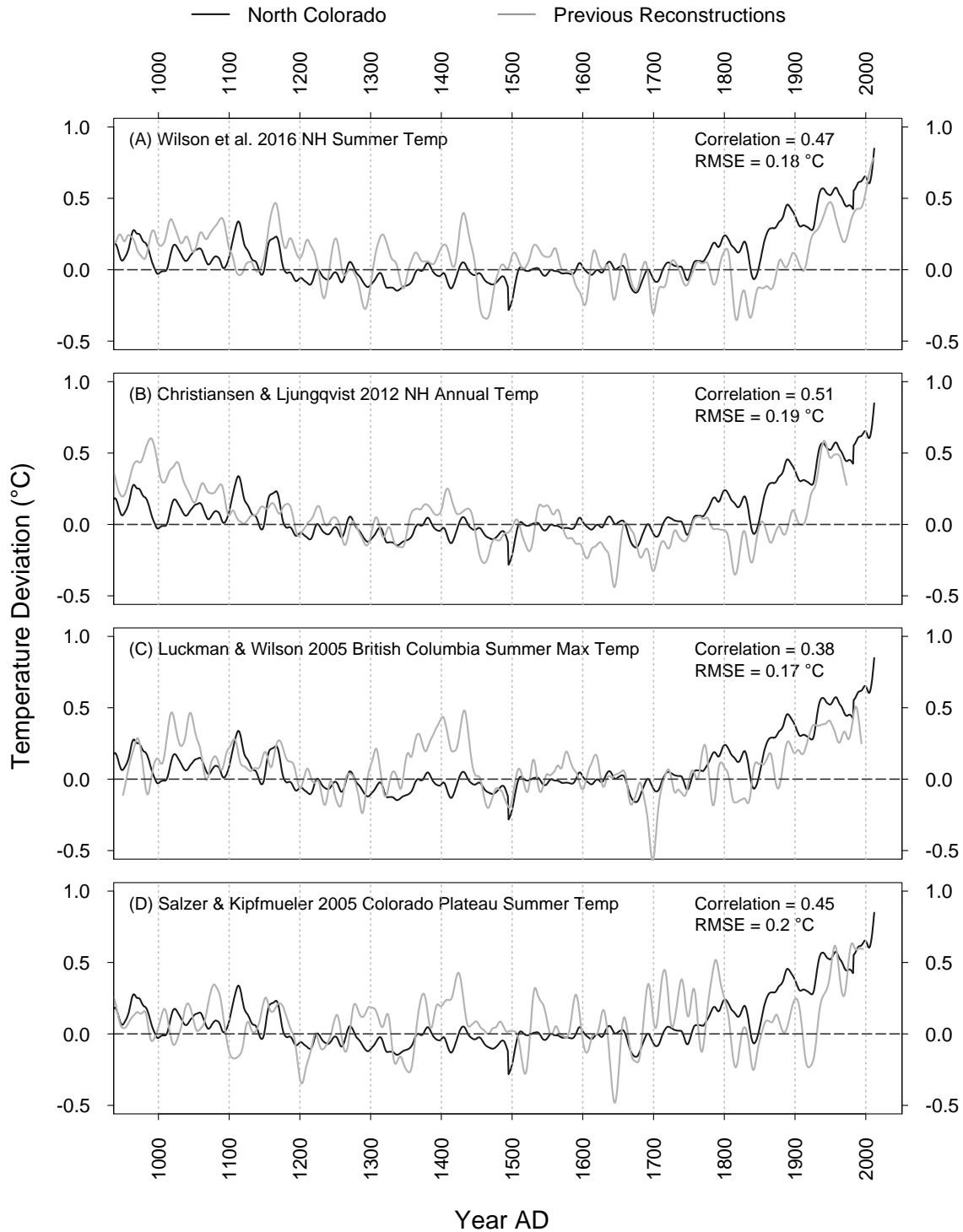


Figure 3.5. Covariation between the current reconstruction for Northern Colorado and selected previous reconstructions of mean temperatures at both hemispheric (A & B) and regional scales (C & D). All reconstructions were scaled to the mean and variance of the PRISM data for the period 1895-2010, smoothed with a 20-year spline function, and normalized relative to a 1400-1850 reference mean. We quantified differences between reconstructions with Pearson

correlation coefficients and RMSE. The target response variable varies between some studies: Christiansen & Ljungqvist (2012) estimated annual mean temperature for the Northern Hemisphere (NH), while Luckman & Wilson (2005) estimated maximum summer temperatures. The two warmest and coldest 30-year periods in this study are shaded red and blue, respectively.

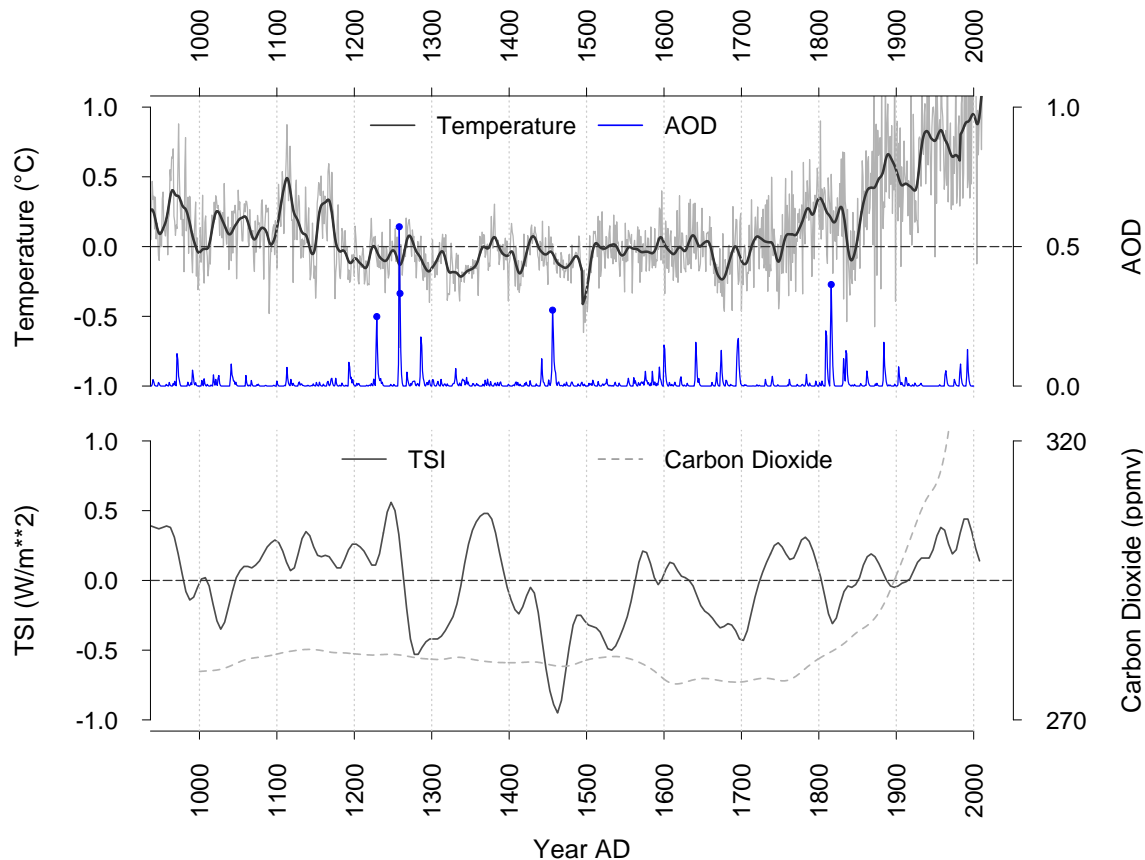


Figure 3.6. Reconstructed temperatures for northern Colorado and selected radiative forcing factors, including sulphate aerosols from volcanism, total solar irradiance in the upper atmosphere, and atmospheric carbon dioxide concentrations. Temperatures are relativized with respect to mean temperature for the pre-industrial period (1400-1850) and smoothed with a 20-year spline function. Estimated annual temperatures are represented by gray vertical lines in the upper panel. Aerosol optical depth (AOD) is a normalized measure of the scatter and absorption of solar radiation by volcanic sulphate aerosols in the stratosphere (data from Crowley & Unterman 2013). Years of extreme aerosol loading (AOD > 2.5) are identified with blue points and follow known major volcanic events (e.g. Tambora in 1815). Total solar irradiance (TSI in W/m^2) is reconstructed from cosmogenic radionuclide (^{10}Be) measurements derived from ice cores (data from Steinhilber *et al.* 2009). TSI is represented by a 40-year running mean relativized to the solar minimum of 1986. Gray shading delimits intervals of low solar irradiance in the historical record (Eddy 1977). Atmospheric carbon dioxide concentrations (ppmv: parts per million by volume) were reconstructed from ice cores and smoothed with a 50-year spline (data from Frank *et al.* 2010).

REFERENCES

- Bigler, C. & Veblen, T.T. (2003) Cameron Pass - PCEN - ITRDB CO633. Cameron Pass - PCEN - ITRDB CO633, National Climatic Data Center, NESDIS, NOAA, U.S. Department of Commerce, Boulder, CO, online data archive, <https://www.ncdc.noaa.gov/paleo/study/5502>. Accessed on 01 June 2014.
- Briffa KR, Jones PD, Bartholin TS, Eckstein D, Schweingruber FH, Karlen W, Zetterberg P, & Eronen M. (1992) Fennoscandian summers from AD 500: temperature changes on short and long timescales. *Climate Dynamics* 7(3):111-9.
- Briffa, KR. & Schweingruber, F.H. (1983a) Medicine Bow Peak - PCEN - ITRDB WY022. National Climatic Data Center, NESDIS, NOAA, U.S. Department of Commerce, Boulder, CO, online data archive, <https://www.ncdc.noaa.gov/paleo/study/2833>. Accessed on 01 June 2014.
- Briffa, KR. & Schweingruber, F.H. (1983b) Pike Peaks - PCEN - ITRDB CO553. National Climatic Data Center, NESDIS, NOAA, U.S. Department of Commerce, Boulder, CO, online data archive, <https://www.ncdc.noaa.gov/paleo/study/2842>. Accessed on 01 June 2014.
- Brown, P.M. & Shepperd, W.D. (1995) Engelmann spruce tree-ring chronologies from Fraser Experimental Forest, Colorado: potential for a long-term temperature reconstruction in the central Rocky Mountains. *USDA General Technical Report*, RM-GTR-262, Fort Collins, CO.
- Brown, P.M., Woodhouse, C.A., Hughes, M.K. & Joyce, L. (1999) Sheep Trail - PCEN - ITRDB WY030. National Climatic Data Center, NESDIS, NOAA, U.S. Department of Commerce, Boulder, CO, online data archive, <https://www.ncdc.noaa.gov/paleo/study/2875>. Accessed on 01 June 2014.
- Buechling, A. & Baker, W.L. (2004) A fire history from tree rings in a high-elevation forest of Rocky Mountain National Park. *Canadian Journal of Forest Research*, **34**, 1259-1273.
- Buechling, A., Martin P.H. & Canham C.D. (2017) Climate and competition effects on tree growth in Rocky Mountain forests. *Journal of Ecology*, doi: <http://dx.doi.org/10.1111/1365-2745.12782>.
- Buechling, A., Martin, P.H., Canham, C.D., Shepperd, W.D. & Battaglia, M.A. (2016) Climate drivers of seed production in *Picea engelmannii* and response to warming temperatures in the southern Rocky Mountains. *Journal of Ecology*, **104**, 1051-1062.
- Burnham, K.P. & Anderson, D.R. (2002) *Model Selection and Multimodel Inference: A Practical Information-theoretic Approach*, 2nd edn. Springer-Verlag, New York, NJ, USA.
- Canham, C.D. & Murphy, L. (2016) The demography of tree species response to climate: sapling and canopy tree growth. *Ecosphere*, **7**, e01474. 10.1002/ecs2.1474.

- Christiansen, B. & Ljungqvist, F.C. (2012) The extra-tropical Northern Hemisphere temperature in the last two millennia: reconstructions of low-frequency variability. *Climate of the Past*, **8**, 765-786.
- Coomes, D.A., Flores, O., Holdaway, R., Jucker, T., Lines, E.R. & Vanderwel, M.C. (2014) Wood production response to climate change will depend critically on forest composition and structure. *Global Change Biology*, **20**, 3632-3645.
- Crowley, T.J. & Lowery, T.S. (2000) How warm was the medieval warm period?. *AMBIO: A Journal of the Human Environment*, **29**, 51-54.
- Crowley, T.J. & Unterman, M.B. (2013) Technical details concerning development of a 1200 yr proxy index for global volcanism. *Earth System Science Data*, **5**, 187-197.
- Daly, C., Halbleib, M., Smith, J.I., Gibson, W.P., Doggett, M.K., Taylor, G.H., Curtis, J. & Pasteris, P.P. (2008) Physiographically sensitive mapping of climatological temperature and precipitation across the conterminous United States. *International Journal of Climatology*, **28**, 2031-2064.
- D'Arrigo, R.D., Kaufmann, R.K., Davi, N., Jacoby, G.C., Laskowski, C., Myneni, R.B. & Cherubini, P. (2004) Thresholds for warming-induced growth decline at elevational tree line in the Yukon Territory, Canada. *Global Biogeochemical Cycles*, **18**, 1-7.
- D'Arrigo, R., Wilson, R., Liepert, B. & Cherubini, P. (2008) On the 'divergence problem' in northern forests: a review of the tree-ring evidence and possible causes. *Global and Planetary Change*, **60**, 289-305.
- Earle, C.J. (1990) Medicine Bows 4 - PCEN - ITRDB WY020. National Climatic Data Center, NESDIS, NOAA, U.S. Department of Commerce, Boulder, CO, online data archive, <https://www.ncdc.noaa.gov/paleo/study/3190>. Accessed on 01 June 2014.
- Eddy, J.A. (1977) Climate and the changing sun. *Climatic Change*, **1**, 173-190.
- Edwards, M.E., Brubaker, L.B., Lozhkin, A.V. & Anderson, P.M. (2005) Structurally novel biomes: a response to past warming in Beringia. *Ecology*, **86**, 1696-1703.
- Edwards, T.L., Crucifix, M. & Harrison, S.P. (2007) Using the past to constrain the future: how the palaeorecord can improve estimates of global warming. *Progress in Physical Geography*, **31**, 481-500.
- Esper, J., Cook, E., Peters, K., Krusic, P. & Schweingruber, F. (2003) Detecting low-frequency tree-ring trends by the RCS method. *Tree-Ring Research*, **59**, 81-98.
- Esper, J. & Frank, D. (2009) The IPCC on a heterogeneous Medieval warm period. *Climatic Change*, **94**, 267-273.

Esper, J., Krusic, P.J., Ljungqvist, F.C., Luterbacher, J., Carrer, M., Cook, E., Davi, N.K., Hartl-Meier, C., Kirilyanov, A., Konter, O. & Myglan, V. (2016) Ranking of tree-ring based temperature reconstructions of the past millennium. *Quaternary Science Reviews*, **145**, 134-151.

Frank, D.C., Esper, J., Raible, C.C., Büntgen, U., Trouet, V., Stocker, B. & Joos, F. (2010) Ensemble reconstruction constraints on the global carbon cycle sensitivity to climate. *Nature*, **463**, 527-530.

Free, M. & Robock, A. (1999) Global warming in the context of the Little Ice Age. *Journal of Geophysical Research: Atmospheres*, **104**, 19057-19070.

Fritts, H.C. (1976) *Tree rings and climate*. Academic Press, New York, NY, USA.

Goffe, W.L., Ferrier, G.D. & Rogers, J. (1994) Global optimization of statistical functions with simulated annealing. *Journal of Econometrics*, **60**, 65-99.

Graybill, D.A. (1983a) Almagre Mountain B - PIAR - ITRDB CO524. National Climatic Data Center, NESDIS, NOAA, U.S. Department of Commerce, Boulder, CO, online data archive, <https://www.ncdc.noaa.gov/paleo/study/3339>. Accessed on 01 June 2016.

Graybill, D.A. (1983b) Mount Goliath - PIAR - ITRDB CO522. National Climatic Data Center, NESDIS, NOAA, U.S. Department of Commerce, Boulder, CO, online data archive, <https://www.ncdc.noaa.gov/paleo/study/3381>. Accessed on 01 June 2016.

Graybill, D.A. (1985) Windy Ridge - PIAR - ITRDB CO523. National Climatic Data Center, NESDIS, NOAA, U.S. Department of Commerce, Boulder, CO, online data archive, <https://www.ncdc.noaa.gov/paleo/study/3422>. Accessed on 01 June 2016.

Graybill, D.A. (1987a) Frosty Park - PIFL - CO535, PAGES North America 2K Version. National Climatic Data Center, NESDIS, NOAA, U.S. Department of Commerce, Boulder, CO, online data archive, <https://www.ncdc.noaa.gov/paleo/study/1000168>. Accessed on 01 June 2016.

Graybill, D.A. (1987b) Milner Pass - PCEN - ITRDB CO543. National Climatic Data Center, NESDIS, NOAA, U.S. Department of Commerce, Boulder, CO, online data archive, <https://www.ncdc.noaa.gov/paleo/study/3377>. Accessed on 01 June 2014.

Graybill, D.A. (1897c) Niwot Ridge B - PIFL - ITRDB CO545. National Climatic Data Center, NESDIS, NOAA, U.S. Department of Commerce, Boulder, CO, online data archive, <https://www.ncdc.noaa.gov/paleo/study/3386>. Accessed on 01 June 2014.

Graybill, D.A. (1987d) Rainbow Curve - PIFL - ITRDB CO547. National Climatic Data Center, NESDIS, NOAA, U.S. Department of Commerce, Boulder, CO, online data archive, <https://www.ncdc.noaa.gov/paleo/study/3398>. Accessed on 01 June 2014.

- Graybill, D.A. (1987e) Timberline Pass - PCEN - ITRDB CO549. National Climatic Data Center, NESDIS, NOAA, U.S. Department of Commerce, Boulder, CO, online data archive, <https://www.ncdc.noaa.gov/paleo/study/3414>. Accessed on 01 June 2014.
- Hansen-Bristow, K. (1979) Niwot Ridge A - PCEN - ITRDB CO083. National Climatic Data Center, NESDIS, NOAA, U.S. Department of Commerce, Boulder, CO, online data archive, <https://www.ncdc.noaa.gov/paleo/study/3462>. Accessed on 01 June 2014.
- Hegerl, G., Crowley, T., Hyde, W. & Frame, D. (2006) Climate sensitivity constrained by temperature reconstructions over the past seven centuries. *Nature*, **440**, 1029-1032, doi: 10.1038/Nature 04679.
- Higuera, P.E., Briles, C.E. & Whitlock, C. (2014) Fire-regime complacency and sensitivity to centennial-through millennial-scale climate change in Rocky Mountain subalpine forests, Colorado, USA. *Journal of Ecology*, **102**, 1429-1441.
- Hoch, G. & Körner, C. (2003) The carbon charging of pines at the climatic treeline: a global comparison. *Oecologia*, **135**, 10-21.
- Jones, P.D., Briffa, K.R., Osborn, T.J., Lough, J.M., Van Ommen, T.D., Vinther, B.M., Luterbacher, J.W.E.R.Z.F.W., Wahl, E.R., Zwiers, F.W., Mann, M.E. & Schmidt, G.A. (2009) High-resolution palaeoclimatology of the last millennium: a review of current status and future prospects. *The Holocene*, **19**, 3-49.
- Jacoby, G.C. & D'Arrigo, R.D. (1995) Tree ring width and density evidence of climatic and potential forest change in Alaska. *Global Biogeochemical Cycles*, **9**, 227-234.
- Jacoby, G.C., Lovelius, N.V., Shumilov, O.I., Raspopov, O.M., Karbainov, J.M. & Frank, D.C. (2000) Long-term temperature trends and tree growth in the Taymir region of northern Siberia. *Quaternary Research*, **53**, 312-318.
- Kienast, F. (1982) Arapahoe - PCEN - ITRDB CO517. National Climatic Data Center, NESDIS, NOAA, U.S. Department of Commerce, Boulder, CO, online data archive, <https://www.ncdc.noaa.gov/paleo/study/3680>. Accessed on 01 June 2014.
- Kipfmüller, K.F. (2008) Reconstructed summer temperature in the northern Rocky Mountains wilderness, USA. *Quaternary Research*, **70**, 173-187.
- Kipfmüller, K.F. & Baker, W.L. (2000) A fire history of a subalpine forest in south-eastern Wyoming, USA. *Journal of Biogeography*, **27**, 71-85.
- Kunstler, G., Albert, C.H., Courbaud, B., Lavergne, S., Thuiller, W., Vieilledent, G., Zimmermann, N.E. & Coomes, D.A. (2011) Effects of competition on tree radial growth vary in importance but not in intensity along climatic gradients. *Journal of Ecology*, **99**, 300-312.

LaMarche, Jr., V.C. & Harlan, T.P. (1968a) Almagre Mountain A - PIAR - ITRDB CO071. National Climatic Data Center, NESDIS, NOAA, U.S. Department of Commerce, Boulder, CO, online data archive, <https://www.ncdc.noaa.gov/paleo/study/3822>. Accessed on 01 June 2016.

LaMarche, Jr., V.C. & Harlan, T.P. (1968b) Mount Evans - PIAR - ITRDB CO072. National Climatic Data Center, NESDIS, NOAA, U.S. Department of Commerce, Boulder, CO, online data archive, <https://www.ncdc.noaa.gov/paleo/study/3839>. Accessed on 01 June 2016.

Ljungqvist, F.C. (2010) A new reconstruction of temperature variability in the extra-tropical Northern Hemisphere during the last two millennia. *Geografiska Annaler: Series A, Physical Geography*, **92**, 339-351.

Ljungqvist, F.C., Krusic, P.J., Brattström, G. & Sundqvist, H.S. (2012) Northern Hemisphere temperature patterns in the last 12 centuries. *Climate of the Past*, **8**, 227-249.

Lloyd, A.H. & Fastie, C.L. (2002) Spatial and temporal variability in the growth and climate response of treeline trees in Alaska. *Climatic Change*, **52**, 481-509.

Loehle, C. (2009) A mathematical analysis of the divergence problem in dendroclimatology. *Climatic Change*, **94**, 233-245.

Lough, J.M. & Fritts, H.C. (1987) An assessment of the possible effects of volcanic eruptions on North American climate using tree-ring data, 1602 to 1900 AD. *Climatic Change*, **10**, 219-239.

Luckman, B.H. & Wilson, R.J.S. (2005) Summer temperatures in the Canadian Rockies during the last millennium: a revised record. *Climate Dynamics*, **24**, 131-144.

Mann, M.E., Zhang, Z., Hughes, M.K., Bradley, R.S., Miller, S.K., Rutherford, S. & Ni, F. (2008) Proxy-based reconstructions of hemispheric and global surface temperature variations over the past two millennia. *Proceedings of the National Academy of Sciences*, **105**, 13252-13257.

Marcott, S. A., Shakun, J. D., Clark, P. U. & Mix, A. C. (2013) A reconstruction of regional and global temperature for the past 11,300 years. *Science*, **339**, 1198-1201.

Marlon, J.R., Bartlein, P.J., Gavin, D.G., Long, C.J., Anderson, R.S., Briles, C.E., Brown, K.J., Colombaroli, D., Hallett, D.J., Power, M.J. & Scharf, E.A. (2012) Long-term perspective on wildfires in the western USA. *Proceedings of the National Academy of Sciences*, **109**, E535-E543.

Rangwala, I. & Miller, J.R. (2012) Climate change in mountains: a review of elevation-dependent warming and its possible causes. *Climatic Change*, **114**, 527-547.

R Core Team (2013) R: A language and environment for statistical computing. R Foundation for Statistical Computing, Vienna, Austria. URL <http://www.R-project.org/>.

- Salzer, M.W. & Kipfmüller, K.F. (2005) Reconstructed temperature and precipitation on a millennial timescale from tree-rings in the southern Colorado Plateau, USA. *Climatic Change*, **70**, 465-487.
- Schurer, A.P., Hegerl, G.C., Mann, M.E., Tett, S.F. & Phipps, S.J. (2013) Separating forced from chaotic climate variability over the past millennium. *Journal of Climate*, **26**, 6954-6973.
- Schweingruber, F.H. (1982) Niwot Ridge C - PCEN - ITRDB CO574. National Climatic Data Center, NESDIS, NOAA, U.S. Department of Commerce, Boulder, CO, online data archive, <https://www.ncdc.noaa.gov/paleo/study/4555>. Accessed on 01 June 2014.
- Sibold, J.S., Veblen, T.T. & González, M.E. (2006) Spatial and temporal variation in historic fire regimes in subalpine forests across the Colorado Front Range in Rocky Mountain National Park, Colorado, USA. *Journal of Biogeography*, **33**, 631-647.
- Steinhilber, F., Beer, J. & Fröhlich, C. (2009) Total solar irradiance during the Holocene. *Geophysical Research Letters*, **36**, L19704, doi:10.1029/2009GL040142.
- Trouet, V., Diaz, H.F., Wahl, E.R., Vial, A.E., Graham, R., Graham, N. & Cook, E.R. (2013) A 1500-year reconstruction of annual mean temperature for temperate North America on decadal-to-multidecadal time scales. *Environmental Research Letters*, **8**, doi:10.1088/1748-9326/8/2/024008.
- Vaganov, E.A., Hughes, M.K., Kirilyanov, A.V., Schweingruber, F.H. & Silkin, P.P. (1999) Influence of snowfall and melt timing on tree growth in subarctic Eurasia. *Nature*, **400**, 149-151.
- Way, D.A. & Oren, R. (2010) Differential responses to changes in growth temperature between trees from different functional groups and biomes: a review and synthesis of data. *Tree Physiology*, **30**, 669-688.
- Williams, J.W. & Jackson, S.T. (2007) Novel climates, no-analog communities, and ecological surprises. *Frontiers in Ecology and the Environment*, **5**, 475-482.
- Wilmking, M., Juday, G.P., Barber, V.A. & Zald, H.S. (2004) Recent climate warming forces contrasting growth responses of white spruce at treeline in Alaska through temperature thresholds. *Global Change Biology*, **10**, 1724-1736.
- Wilson, R., Anchukaitis, K., Briffa, K.R., Büntgen, U., Cook, E., D'Arrigo, R., Davi, N., Esper, J., Frank, D., Gunnarson, B. & Hegerl, G. (2016) Last millennium northern hemisphere summer temperatures from tree rings: Part I: The long term context. *Quaternary Science Reviews*, **134**, 1-18.
- Wilson, R., D'Arrigo, R., Buckley, B., Büntgen, U., Esper, J., Frank, D., Luckman, B., Payette, S., Vose, R. & Youngblut, D. (2007) A matter of divergence: tracking recent warming at hemispheric scales using tree ring data. *Journal of Geophysical Research*, **112**, doi:10.1029/2006JD008318.

Wilson, R.J. & Luckman, B.H. (2003) Dendroclimatic reconstruction of maximum summer temperatures from upper treeline sites in Interior British Columbia, Canada. *The Holocene*, **13**, 851-861.

Woodhouse, C.A. (1989) Island Lake - PIFL - ITRDB CO511. National Climatic Data Center, NESDIS, NOAA, U.S. Department of Commerce, Boulder, CO, online data archive, <https://www.ncdc.noaa.gov/paleo/study/5306>. Accessed on 01 June 2014.

APPENDIX

Appendix S1.1: Comparison of PRISM and TopoWx Gridded Temperature Datasets

We used instrumental climate records obtained from long term meteorological stations at Fraser to evaluate the performance of two existing gridded temperature datasets, PRISM (Daly *et al.* 2008) and TopoWx (Oyler *et al.* 2014). Both datasets provide continuous estimates of daily maximum (T_{max}) and minimum temperature (T_{min}) at high spatial resolution (30 arcsec or 800 m pixel size). PRISM also provides an interpolated precipitation dataset. PRISM and TopoWx are both derived from elevation-based regression models trained with standardized and quality controlled meteorological observations. TopoWx additionally integrates remotely sensed estimates of the radiometric temperature of the ground surface as a covariate (Oyler *et al.* 2014). PRISM weights individual meteorological stations based on terrain features known to cause anomalies in the associated climate regime. See Daly *et al.* (2008) and Oyler *et al.* (2014) for full methods.

Goodness of fit measures (GOF) were computed to evaluate the degree of agreement between aggregated annual and seasonal station data from Fraser and the corresponding predicted values from PRISM and TopoWx, including mean absolute error (MAE), percent bias (Pbias) and the proportion of variance (R^2) explained by the regression model relative to the total variability in observations explained by the simple mean of the data ($1 - \text{sum of squares error} / \text{sum of squares total}$). R^2 defined in this way is equivalent to both the Nash-Sutcliffe efficiency (NSE; Nash & Sutcliffe 1970) as well as the Reduction of Error (RE) statistic commonly used to evaluate tree ring based climate models (Fritts 1976; Cook *et al.* 1987). The time period of GOF analyses spanned years from 1980 to 2008.

For use in GOF analyses, we aggregated daily instrumental climate data from five stations at Fraser to monthly, seasonal, and annual values after first inspecting records for completeness and potential instrumental errors associated with extreme values. Annual precipitation sums were computed over a 12-month window from Oct 1st to September 31st, defined as a water year. We did not infill missing daily values to maintain independence of observations. Adopting criteria used by Daly *et al.* (2008), we excluded aggregated monthly or seasonal variables with less than 85% data completeness. Extreme temperature values that exceeded a threshold distance of 5 standard deviations from corresponding means were also excluded. Potential temporal trends in climate were examined using linear regression (McGuire *et al.* 2012). Data from the independent climate stations used for testing were highly inter-correlated with a mean correlation coefficient of 0.98, indicating a strong common climate signal and minimal local temperature variation or noise that could bias evaluations of PRISM and TopoWx (Pielke *et al.* 2002).

GOF measures indicate that PRISM and TopoWx provide generally comparable prediction accuracy for temperature variation at climate station locations in Fraser (Fig. S1.2). Values of MAE for seasonal *Tmin* and *Tmax* range from 0.81 to 2.03 °C for PRISM and from 0.98 to 1.79 °C for TopoWx. Both models tend to slightly overestimate *Tmax* and underestimate *Tmin* across seasons. The warm bias for *Tmax* is largest in winter, and higher for PRISM than TopoWx. Model fit is relatively strong for *Tmin* across seasons for both models, despite ubiquitous temperature inversions caused by cold air drainage that could potentially bias climate model predictions at high elevations. However, both PRISM and TopoWx fail to capture an extreme multi-year increase in summer *Tmin* that occurred between 2001 and 2003 (Fig. S1.3), corresponding to a period of extreme drought, high temperatures, and low snowpack across

Colorado (Pielke *et al.* 2005). Model fit to seasonal T_{max} is relatively poor for PRISM, with values of R^2 ranging from -0.46 to 0.07. Negative R^2 values indicate that model predictions provide a weaker fit to the observational data than the simple overall mean of the observations. GOF measures for TopoWx T_{max} are variable with poor fit to fall and winter T_{max} , but relatively strong model predictions of summer and spring T_{max} .

GOF statistics indicate that PRISM provides relatively accurate predictions of both annual and seasonal precipitation sums at Fraser at all elevations. MAE ranged from 16 to 46 mm and mean R^2 across all seasons was 0.5. PRISM tended to underestimate station precipitation with a mean negative bias across seasons of ~10%.

In summary, TopoWx and PRISM provide arguably comparable predictions of T_{min} , while TopoWx provides slightly more accurate predictions of T_{max} . Therefore, we used TopoWx temperature data and PRISM precipitation data in all modeling analyses.

Appendix S2.1: Distribution of field samples

Our stratified random sampling design captured a broad range of tree sizes, stand structures, and climates (Table 2.1 & S2.1). We sampled a total of 777 target trees and processed a total of 1923 associated core samples. Individual species sample sizes ranging from 131 to 179 trees (Fig. S2.1). Target tree DBH ranged from 10 to 96 cm and ages ranged from 24 to 521 years. Neighborhood conditions varied from open forest stands with essentially free growing target trees, to dense neighborhoods with more than 200 trees within the 15 m search radius of each plot. Elevations for all samples ranged from ~1300 to over 3600 m. The average breadth (maximum– minimum) of mean annual temperature within sites was substantial, ranging from a low of 6.2°C for *P. ponderosa* to a high of 7.8°C for *P. menziesii* (Fig. S2.2). For all study sites combined, the breadth of mean annual temperature ranged from 9.9°C for *P. contorta* to 12.6°C

for *P. menziesii*. The average breadth of annual precipitation within sites was similarly large, ranging from 620 mm for *P. ponderosa* to 1040 mm for *P. engelmannii*. For all study sites and plots combined, the breadth of mean annual precipitation ranged from 863 mm for *P. ponderosa* to 2558 mm for *P. engelmannii*. The climate niche breadth of our samples is comparable to or exceeds the climate breadth captured by permanent sampling plots associated with the Forest Inventory and Analysis Program of the U.S. Forest Service (Fig. S2.3).

Appendix S2.2: Growth models based on seasonal climate

We considered seasonal climate predictors in the event that future climate forcings result in differential changes in temperature or precipitation among seasons or a possible decoupling of annual and seasonal climate. We considered alternate combinations of seasonal temperature and precipitation variables based on winter, spring, and summer periods. Seasonal periods were defined *a priori* according to 3 month intervals beginning with December in the year preceding growth. The best fitting seasonal climate predictors were selected based on model parsimony and likelihood (minimum AICc). The strongest seasonal temperature and precipitation predictors for each species were subsequently used to generate a full model of the same form as the best fitting full model based on annual climate. Full seasonal models thus included climate, crowding, age and size functions (Table S2.2).

Seasonal climate predictors generated more parsimonious full models of growth, compared with annual climate variables, for only two study species, *A. lasiocarpa* and *P. contorta*. Rollinson *et al.* (2016) similarly found only modest increases in explanatory power for models of tree growth for species in eastern North America when using seasonal vs. annual climate predictors. We argue that the use of annual climate variables in empirical models provide unbiased, robust predictions of tree growth due to high correlations between annual climate and

other permutations of temperature and precipitation. Further, models developed using annual climate facilitate more direct model comparisons between species and among studies and may more readily contribute to scientific and policy debates concerning global climate change, which have generally been framed in terms of trends in mean annual temperature.

Table S1.1. Warming trends in station observations of *Tmin* and *Tmax* (°C / decade) by elevation and season derived from the slopes of the linear regression of temperature on year for the period 1970 to 2008. Trends in annual temperature are calculated for the entire period as well as for 20 year subsets.

Variable	Elevation (m)	Annual (1970- 2008)	Annual (1970- 1989)	Annual (1990- 2008)	Winter	Spring (1970-2008)	Summer	Fall
<i>Tmin</i>	2770	.56**	0.76**	0.47	0.4*	0.61**	0.61**	0.49**
<i>Tmin</i>	3230	0.58**	0.03	0.86**	0.47*	0.67**	0.48**	0.61**
<i>Tmax</i>	2770	0.50**	0.3	0.94**	0.43**	0.62**	0.21	0.58**
<i>Tmax</i>	3230	0.62**	0.44	1.05**	0.45**	1.00**	0.34	0.52**

Significance levels: * $p < 0.05$; ** $p < 0.01$

Table S1.2. Goodness of fit and model comparison measures for hierarchical models of radial growth. Response variable is raw ring width. Size represents the diameter of the main stem at 1.3 m from the root crown. Shoot period represents the period of shoot extension growth (April to July). These models incorporate effects that occur in the year concurrent with growth and in the preceding or lag1 year. A null model predicts ring width from tree size in the year concurrent with growth (lag0). Statistics are shown for the most parsimonious models selected by AICc (corrected for small sample size).

Model	Variables	Sample size	¹ NP	AICc	R ²	Bias
Null	PotGrowth Size lag0	7023	17	35939	0.214	0.998
Concurrent year	PotGrowth Size lag0	7023	19	35841	0.216	0.997
Lag year	² <i>ppt</i> shoot period PotGrowth Size lag0	7023	21	35839	0.222	0.984
Full	³ <i>Tave</i> summer lag1 <i>ppt</i> spring lag1 PotGrowth Size lag0 <i>ppt</i> shoot period <i>Tave</i> summer lag1 <i>ppt</i> spring lag1	7023	23	35788	0.225	0.997

¹ number of parameters

² precipitation

³ average temperature

Table S2.1. Climate summary for target species by sample site for the analysis period (1992-2011). Sites arranged from south to north. Species acronyms are defined in Table S3 and site acronyms are defined in the methods section.

Species	Site	Annual Mean Temperature (°C)				Annual Total Precipitation (mm/year)			
		Mean	¹ SD	² CV	Range	Mean	¹ SD	² CV	Range
ABLA	LNF	6.1	0.9	0.15	3.9, 8	926	184.8	0.20	510, 1269
	SNF	2.6	0.8	0.31	-0.1, 4.7	699	194.8	0.28	219, 1115
	RNF	1.8	1.3	0.72	-1.4, 4.8	655	146.9	0.22	295, 1118
	BNF	1.9	1.5	0.79	-2.7, 5.8	670	101.8	0.15	389, 945
	GNP	3.4	1.4	0.41	-2.3, 6	1341	344.2	0.26	685, 2777
PIEN	LNF	6.3	1.1	0.17	3.9, 9.5	881	198.7	0.23	383, 1276
	SNF	2.5	1.3	0.52	-1, 6.1	748	180.6	0.24	220, 1150
	BNF	2.3	1.7	0.74	-3, 6.7	650	101.9	0.16	385, 942
	GNP	3.6	1.3	0.36	-2.3, 6	1302	333.6	0.26	646, 2777
PICO	SNF	5.1	0.8	0.16	2.6, 7.1	606	146.2	0.24	196, 867
	RNF	2.5	1.4	0.56	-1.4, 5.4	606	167.4	0.28	290, 1139
	BNF	2.7	1.6	0.59	-2.8, 6.1	632	101	0.16	307, 913
	GNP	3.1	1.4	0.45	-1.5, 6	1339	322.1	0.24	618, 2584
PIPO	LNF	9.8	1.7	0.17	5.7, 13.6	619	163.4	0.26	180, 1030
	SNF	6.8	1.2	0.18	3.3, 9	523	140.5	0.27	168, 863
	BNF	5.2	1.5	0.29	1.2, 9.3	519	108	0.21	267, 833
PSME	LNF	8.3	1.2	0.14	5.1, 11.3	701	172.8	0.25	254, 1216
	SNF	6.1	1.8	0.30	0.2, 9	577	156.6	0.27	167, 1083
	BNF	4	1.8	0.45	-1.3, 8.4	591	99.1	0.17	284, 832
	GNP	3.8	1.2	0.32	-0.5, 6	1267	281.5	0.22	645, 2128

¹ Standard deviation

² Coefficient of Variation

Table S2.2. Model comparison statistics (AICc and R^2) for the best fitting full models of RG based on annual vs. seasonal climate variables. Climate predictors in the seasonal models include temperature (T) and precipitation (P) for the months specified. Lag refers to climate in the year preceding growth. The best fitting models based on AICc are bolded.

Species	Annual Model			Seasonal Model			
	AICc	¹ Bias	R^2	AICc	Bias	R^2	Climate Predictors
ABLA	4185.1	1.01	0.36	4094.4	1.01	0.39	T summer, P spring, T lag summer, P lag summer
PIEN	5684.3	1.00	0.48	5760.8	1.01	0.45	T summer, P spring, T lag summer, P lag summer
PICO	1811.8	1.01	0.48	1748.3	1.01	0.49	T spring, P spring, T lag summer, P lag summer
PIPO	4563.1	1.03	0.75	4726.1	1.03	0.67	T spring, P winter, T lag spring, P lag winter
PSME	8179.6	1.02	0.42	8322.0	0.99	0.47	T summer, P spring, T lag summer, P lag summer

¹ Bias = slope of observed versus predicted *RG*

Table S2.3. Maximum likelihood estimates, with support intervals in brackets, for model parameters from the best fitting models of radial growth for each focal species. PotGrowth parameters (mm/year) are site specific intercept terms representing potential radial growth for a free growing tree under optimum climate conditions. Size effects were excluded from final models for all species except *P. ponderosa*. Precipitation effects were differentiated by site in final models only for *P. menziesii* and corresponding parameters are listed at the end of the table.

Parameter	Species				
	<i>A. lasiocarpa</i>	<i>P. engelmannii</i>	<i>P. contorta</i>	<i>P. ponderosa</i>	<i>P. menziesii</i>
Acronym	ABLA	PIEN	PICO	PIPO	PSME
PotGrowth (BNF)	225.7 (218.9-230.3)	158.8 (155.6-162.2)	19.1 (18.5-19.3)	1000 (970-1000)	12.1 (11.7-12.3)
PotGrowth (GNP)	29.6 (29.3-30.2)	4.89 (4.84-4.99)	6.81 (6.67-6.95)	NA	8.61 (8.44-8.81)
PotGrowth (LNF)	21.2 (19.7-22.9)	7.83 (7.44-8.11)	NA	240 (230-242)	4.71 (4.53-4.81)
PotGrowth (RNF)	11.8 (11.4-12.2)	NA	7.05 (6.98-7.32)	NA	NA
PotGrowth (SNF)	15.2 (14.9-15.8)	999.9 (980-1000)	46.2 (44.9-48.6)	1000 (960-1000)	8.12 (7.88-8.28)
age.a	0.09 (0.09-0.097)	0.79 (0.77-0.81)	0.01 (0.01-0.02)	0.007 (0.006-0.007)	0.62 (0.6-0.63)
age.b	3.1 (3.1-3.12)	2.91 (2.91-2.92)	4.02 (4.02-4.021)	3.05 (3.04-3.05)	2.954 (2.95-2.94)
size.a	NA	NA	NA	126.1 (122.3-138)	NA
size.b	NA	NA	NA	2.22 (2.1-2.26)	NA
temp.a (BNF)	9830.0 (6951-10000)	9956 (-100-10000)	3190 (2894-10000)	9947 (-100-15000)	227 (227-230)
temp.a (GNP)	23.7 (23.1-23.9)	7351 (6904-7645)	8.44 (8.27-8.64)	NA	9997 (9687-10000)
temp.a (LNF)	-100 (-100-125)	6.8 (6.5-6.9)	NA	9.12 (8.72-9.31)	7584 (556-10000)

Parameter	Species				
	<i>A. lasiocarpa</i>	<i>P. engelmannii</i>	<i>P. contorta</i>	<i>P. ponderosa</i>	<i>P. menziesii</i>
temp.a (RNF)	7234.1 (6794.1-7595.8)	NA	2613 (334-10000)	NA	NA
temp.a (SNF)	1861.0 (-100 -2786.4)	4733 (-100-10000)	9990 (9285-10000)	14955 (-100-15000)	5694 (5322-6210)
temp.b (BNF)	1885.6 (0.001-2685.6)	0.001 (0.001-26.8)	961.4 (0.001-1061)	¹ 2.89 (2.4-3.1)	134.7 (133.4-134.8)
temp.b (GNP)	20.4 (20.1-20.8)	6881 (6674-7293)	2.82 (2.68-2.96)	NA	9990 (9791-10000)
temp.b (LNF)	125.1 (115.1-140.9)	1.88 (1.78-2.1)	NA	NA	187.2 (0.001-2742)
temp.b (RNF)	6485.0 (6225.6-6901.4)	NA	124.4 (0.001-1025)	NA	NA
temp.b (SNF)	8680.0 (347.2-10000)	2.53 (0.001-23.7)	4590 (3672-4960)	NA	9873 (9084-10000)
temp.lag1.a (BNF)	-100 (-100-98.6)	-100 (-100- -98.6)	-28.96 (-29.6- -28.2)	15000 (14850-15000)	3978 (-500-10000)
temp.lag1.a (GNP)	577.8 (-100-10000)	3032 (2406-3371)	-93.5 (-100-1767)	NA	9201 (7169-10000)
temp.lag1.a (LNF)	9999.0 (2122.0-10000)	6044 (1314-10000)	NA	9477 (9094-10582)	-282 (-500-1454)
temp.lag1.a (RNF)	5.1 (4.8-5.2)	NA	0.84 (0.65-1.29)	NA	NA
temp.lag1.a (SNF)	338.0 (-100-10000)	9051 (9051-9052)	-99.6 (-100-2419)	14336 (14192-14623)	9999 (8219-10000)
temp.lag1.b (BNF)	44.0 (44.0-44.1)	39.5 (39.5-39.6)	22.7 (22.44-22.9)	¹ 10000 (9900-10000)	75.2 (0.001-156.6)
temp.lag1.b (GNP)	0.001 (0.001-36.1)	6187 (5568-7850)	7329 (440-10000)	NA	2568 (0.001-3311)

Parameter	Species				
	<i>A. lasiocarpa</i>	<i>P. engelmannii</i>	<i>P. contorta</i>	<i>P. ponderosa</i>	<i>P. menziesii</i>
temp.lag1.b (LNF)	871.7 (0.001-4166.6)	491.8 (0.001-2355)	NA	NA	4586 (1651-10000)
temp.lag1.b (RNF)	3.07 (2.9-3.3)	NA	4.71 (4.47-5.4)	NA	NA
temp.lag1.b (SNF)	13.4 (0.001-37.8)	2746.9 (2746-2747)	6293 (314-10000)	NA	2978 (0.001-3629)
prec.a	7.06 (0-10000)	868.8 (851.4-888.6)	97123 (0-100000)	2092 (2071-2155)	NA
prec.b	39289 (393-100000)	0.65 (0.63-0.69)	31970 (320-100000)	1.33 (1.31-1.35)	NA
prec.lag1.a	77687 (0-100000)	14821 (13783-15843)	36296 (362-100000)	83567 (0-100000)	NA
prec.lag1.b	0.1 (0-100000)	2.3 (2.26-2.35)	58231 (582-100000)	0.1 (0.1-100000)	NA
Alpha (α)	1.23 (1.21-1.26)	1.03 (1.01-1.05)	0.96 (0.95-0.98)	0.37 (0.31-0.4)	0.00001 (0-0.046)
Beta (β)	0.0 (0-0.02)	0.06 (0.04-0.08)	0.77 (0.76-0.79)	0.91 (0.85-0.93)	0.017 (0-0.052)
C	107.1 (102.4-111.7)	9.52 (9.23-9.81)	37.2 (35.9-37.9)	7.47 (7.12-8.26)	0.23 (0.21-0.26)
Gamma (γ)	--1.25 (-1.28-1.22)	-0.32 (-0.33-0.31)	-0.36 (-0.37-0.34)	0.05 (0.04-0.08)	0.0066 (0-0.042)
int	0.0 (0.0-0.01)	0.097 (0.085-0.11)	0 (0-0.013)	0.2 (0.18-0.21)	0 (0-0.02)
Sigma (σ)	0.44 (0.43-0.45)	0.35 (0.347-0.36)	0.43 (0.426-0.44)	0.34 (0.32-0.35)	0.55 (0.53-0.56)
² prec.a (BNF)	NA	NA	NA	NA	686.6 (672.9-720.2)
² prec.a (GNP)	NA	NA	NA	NA	981.5 (952.1-1031)
² prec.a (LNF)	NA	NA	NA	NA	1666 (1549-1922)
² prec.a	NA	NA	NA	NA	1232 (1195-1292)

Parameter	Species				
	<i>A. lasiocarpa</i>	<i>P. engelmannii</i>	<i>P. contorta</i>	<i>P. ponderosa</i>	<i>P. menziesii</i>
(SNF)					
² prec.b (BNF)	NA	NA	NA	NA	0.32 (0.280-0.34)
² prec.b (GNP)	NA	NA	NA	NA	0.39 (0.36-0.45)
² prec.b (LNF)	NA	NA	NA	NA	1.08 (0.92-1.16)
² prec.b (SNF)	NA	NA	NA	NA	1.1 (0.92-1.16)
² prec.lag1.a (BNF)	NA	NA	NA	NA	688 (667-735)
² prec.lag1.a (GNP)	NA	NA	NA	NA	55759 (0.001-100000)
² prec.lag1.a (LNF)	NA	NA	NA	NA	64566 (0.001-100000)
² prec.lag1.a (SNF)	NA	NA	NA	NA	92109 (0.001-100000)
² prec.lag1.b (BNF)	NA	NA	NA	NA	0.43 (0.37-0.47)
² prec.lag1.b (GNP)	NA	NA	NA	NA	77494 (775-100000)
² prec.lag1.b (LNF)	NA	NA	NA	NA	92727 (927-100000)
² prec.lag1.b (SNF)	NA	NA	NA	NA	0.001 (0.001-4.59)

¹ Variance of function not differentiated in best model for *Pinus ponderosa*

² Differentiated parameters for precipitation effects only significant for *P. menziesii*

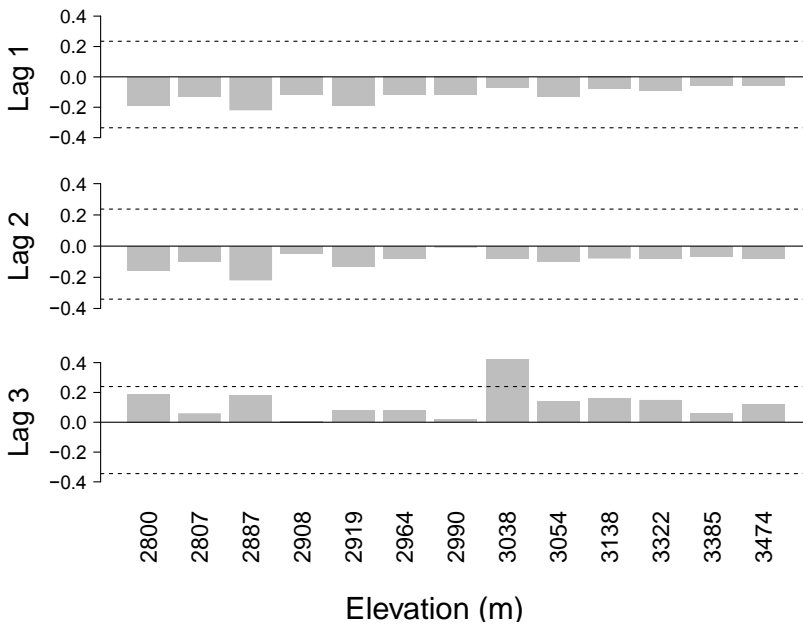


Figure S1.1. Autocorrelation function for each seed plot, designated by elevation, showing degree of serial correlation (y axis) for 3 lag years based on the untransformed time series of seed counts. Dashed 95% confidence intervals were computed following Salas et al. (1980): $CI = \frac{-1 \pm 1.96\sqrt{N-K-1}}{N-K}$, where N is sample size and K is lag.

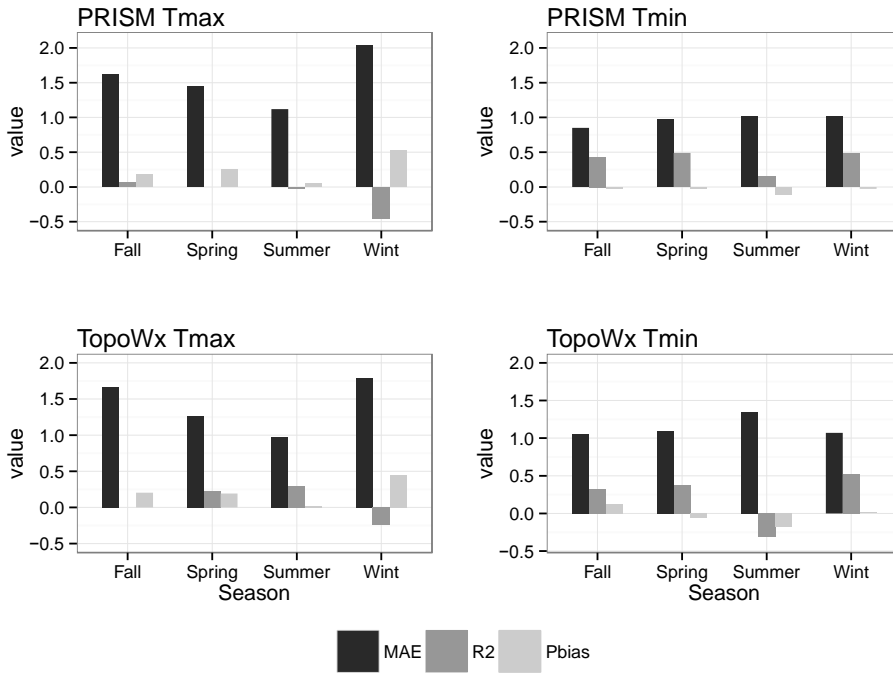


Figure S1.2. GOF statistics, including mean absolute error (MAE), R^2 of the regression of observed vs. predicted temperature, and percent bias (Pbias), comparing PRISM and TopoWx estimates of seasonal T_{max} and T_{min} at Fraser climate stations.

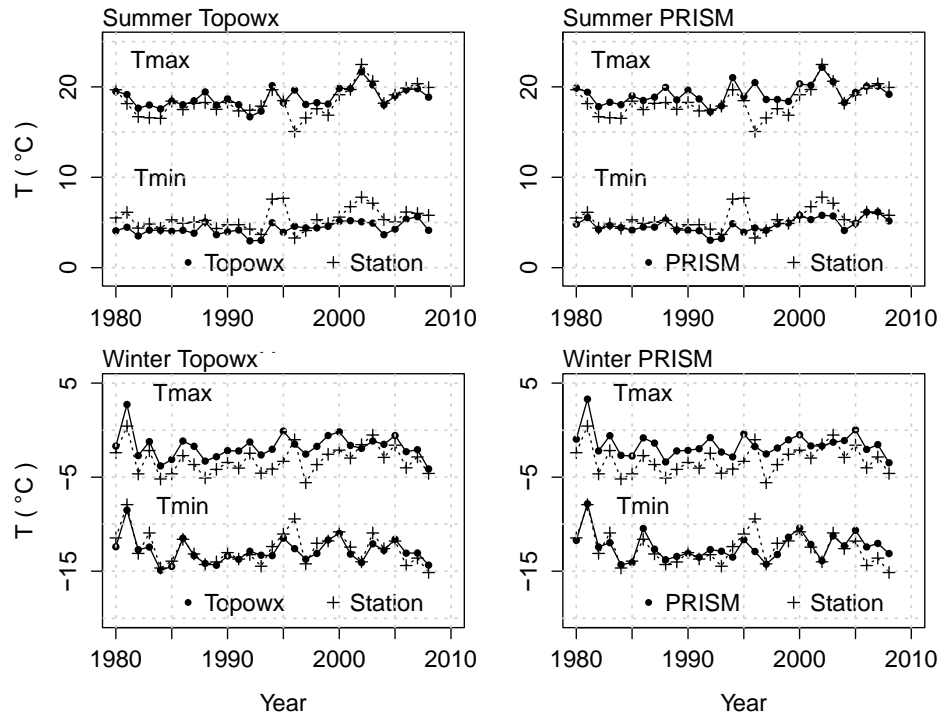


Figure S1.3. Time series of PRISM and TopoWx estimates of annual T_{min} and T_{max} for summer and winter. Station data are represented by grey dashed lines and model estimates by black solid lines.

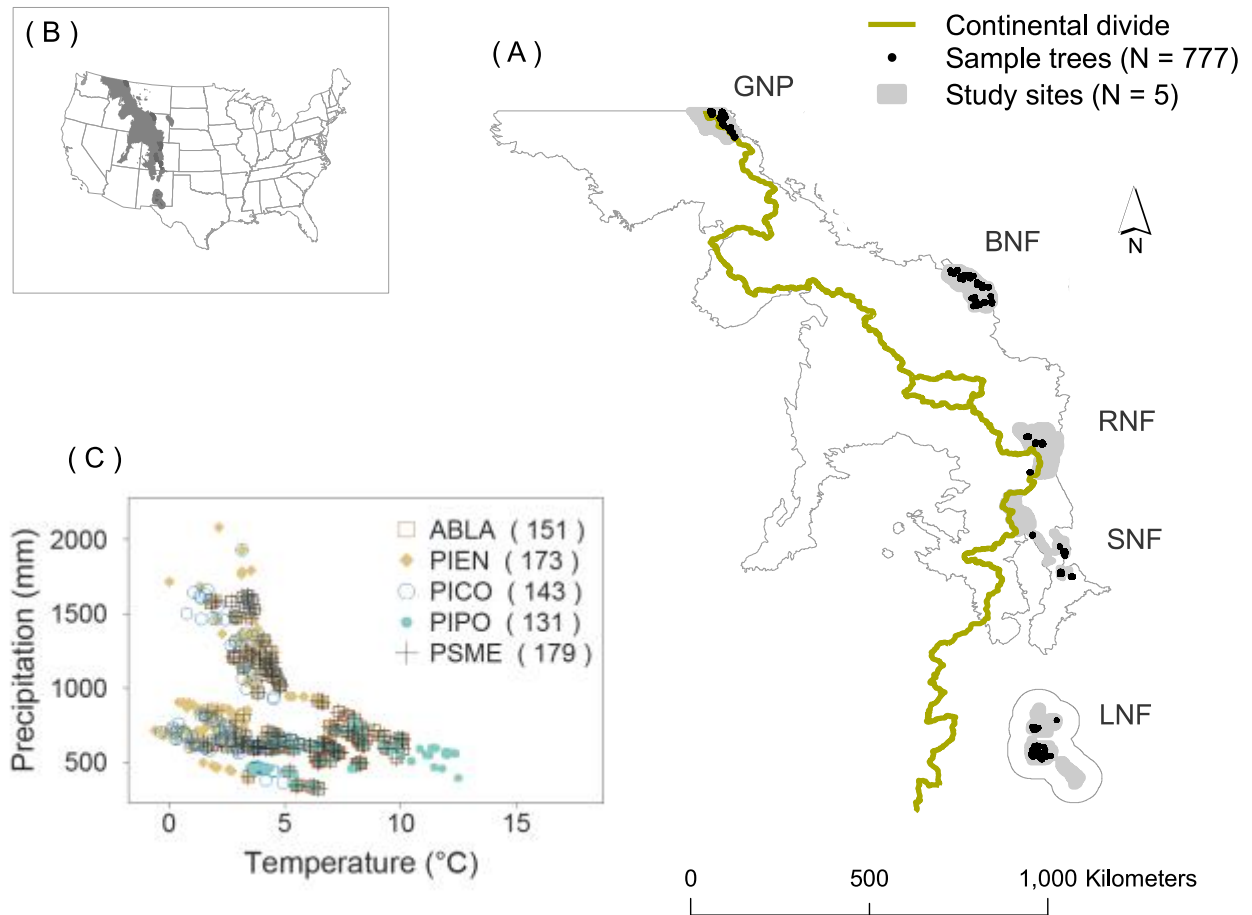


Figure S2.1. (A) Location of the 5 study sites and all sample trees within the Rocky Mountain ecoregion of the western United States. (B) Location of the Rocky Mountain ecoregion within the United States. (C) Distribution of all sample trees by species across gradients of total annual precipitation and mean annual temperature averaged over the 20-year study period (tree sample sizes in brackets).

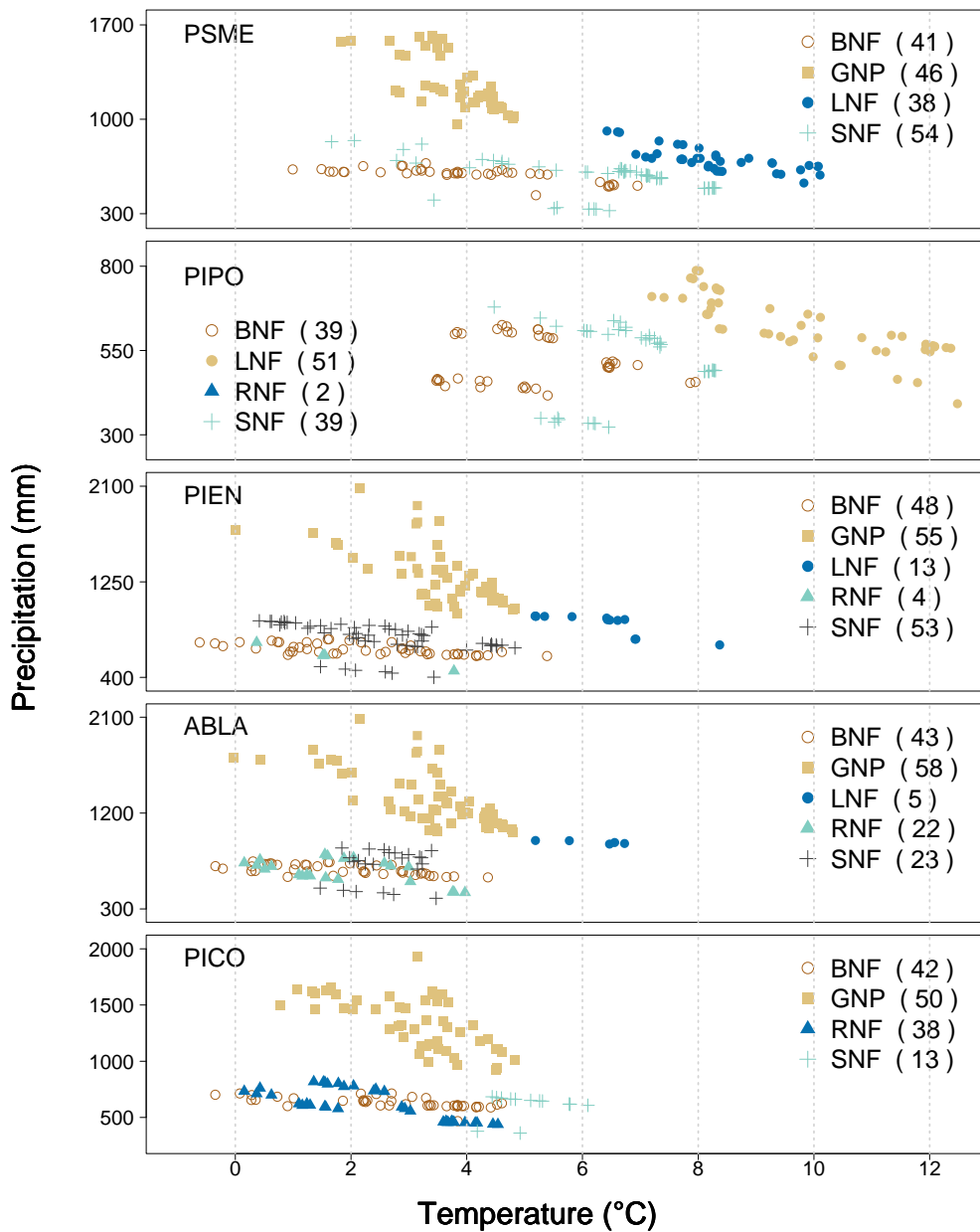


Figure S2.2. Distribution of sample trees across gradients of mean annual temperature and total annual precipitation by species and sample site (sample sizes for each species and site in brackets). Annual climate data were averaged over the 20-year period of the study for this figure. Sites with less than 5 sample trees for a given species were excluded from modeling analyses.

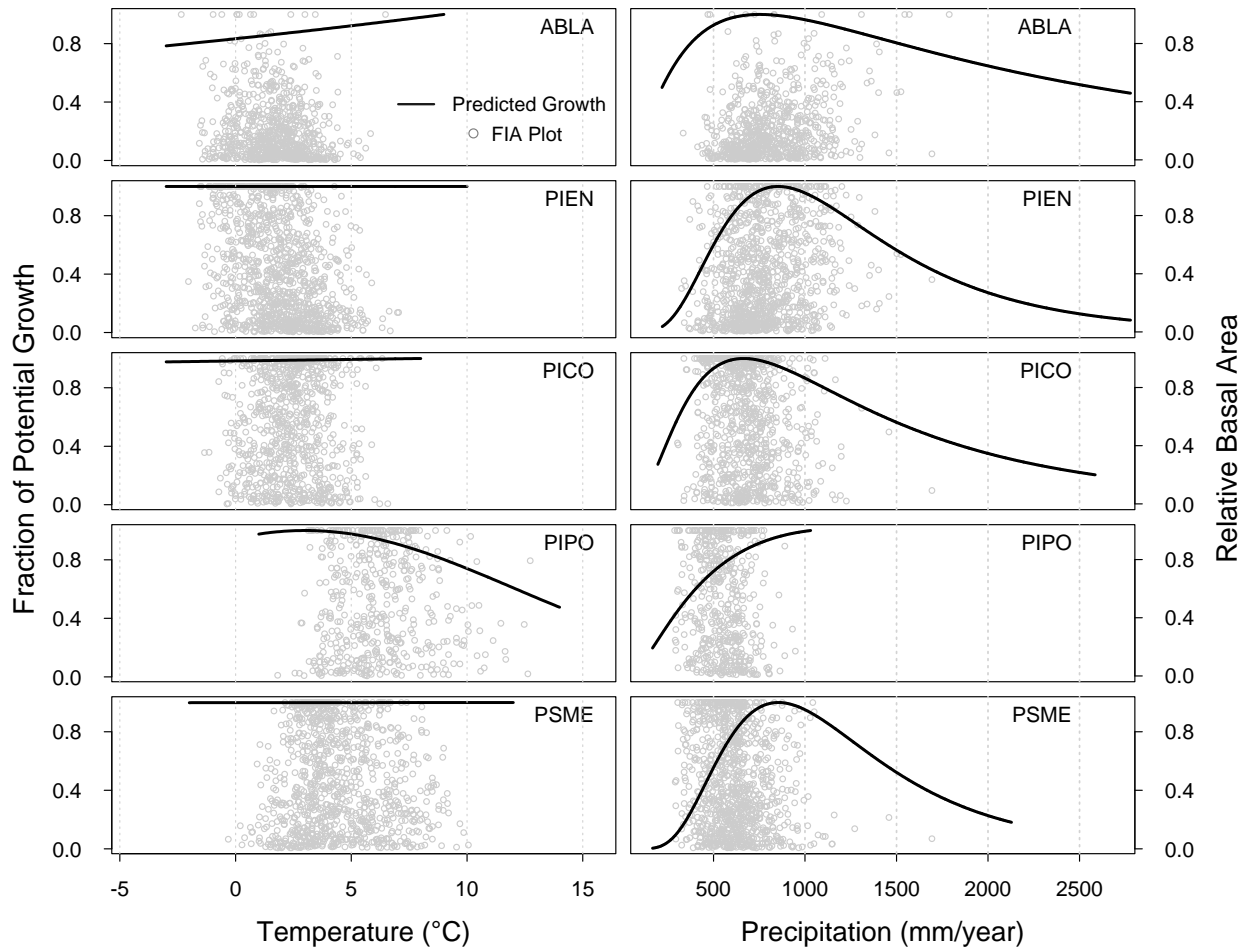


Figure S2.3. Comparisons of the climate niche breadth associated with target trees in this study and Forest Inventory and Analysis (FIA) plots from the U.S. Forest Service located on the east slope of the Rocky Mountains (from Martin & Canham *in prep*). Growth responses to annual climate parameters in the year concurrent with growth are plotted as smooth curves representing the fraction of potential radial growth for 30 cm DBH, free growing trees from all study sites combined. The length of each curve defines the observed climate breadth of the corresponding field data. FIA point data represent the fraction of total biomass of a given species at a particular plot location and delimit the associated realized climate niche of each species in the Rocky Mountain ecoregion.

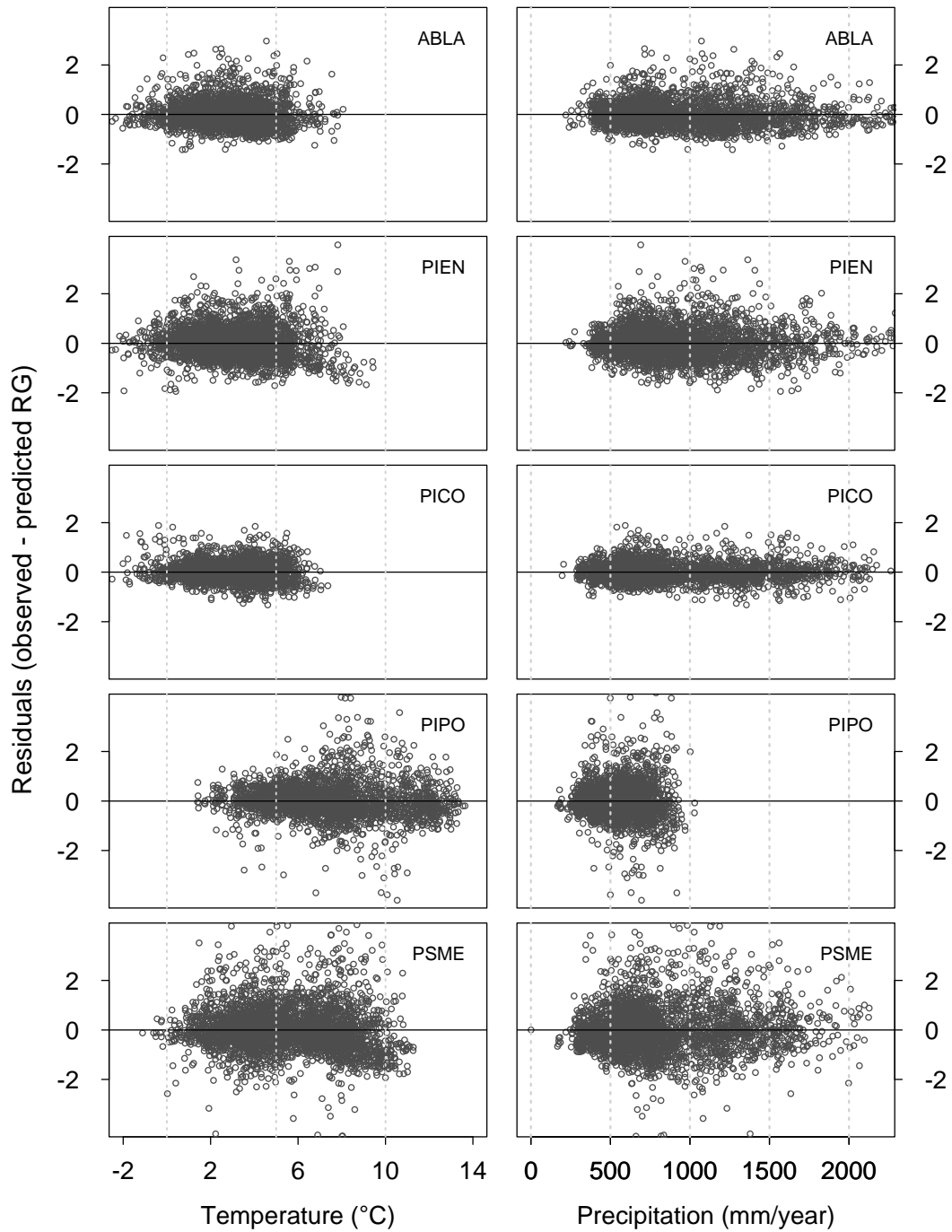


Figure S2.4. Regression residuals (observed – predicted radial growth) from full models plotted as a function of annual mean temperature and annual total precipitation.

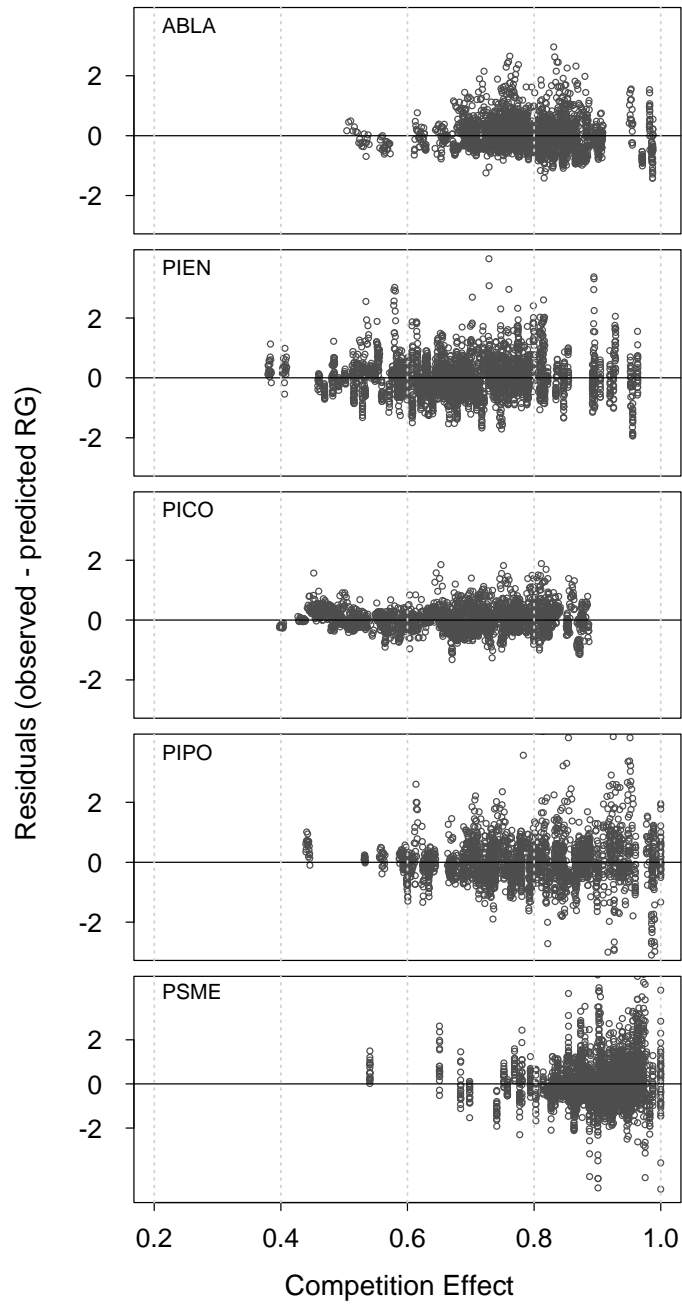


Figure S2.5. Regression residuals (observed – predicted radial growth) for full models plotted as a function of competition effects.

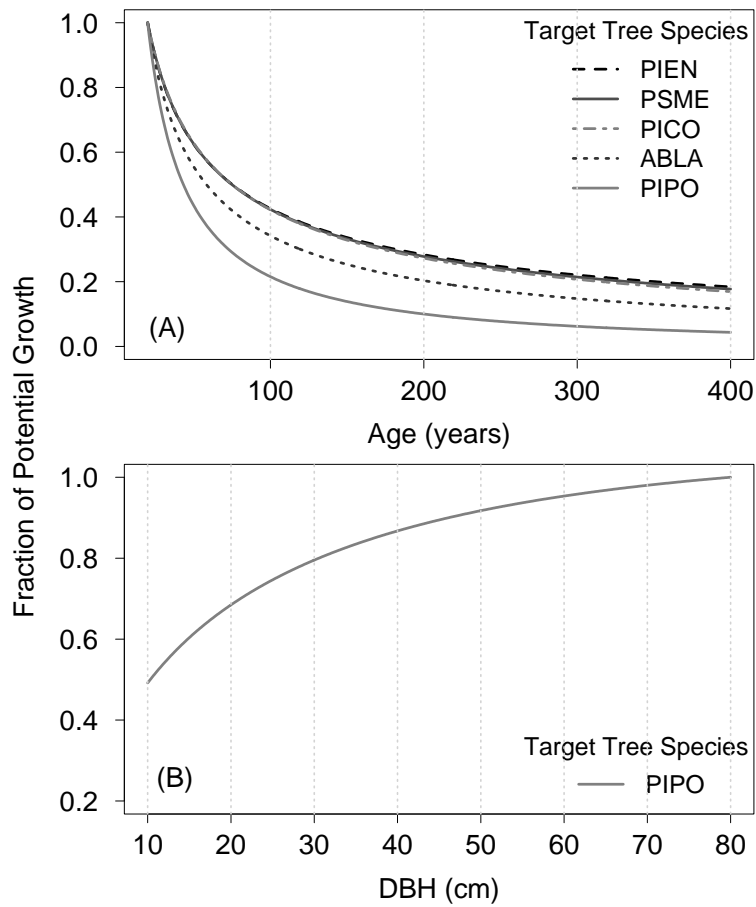


Figure S2.6. Fraction of maximum potential radial growth as a function of age (panel A) and stem diameter (panel B) for a free growing tree in its optimum climate. Size effects were only significant for PIPO in the final full models of growth that included age and locally differentiated responses to climate.

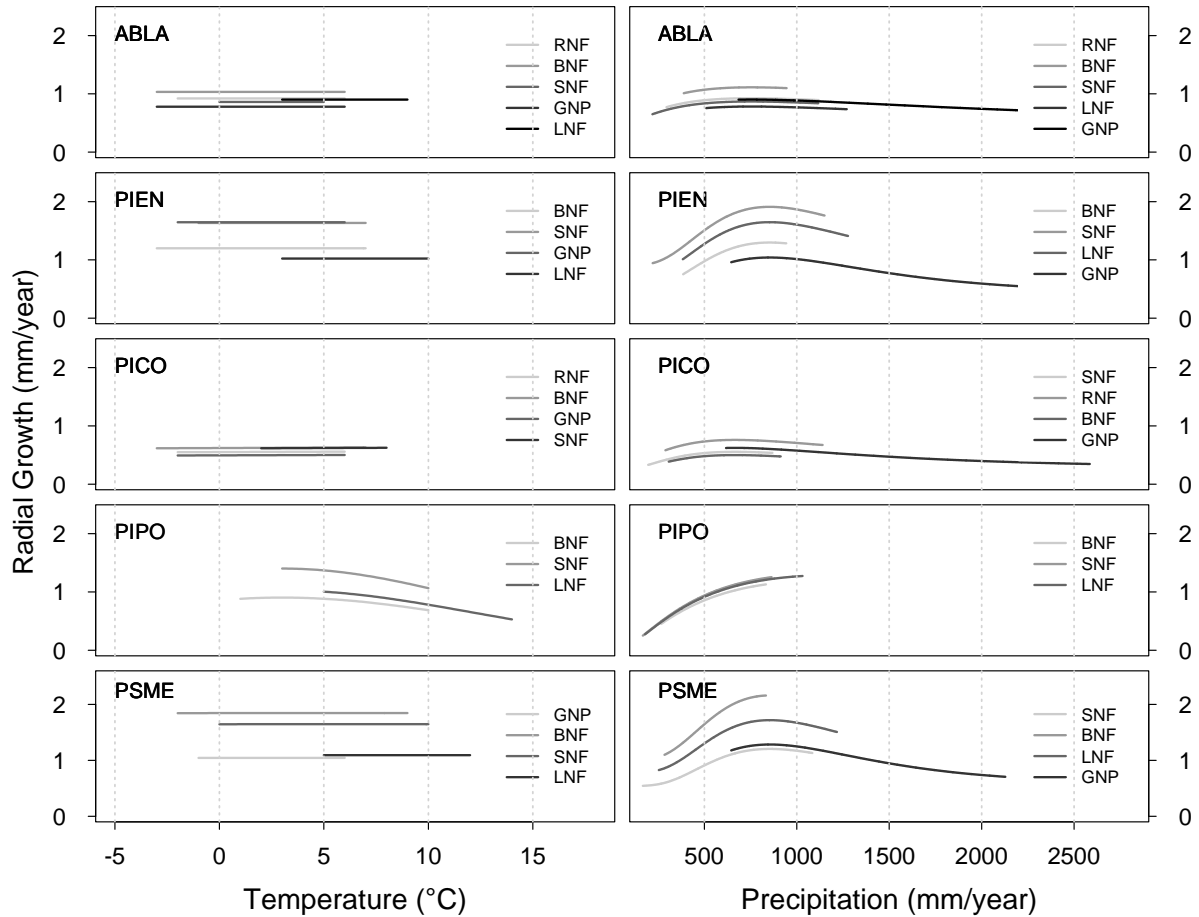


Figure S2.7. Radial growth responses by study site to concurrent annual temperature and precipitation for a 30 cm tree. These responses are based on models that include age and crowding effects, but do not account for locally differentiated responses to site specific climates. Hence, the amplitude of each response curve varies by site, but not their shape. Crowding effects are held constant at the overall mean level for a species. The grey color scale corresponds to a gradient of mean annual temperature or precipitation for a species across sites (darker shades representing higher site climate means). The length of each site curve defines the observed climate breadth of the corresponding field data for that site.

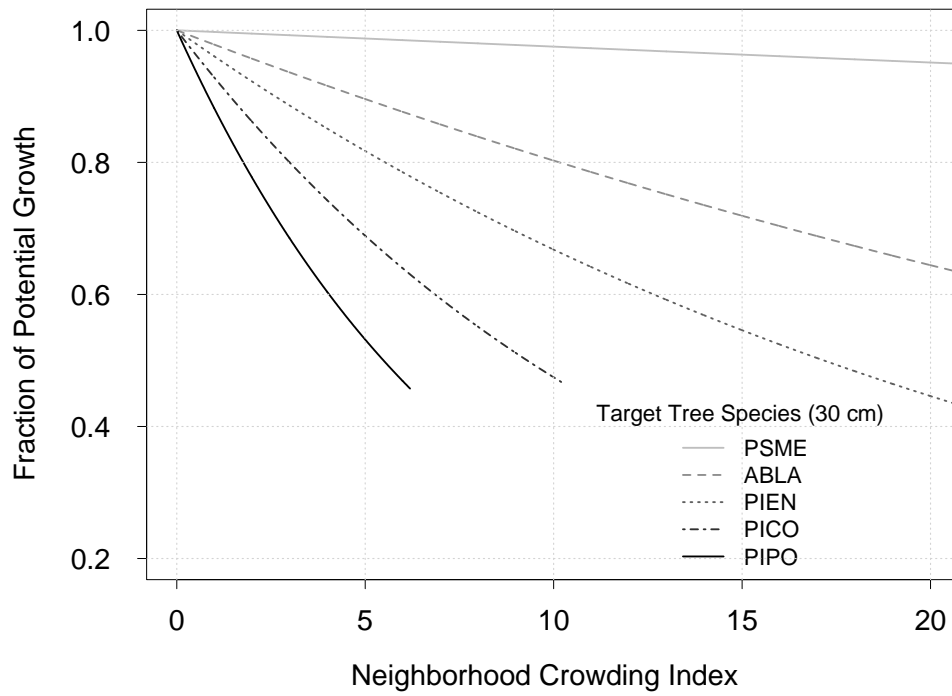


Figure S2.8. Fraction of maximum potential radial growth as a function of neighborhood crowding based on the best fitting full model for a 30 cm tree under optimum climate conditions.

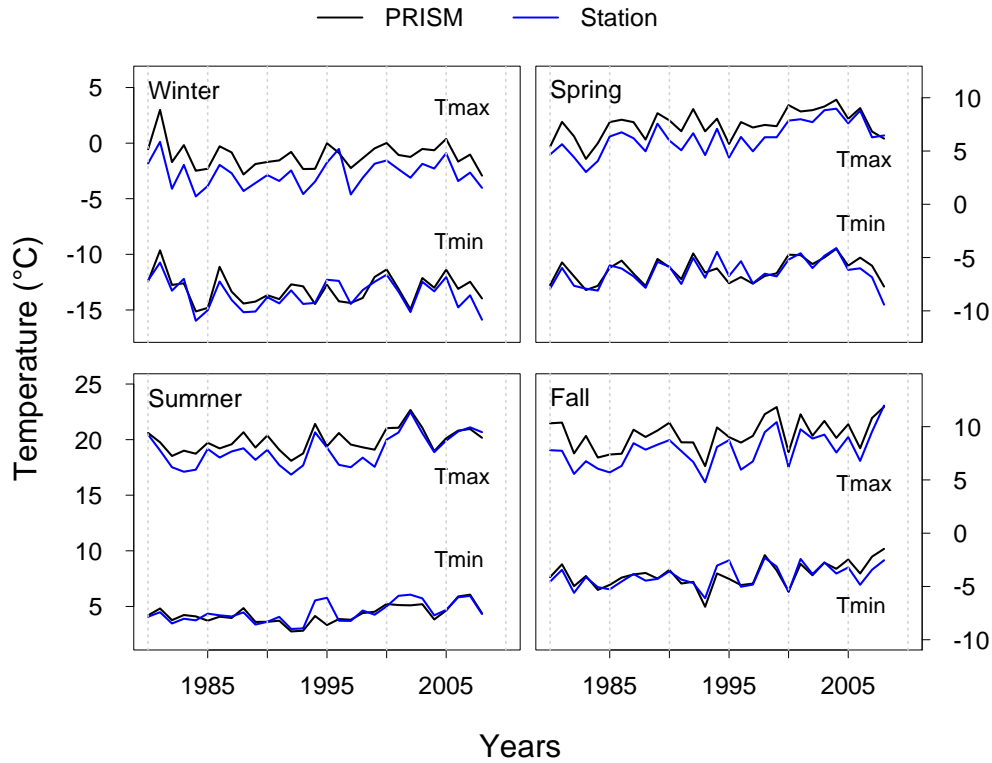


Figure S3.1. Time series of spatially explicit gridded PRISM data and independent instrumental climate records collected by the U.S. Forest Service at Fraser Experimental Forest in central Colorado. Instrumental data were collected from 5 weather stations distributed on an elevation gradient from 2770 to 3230 m. Daily minimum and maximum data were screened for anomalous values and aggregated to produce seasonal means (3 month intervals beginning with December of the prior year).

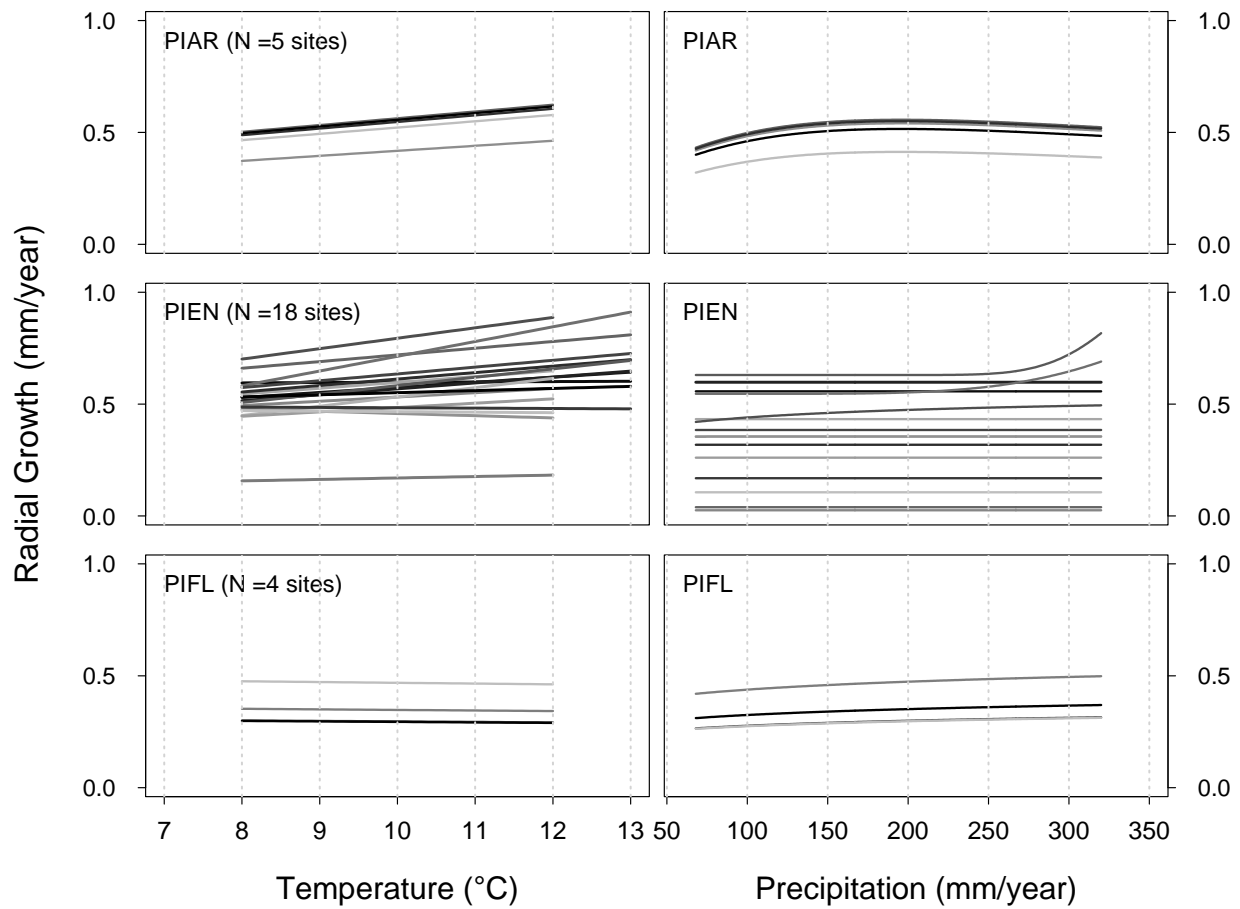


Figure S3.2. Radial growth responses by study site to concurrent summer temperature and precipitation for a 30 cm tree based on parameters from the best fitting models (see Table 3.3). Dissimilar slopes and shapes for the response curves for *P. engelmannii* reflect differentiated climate functions for this species (variable mode and variance depending on location). The grey color scale corresponds to a gradient of mean annual temperature or precipitation for a species across sites (darker shades representing higher site climate means). Species acronyms defined as: PIAR: *P. aristata*; PIEN: *P. engelmannii*; and PIFL: *P. flexilis*.

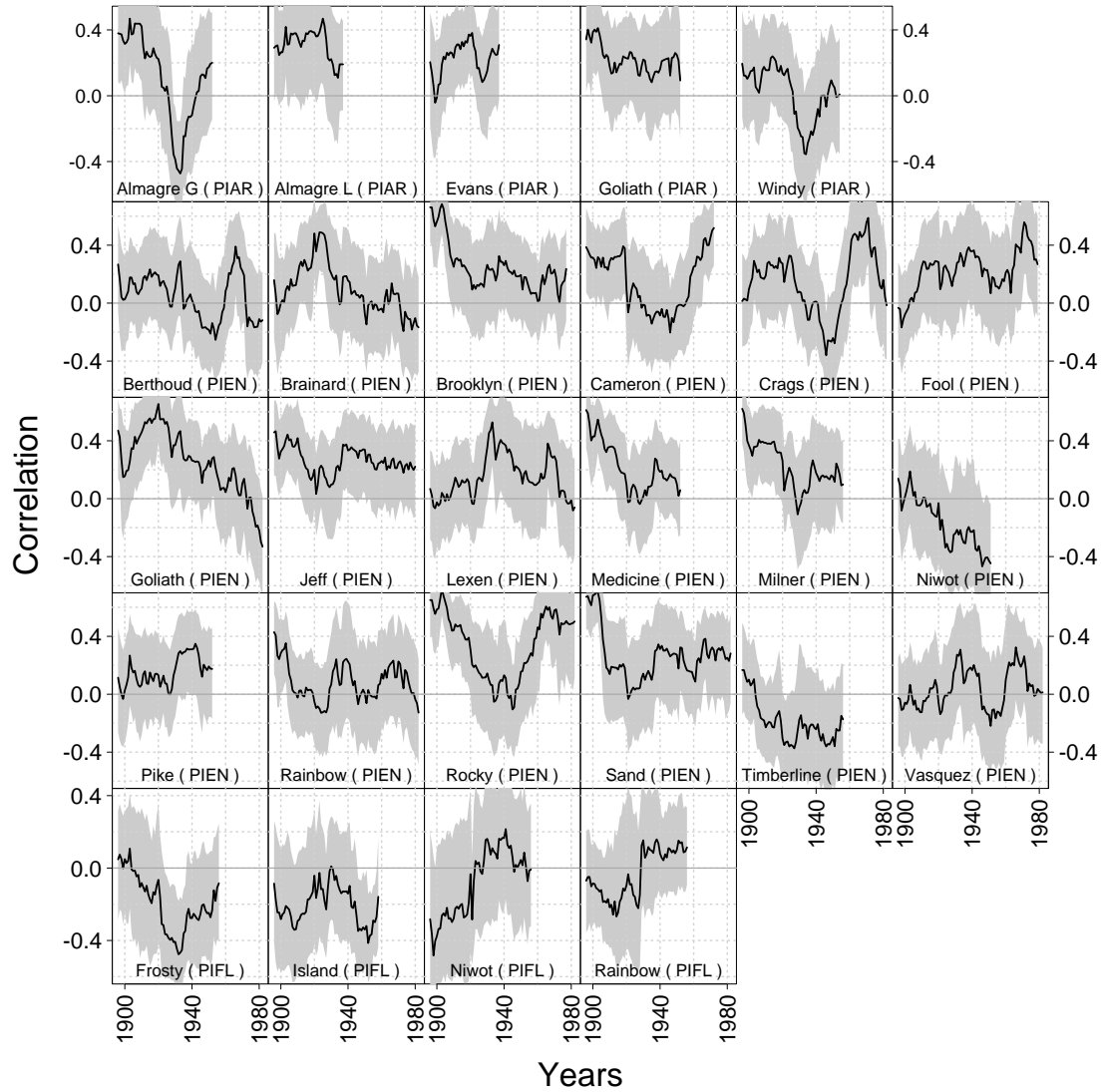


Figure S3.3. Moving window correlation between composite site indices of normalized BAI and site-specific mean summer temperatures. A window length of 30 years was progressively advanced by one year. Years on the abscissa represent start years for each 30 year window. Three species were analyzed including *Pinus aristata* (PIAR) in the upper row, *Picea engelmannii* (PIEN) in the middle three rows, and *Pinus flexilis* (PIFL) in the bottom row.

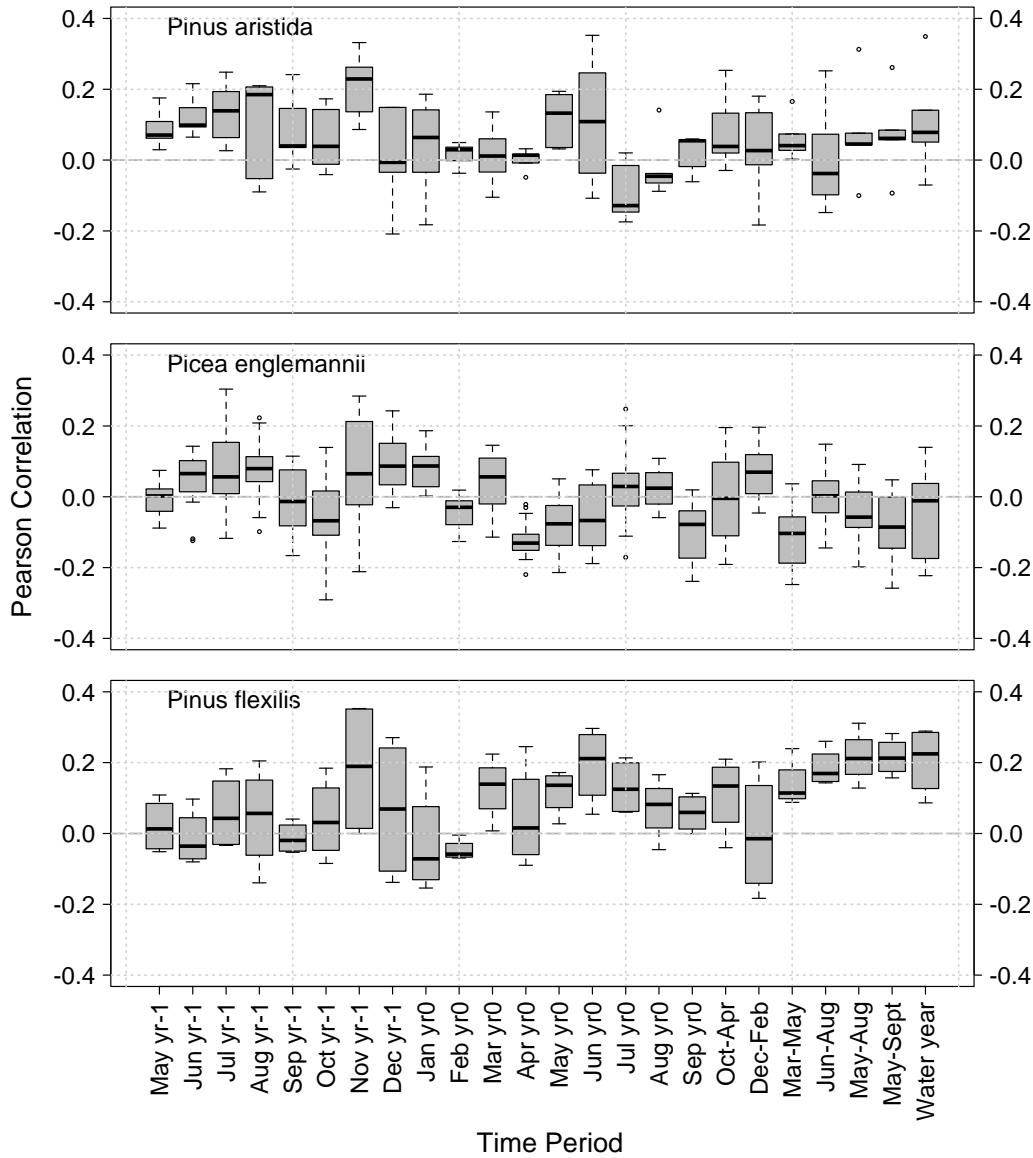


Figure S3.4. Linear correlations between site-specific mean normalized basal area increment (BAI) and mean regional precipitation for a range of time periods for 3 species. Regional precipitation indices were obtained by summing site-specific precipitation values across all sites. Months range from May of the year prior to growth (yr-1) to September of the year concurrent with growth (yr0). Seasonal windows were tested for the year concurrent with growth only. Water year precipitation represents total precipitation across months from October of the prior year to September of the concurrent year. Boxplots delimit medians, 25th and 75th percentiles, and extreme site values.

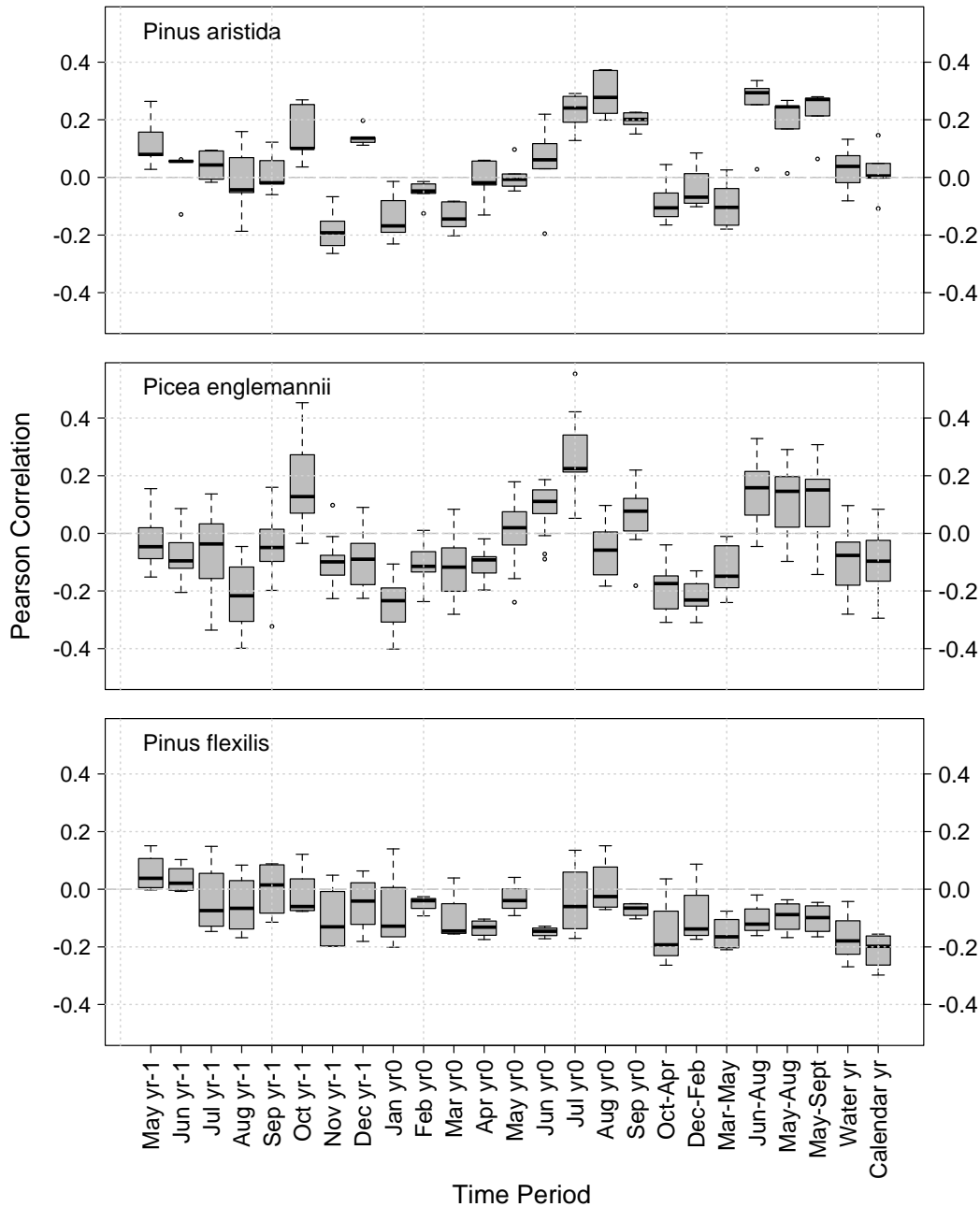


Figure S3.5. Linear correlations on inter-annual time scales between site-specific mean normalized basal area increment (BAI) and regional mean temperature for 3 species. Regional temperature indices were obtained by averaging site-specific temperatures across all sites. Monthly correlations range from May of the year prior to growth (yr-1) to September of the year concurrent with growth (yr0). Seasonal windows were tested for the year concurrent with growth only. Water year temperature represents mean temperature across months from October of the year preceding growth to September of the concurrent year. Calendar year temperature ranges from January to December of the year concurrent with growth. Boxplots delimit medians, 25th and 75th percentiles.

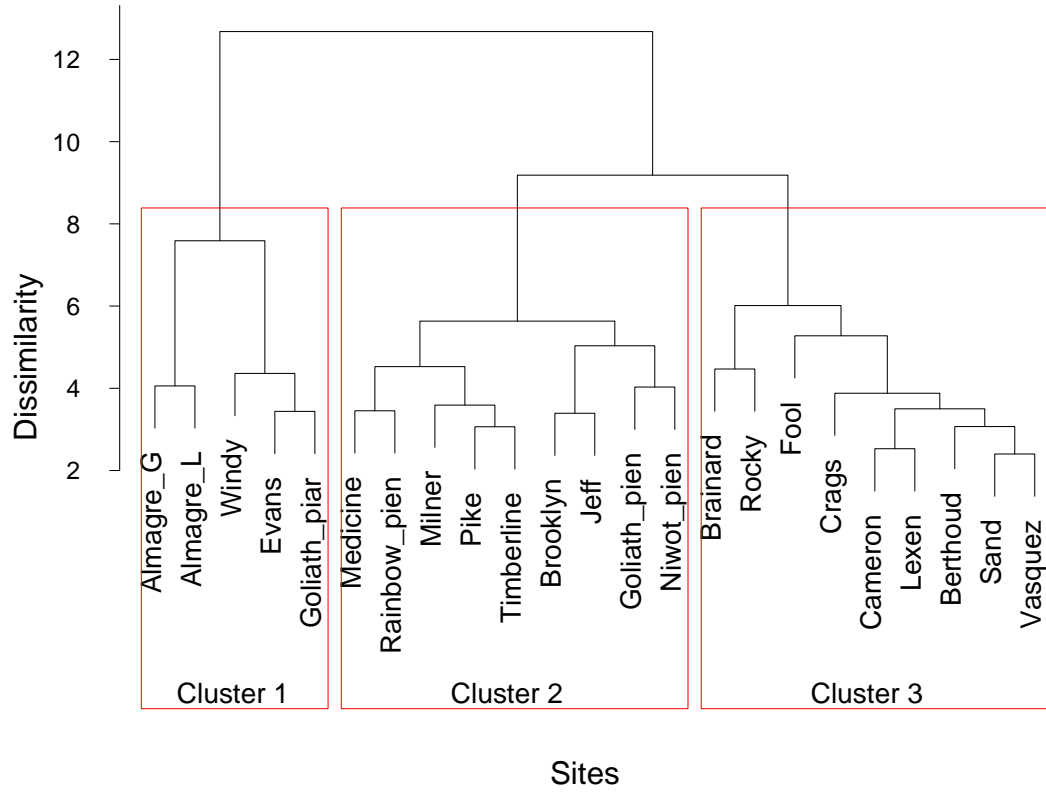


Figure S3.6. Hierarchical cluster analysis of all *P. engelmannii* and *P. aristata* populations based on normalized BAI. Cluster 1 is comprised of exclusively of *P. aristata* populations. Clusters 2 and 3 are comprised of *P. engelmannii* populations only.